NORTHWESTERN UNIVERSITY

# The Role of Mental Disorder Susceptibility Molecule CNTNAP2 in Interneuron Function and Pathology

A DISSERTATION

SUBMITTED TO THE GRADUATE SCHOOL IN PARTIAL FULLFILLMENT OF THE REQUIREMENTS

for the degree

DOCTOR OF PHILOSOPHY

Field of Neuroscience

By

Ruoqi Gao

EVANSTON, ILLINOIS

December 2018

## ABSTRACT

Contactin associated protein like 2 *(CNTNAP2)* has emerged as a prominent susceptibility gene implicated in multiple complex neurodevelopmental disorders, including autism spectrum disorders (ASD), intellectual disability (ID), and schizophrenia (SCZ). The presence of seizure comorbidity in many of these cases, as well as inhibitory neuron dysfunction in *Cntnap2* knockout (KO) mice, suggests CNTNAP2 may be crucial for proper inhibitory network function. However, underlying cellular mechanisms are unclear. Here we show that cultured *Cntnap2* KO mouse neurons exhibit an inhibitory neuron-specific simplification of the dendritic tree. These alterations can be replicated by acute knockdown of CNTNAP2 in mature wild-type (WT) neurons and are caused by faulty dendrite stabilization rather than outgrowth. Using structured illumination microscopy (SIM) and stimulated-emission depletion microscopy (STED), two super-resolution imaging techniques, we uncovered relationships between nanoscale CNTNAP2 protein localization and dendrite arborization patterns. Employing yeast two-hybrid screening, biochemical analysis, in situ proximity ligation assay (PLA), SIM, and phenotype rescue, we show that these effects are mediated at the membrane by the interaction of CNTNAP2's C-terminus with calcium/calmodulin-dependent serine protein kinase (CASK), another ASD/ID risk gene. Finally, we show that adult *Cntnap2* KO mice have reduced interneuron dendritic length and branching in particular cortical regions, as well as decreased CASK levels in the cortical membrane fraction. Taken together, our data reveal an interneuron-specific mechanism for dendrite stabilization that may provide a cellular mechanism for inhibitory circuit dysfunction in CNTNAP2-related disorders.

# ACKNOWLEDGMENTS

I would like to foremost acknowledge my mentor, Dr. Peter Penzes, for giving me the opportunity to work in his lab. He not only provided valuable technical and conceptual feedback for a great portion of these projects, but he also instilled in me a sense of pride in my work. The latter was critical as it gave me the confidence and persistence to fight through the inevitable technical and mental hurdles. I would also like to especially thank Dr. Sehyoun Yoon for his invaluable mentorship on experimental design, planning, and data interpretation. Dr. Marc Forrest was also an invaluable resource to me, especially on habits of organization. My gratitude also goes out to my collaborators Dr. Alexandria Melendez-Zahdi, Dr. Nicholas Piguel, and Dr. Maria Dolores Martin-de-Saavedra for their patience and hard work on several key experiments. I would also like to express my gratitude to the other postdocs in the lab who have helped me with advice along the way, including Dr. Kristoffer Myczek, Dr. Colleen Zaccard, Dr. Marc de los Santos, and Dr. Christopher Pratt. Finally, I would like to thank my committee, Dr. Geoffrey Swanson, Dr. Richard Miller, and Dr. Gianmaria Maccaferri for guiding me in the right direction.

TABLE OF CONTENTS

# LIST OF FIGURES

# CHAPTER 1: General Introduction

## 1.1. Background

ASD and SCZ are two highly heritable spectrum disorders with complicated genetic etiologies but overlapping behavioral phenotypes [1]. ASDs are a group of neurodevelopmental disorders characterized by repetitive behaviors and problems with social interaction and communication while SCZ is a disease afflicting thought, perceptions of reality, affect, and cognition[2]. Genetic linkage and genome-wide association studies (GWAS) have discovered a plethora of disease-associated genes, but few have been widely reproducible because each individual gene likely holds small influence on the overall disease pathogenesis[3, 4]. Moreover, given the conditions' heterogeneous natures, many studies lack the required power to consistently reproduce these weak associations[5]. The behavioral symptoms of ASD and SCZ, however, are intriguingly similar; social interaction deficits, cognitive deficits, emotional processing problems, and executive functions dysfunction are all behavioral features commonly observed in both disorders[6, 7]. In addition, subsets of autism patients have auditory and visual hallucinations, similarly to acutely ill patients with SCZ[8]. Indeed, autism was initially believed to be an early manifestation of SCZ and was once referred to as "schizophrenia syndrome of childhood"[9, 10].

These observations suggest that while the genetics are diverse, the two diseases may convergence upon common pathophysiological mechanisms. One emerging hypothesis maintains that alterations in the ratio of excitatory to inhibitory cortical activity (E/I imbalance) could explain the diseases' similar social and cognitive deficits. Such imbalances may arise from problems in initial neural circuit formation or maintenance, as many of the genes derived from linkage and association studies code for proteins involved with these processes[4, 11]. In addition, postmortem studies have discovered structural/functional changes in both glutamatergic

excitatory and GABAergic inhibitory circuits in individuals with ASD and SCZ[12-14].

The end goal, however, is to provide biological evidence that risk variants impact the pathogenesis of the diseases through specific shared pathways, such as E/I imbalance, so that future therapies can be developed in a directed manner. For this purpose, we will briefly discuss the cellular physiology of E/I balance, review evidence of its dysregulation in ASD and SCZ, and discuss how *CNTNAP2*, a gene implicated in multiple complex psychiatric disorders is involved with E/I homeostasis and pathology.

## 1.2. The physiology of E/I balance

### 1.2.1. Excitatory/Inhibitory synapses

Excitatory and inhibitory synapses, although found on pyramidal and interneuron cells alike, have different architectures. While glutamatergic synapses are found almost exclusively on dendritic spines[2], GABAergic synapses are localized along the dendritic shaft, somata, and axon initial segments[15]. Excitatory synapses contain an electron-dense postsynaptic density (PSD) that directly opposes a pre-synaptic active zone while inhibitory synapses are missing this feature and are more symmetric. Likewise, the two also harbor different molecular constituents, which are often used as markers for identification purposes in immunofluorescent studies. Excitatory synapses maintain pre-synaptic vesicular glutamate transporters (VGLUTs), which pack the excitatory neurotransmitter glutamate into synaptic vesicles for release. The postsynaptic side harbors the postsynaptic density protein-95 kDa (PSD-95), a multimeric scaffold that anchor N-methyl-D-aspartate receptors (NMDARs) and 2-amino-3-(3-hydroxy-5-methyl-isoxazol-4-yl)propanoic acid receptors (AMPARs) to the surface. Inhibitory synapses have pre-synaptic vesicular GABA

transporters (VGATs), which pack the inhibitory neurotransmitter y-aminobutyric acid (GABA) into synaptic vesicles for release, while the adaptor protein gephyrin help cluster y-aminobutyric acid receptors (ionotropic GABAARs and metabotropic GABABRs) and glycine receptors (largely in spinal cord, brainstem, and retina[16]) onto the postsynaptic surface. Both synapse types are held together by trans-synaptic interactions between pre- and post-synaptic cell adhesion molecules (CAMs)[17] (Figure 1.1).

### 1.2.2. Dendritic arbors

The structure and arborization of dendrites has a profound impact on the processing of neuronal information because it determines the extent of a neuron's synaptic field. The establishment of the dendritic arbor is highly plastic and involves dendrite extension, addition, elongation, retraction. Much of this early process is dependent on robust synapse formation and hence is particularly sensitive to experience and activity[18]. However, by adulthood, the arbor becomes stabilized and is no longer as dependent on synaptic activity. This mechanistic separation allows mature neurons the ability to fine-tune synaptic connections while retaining a stable dendrite field[19].

### 1.2.3. Pyramidal neurons

Pyramidal cells comprise the majority of the neuronal population and are primarily responsible for long-range glutamatergic transmission in the mammalian forebrain. The dendrites of pyramidal neurons are usually regarded as input structures and receive excitatory synaptic contacts from other

a.

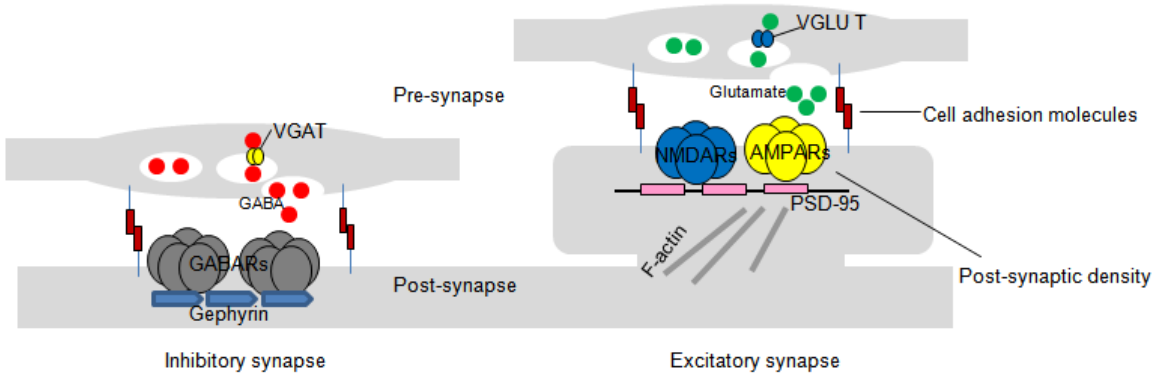


**Figure 1.1**. **Simplified architecture of excitatory and inhibitory synapses on pyramidal cells.** Pre-synaptic terminals of excitatory synapses release glutamate neurotransmitters that are post-synaptically received by glutamate receptors (NMDARs and AMPARs) on dendritic spines – small membranous protrusion stemming from the dendrite. The tip of each spine contains an electrodense region called the PSD, which is comprised of cytoskeleton anchoring proteins, such as PSD-95, designed to scaffold glutamate receptors (NMDARs and AMPARs) to the spine's surface and to dock hundreds of signaling molecules (not shown) to the underside. Inhibitory synapses are localized to the dendritic shaft. Pre-synaptic terminals release GABA to be received by post-synaptically by GABARs anchored onto the post-synaptic surface by gephyrins (gephyrins also scaffold glycine receptors, which are activated by glycine neurotransmitters – not shown). Noticeably missing is the PSD. Both synapse types are structurally maintained by trans-synaptic adhesions through CAMs.

excitatory neurons on small protrusions called dendritic spines. Thousands of spines stud the pyramidal cell's apical and basal dendritic branches, increasing the neuron's receptive surface area and allowing for integration of thousands of excitatory signals to influence the output[20]. Due to this capability to control neuron activity, spines are morphologically regulated to meet the dynamic demands of the growing brain and thus intimately linked to cognitive function[21]. For instance, during development, spines actively participate in synaptogenesis and contribute to the formation of neuronal circuits[21]. Activity-dependent spine maintenance or elimination, on the other hand, is important for the remodeling of established neuronal circuits during post-natal and adolescence periods[22, 23]. These complicated dynamics are regulated by equally complex molecular pathways, involving cytoskeletal remodeling, trans-synaptic adhesion, receptor trafficking, protein translation, ubiquitination, and gene expression[24-26].

### 1.2.4. GABAergic neurons

Cortical GABAergic neurons comprise only 20-30% of the entire neuron population but play crucial roles in regulating neuronal excitability due to their synaptic strengths, high firing rates, and abilities to synthesize the inhibitory neurotransmitter y-aminobutyric acid (GABA) by two isoforms of glutamic acid decarboxylase (GAD65 and GAD67)[27]. Unlike pyramidal neurons, which have long-projecting axons and homogenously characteristic spine-studded pyramidal-shaped arbors that can span several cortical layers, cortical interneurons communicate within spatially restricted regions and are relatively aspiny. Moreover, they are categorized into many subpopulations - classified by a combination of morphological, physiological and molecular properties - each of which possesses specialized functions for regulating pyramidal activity[27, 28]. Of these, interneurons possessing the calcium-binding protein parvalbumin (PV+) greatly

influence the generation and timing of a pyramidal cell's action potentials due to the strategic location of their inhibitory synapses and their fast-spiking electrophysiological properties[29, 30]. For example, the chandelier subtypes electrophysiologically exhibit fast-spiking firing patterns[30] and have long linear axon terminals called cartridges that synapse onto the axon initial segment of pyramidal neurons[31]. Basket subtypes, on the other hand, have identical fast-spiking electrophysiological features[29], but their axons target the cell bodies and proximal dendrites of pyramidal neurons[32]. Thus, both parvalbumin-positive subtypes are situated near the axon and have tight control over the excitatory cell's firing rhythms. Moreover, their biophysical abilities to generate fast synchronized inhibition patterns onto and to receive rhythmic feedback inhibition from pyramidal cells provide the temporal synchrony necessary for generation of network oscillations[33] (Figure 1.2). For the purposes of this introduction, we will focus largely on PV+ interneurons because they play an essential role in proper cognitive function and are noticeably afflicted in ASD and SCZ patients. For a more comprehensive review on interneuron classification and function, we would like to direct the reader to pertinent articles[27, 34].

### 1.2.5. Excitatory/Inhibitory balance

Information transfer in the brain relies on a functional balance between excitatory and inhibitory networks. At the level of individual neurons, this balance involves the maintenance of appropriate ratios of excitatory versus inhibitory synaptic inputs[35]. Activation of an excitatory synapse by glutamate depolarizes the cell and increases the likelihood that the cell will fire an action potential while activation of an inhibitory synapse by GABA does the opposite. Thus, the E/I synaptic ratio is critical for keeping the cell's overall firing patterns within a narrow range[36]. However, this ratio is highly asymmetric across development and between neuronal subtypes. For example, individual

pyramidal cell dendrites in the cultured hippocampal cultures have E/I ratios of 2:1 at 14 days but 4:1 at 19 days [37] while hippocampal PV+ and calretinin-positive interneuron subtypes have 14:1 and 3:1 ratios respectively[38]. Surprisingly, the ratios themselves are tightly regulated with minimal variance even between branches on a single neuron. Yet how do neurons establish and maintain this long- term internal consistency despite such external variability? In a landmark paper, Turrigiano *et al.*[39] discovered chronic activity blockade with tetrodotoxin (TTX) and bicuculline increased and decreased the amplitude of miniature excitatory postsynaptic currents (mEPSC) respectively in cultured neurons, while drug washout restored firing rates to control levels. Thus, in response to outside influences forcibly altering activity, compensatory mechanisms are recruited to restore the initial circuit set point. These responses include modulation of excitatory and inhibitory postsynaptic strength, alterations in presynaptic neurotransmitter release probability, and adjustment of intrinsic membrane excitability[40], all of which affect and are influenced by neuronal architecture, including dendritic spines and arbors. Collectively, multiple levels of homeostatic control exist to ensure the neuron's output is appropriately stable.

Since neural circuits are defined by inter-neuronal communications, output precision in individual cells becomes essential to network function. Cortical interneurons use rhythmic inhibition to create narrow windows for effective excitation, entraining excitatory pyramidal cells to fire certain oscillatory patterns[41-45]. Specific classes of interneurons contribute to the frequency of these particular patterns. For example, the synchronization of neuronal network activity in the human cortex and hippocampus at gamma frequencies (30–80 Hz) is essential for integrating information from different brain regions and is thus relevant for cognition, learning, and memory. Gamma oscillations emerge from the synchronized firing of interconnected excitatory glutamatergic and

a.

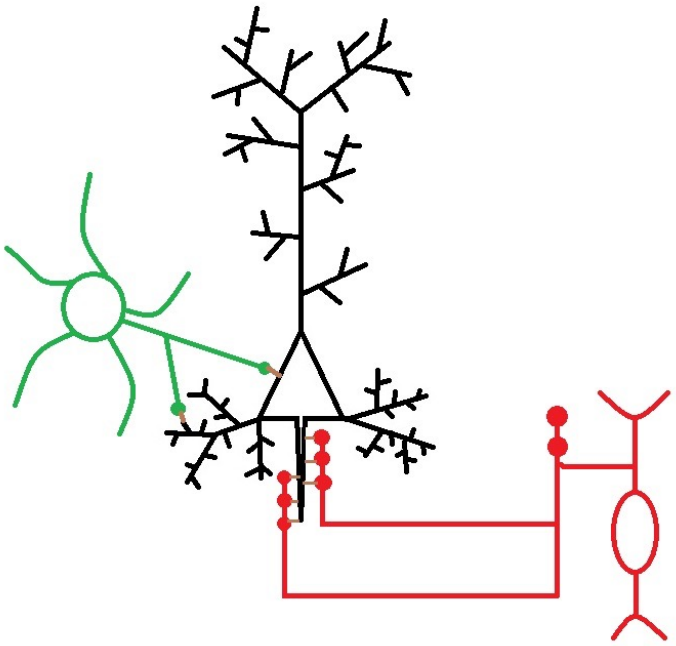

**Figure 1.2. PV+-containing interneurons regulate pyramidal cell firing.** (a) Both basket (green) and chandelier cells neurons (red) contain PV+ and have fast-spiking electrophysiological properties. Chandelier cells have long linear axon terminals called cartridges that synapse onto the axon initial segment of pyramidal neurons (black) while basket cell axons target the cell bodies and proximal dendrites of pyramidal neurons. Due to the strategic location of their synapses, both subtypes greatly influence the generation and timing of a pyramidal cell's action potentials.

primarily inhibitory fast-spiking GABAergic PV+ interneurons (Figure 1.2) and its power (i.e. amplitude) is modulated by the E/I balance at distinct synaptic sites in the circuit and the intrinsic excitable properties of the neurons[46]. Given the dynamic variability of early postnatal brain development and its activity-dependent shifts, such internal consistency - from single synapses to entire circuits - requires tight control and is essential for proper circuit formation and adaption to the onset and maturation of sensory input. Genetic perturbations to synaptic homeostatic mechanisms, if uncorrected, can serve as pathophysiological initiation points that lead to network destabilization, which in turn can impact behavior. To illustrate this point, Bateup *et al.*[47] showed loss of *TSC1*, a gene encoding a regulator of mTOR signaling in hippocampal cultures resulted in a primary decrease of inhibitory synaptic transmission, followed closely by a futile secondary homeostatic response, and concluded with an overall increase in network hyperexcitability. Moreover, optogenetic manipulation of specific excitatory and inhibitory circuits directly caused changes in social and cognitive behavior in mice[48]. Thus, circuits tend to be malleable but vulnerable during postnatal development; notably, several neurodevelopmental disorders, such as ASD and SCZ, manifest during this plasticity period[49, 50].

## 1.3. Neuropathological features of SCZ

One of the defining neuropathological features of SCZ is gray matter loss[51-53]. Postmortem studies have examined brain regions showing the highest indices of gray matter loss and have consistently found reductions in spine density in these parts. Intriguingly, these areas have also been associated with functions which are perturbed in SCZ. For example, the dorsolateral prefrontal cortex (DLPFC) is critical for working memory function and schizophrenic individuals show reduced activity of this region during working memory tasks. Spine loss in the DLPFC has been

reproducibly reported, particularly in layer 3 neurons[54]. Moreover, there is also a profound reduction in spine density on pyramidal neurons in the primary auditory cortex, which could explain why schizophrenics suffer from auditory hallucinations[55]. Finally, reductions in hippocampal volume and reduced spine density on CA3 dendrites in SCZ[56, 57] could be the physiological reason why patients have problems with memory and spatial learning. Collectively, these studies reveal strong associations between brain region-specific loss of gray matter, reduced spine density and functional hypoactivity in SCZ.

Dysfunction of DLPFC inhibitory PV+ basket cells is also thought to play a major role in SCZ's working memory deficits. Coordinated firing of DLPFC pyramidal cells at the gamma frequency between a stimulus cue and behavioral response is essential for accurate working memory and relies largely on fast spiking PV+ GABAergic interneurons[58]. For example, PV+ neurons in the monkey DLPFC are active during the delay period of working memory tasks[59], and are responsible for spatial tuning of neuronal responses during this period[60]. In addition, injection of GABA antagonists into the DLPFC disrupts working memory[61]. Fittingly, gamma-frequency oscillations are abnormal in the prefrontal cortex of patients with SCZ who are performing working-memory tasks[45, 62, 63]. Interestingly, multiple postmortem studies have reproducibly found lower levels of PV+ mRNA and GAD67, the principal synthesizing enzyme for GABA, in DLPFC PV+ neurons, but found the absolute number of PV+ cells unchanged, suggesting a functional rather than a numerical deficit[64, 65]. Furthermore examination of PV+ chandelier axon terminals[66] revealed selective reduction of GAT1 - a GABA reuptake transporter - and upregulated levels of the GABAA receptor α2 subunit in the axon initial segments of pyramidal neurons, possibly as a compensation to the lowered GABA levels[67]. In conclusion, these findings suggest hyper-

excitability and gamma wave disruption in particular brain regions can be etiological contributions of SCZ.

## 1.4. Neuropathological features of ASD

Early brain overgrowth and neuronal hyperexcitability are two well-established phenotypes in ASD[68, 69]. About 25–30% of autistic children experience excessive increase in brain size between the first and second year of life when compared with healthy controls[70] while 30% struggle with epilepsy[71]. One possible biological mechanism connecting the two phenotypes is increased spine density, as recent evidence examining post-mortem ASD human brain tissue revealed an increase in spine density on apical dendrites of pyramidal neurons from cortical layer 2 in frontal, temporal and parietal lobes and layer 5 in the temporal lobe[14]. Furthermore, these trends are also observed in tissue from individuals with diseases co-morbid with autism. For instance, the fragile X brain is characterized by macrocephaly, elevated spine density and elongated, tortuous spine morphologies[72]. However, other studies have revealed contradicting findings: several case studies have found smaller neurons and simplified dendrite morphology in the limbic system, consistent with a curtailment of developmental maturity[73, 74]. While these discrepant results must be taken with caution due to lack of large samples (only around 120 postmortem ASD brains have been studied since 1980) and closely matched control groups[75], they also suggest a degree of heterogeneity in the autistic brain, which may be due to brain-region dependent changes caused by alterations in region-specific genetic factors[76]. Indeed, fMRI studies have consistently reported patterns of long-distance “under connectivity” with short-range “over connectivity” in brains of ASD adult patients[77].

Evidence for alterations in GABAergic circuits in ASD also come from postmortem studies showing significantly reduced GAD65/GAD67 levels in the parietal cortex and cerebellum[78, 79] and alterations in GABAA and GABAB receptors in postmortem brains of autistic subjects[80-82]. These alterations may be the result of widespread changes in GABA innervation and/or release, which may lower the threshold for developing seizures, given the high co-morbidity of ASD and epilepsy[83]. In support of this hypothesis, another study showed that ASD patient brains had lower numbers of PV+ interneurons in the prefrontal cortex[84]. As PV+ interneurons provide strong perisomatic innervations of pyramidal cells, a reduction in its absolute number could explain the aberrant GABAergic transmission and predisposition for epileptic symptoms in autism[85]. Together, these results suggest heterogenous changes in glutamatergic and GABAergic systems in the ASD brain can converge upon an overall increased ratio of excitation/inhibition, which can manifest in epileptic symptoms, macroscopic changes in brain volume, and behavioral alterations.

## 1.5. *CNTNAP2* mutations are associated with complex mental disorders

### 1.5.1. Syndromic genes provide key insights into disease pathophysiology

Abnormalities in synapses and dendrites of excitatory and inhibitory neurons have emerged as key cellular substrates in the pathogenesis of several psychiatric disorders, including ASD, ID, and SCZ[2]. Indeed, disease-specific disruptions in dendritic architecture and synaptic morphology or number accompany a large number of brain disorders, suggesting that such alterations may serve as common substrates for many neuropsychiatric disorders, particularly those that involve deficits in information processing[86]. It has been proposed that different mutations within a gene, in concurrence with environmental context and gene/gene interactions[87], can lead to a spectrum of clinical outcomes[88]. As a result, understanding how individual genetic disruptions impact the

system in is critical but difficult. How can we ascertain, especially in disorders with polygenic causes, which genetic disturbances are the most profound and upon which substrates they act?

In a subset of cases, alterations of a single gene can lead to syndromic disease. For example, mutations in *TSC1*/*TSC2* and *FMRP* are respectively causative for tuberous sclerosis complex and Fragile X syndrome – two distinct forms of syndromic autism. Dedicated functional research have shown dendritic spine pathology as a common convergence point of both genes, leading to investigation of mTOR signaling and mRNA regulation as potential ASD mechanisms[2]. Investigation of monogenic disorders with psychiatric features, therefore, have tremendous potential to uncover shared pathways implicated in complex mental disorders.

### 1.5.2. *CNTNAP2* as a monogenic disease gene

Genetic studies over the past decade have reproducibly associated *CNTNAP2* mutations and variants with ASD[89-92], SCZ[93, 94], ID[95], as well as an array of other diseases and co-morbidities, including attention deficit hyperactivity disorder (ADHD)[96], Tourette's syndrome[97], Pitt-Hopkin's syndrome[98], language impairment[99, 100] and epilepsy[94]. Many of the initial reports of disease association were from patients exhibiting complex symptomology that harbored large chromosomal translocations or deletions, making it difficult to pinpoint the genetic culprit behind reported endophenotypes[90, 101]. However, clinical cases of patients with similar symptomology but micro-deletion or point mutations specifically on the *CNTNAP2* gene locus soon emerged, suggesting at least some of the deficits could be directly related to CNTNAP2[89, 95]. Conflictingly, however, reports demonstrating the presence of heterozygous mutations in normal populations have also been published[102, 103], suggesting *CNTNAP2* homozygous

mutations may be highly penetrant.

Strength for this theory came in a landmark genetic study on an Old Order Amish family: several proband members harbored a co-segregating homozygous nucleotide deletion that resulted in premature termination of the CNTNAP2 protein, causing a truncated and supposedly non-functional version to be produced[104, 105]. The afflicted patients suffered from a wide range of issues, such as epilepsy, severe ID, autistic traits, and motor delays; moreover, the majority of these patients suffer from language issues, ranging from verbal regression to the total absence of speech. Since this initial discovery, several other independent cohorts, all harboring the same eclectic range of issues, have been reported[98, 106-109]. Interestingly, while almost all such cases possess bi-allelic genetic deletions, there are no consistent patterns of perturbation. Cases range from premature termination near the N-terminus to seemingly arbitrary deletions of several exons within the extracellular region[106]. These data suggest the diverse group of homozygous mutations may simplify nullify the overall function of the protein.

Indeed, thorough characterization of the *Cntnap2* KO mouse revealed many of the same core behavioral abnormalities, including autistic-like behavior, seizures, and cortical dysplasia[110]. Together, it appears total CNTNAP2 loss is causative for a syndromic constellation of symptoms, now termed cortical dysplasia focal epilepsy (CDFE), and that heterozygous *CNTNAP2* variants have lower and more variable individual burdens on protein function and disease pathophysiology. These differences also highlight the validity of using the KO model as a legitimate disease model.

### 1.5.3. CNTNAP2's expression patterns

CNTNAP2 is highly expressed throughout the central nervous system, with highest expression in the frontal and anterior lobes, striatum and dorsal thalamus[111], which recapitulates the corticostriato-thalamic circuitry known to control higher order functions such as. Relatedly, CNTNAP2 is also highly enriched in perisylvian regions of the human brain[112] – a region involved in speech – with these expression patterns highly conserved in homologous areas in lower species[113]. In additional, CNTNAP2 is highly expressed embryonically in the medial ganglionic eminence, suggesting its possible roles in both interneuronal function and migration[110].

From a temporal perspective, a study utilizing a CNTNAP2-LacZ knock-in reporter model showed CNTNAP2 to be first expressed perinatally around the brainstem region and slowly increasing through adulthood, progressing to the midbrain and forebrain in a posterior to anterior pattern. In the cortex, expression is first detected in the marginal zone at P0 and gradually migrates into deeper layers over the next two weeks[114].

### 1.5.4. CNTNAP2's known molecular mechanisms

CNTNAP2 is a neurexin superfamily member with a single pass transmembrane structure characteristic of type-I CAMs. The majority of its domains – four laminin G (LamG), two epidermal growth factor-like (EGF), one discoidin homology (Discoidin), and one fibrinogen-like (FBG-like) domains – are located within the extracellular region. Intriguingly, the C-terminus is one of the smallest within the neurexin superfamily, harboring enough space for only one 4.1B and one PDZ type II binding site (Fig 1.3).

Extracellularly, CNTNAP2 participates in cell-cell adhesions, particularly with its canonical binding partner CNTN2 (TAG-1)[115]. This particular interaction process is critical for several developmental features, including migration[116], the maintenance of axo-glial integrity in axons[115], and clustering of Kv1.1 potassium subunits[115]. In accordance, *Cntnap2* KO mice exhibit migration deficits (ectopic neurons within the corpus callosum), possess axon excitability defects[117], and have deficits in potassium channel clustering at the axonal juxtaparanodes[117]. Recent studies have also surprisingly shown a strong interaction with CNTN1, albeit with unknown consequences[118]. A recent proteomics study showed CNTNAP2 to complex with several members of the transmembrane ADAM family (ADAM11, ADAM2, and ADAM 23) and the secreted ligand LGl1[79]. Because ADAM22 and LGl1 interact[119] and are involved with potassium channel trafficking[120, 121], while antibodies to CNTNAP2 and LGI1 have been found in several autoantibody-mediated neurological diseases[122], these candidates are likely components of the voltage-gated potassium channel (VGKC) complex. Whether these members bind directly or are bridged by other proteins is unknown.

While literature regarding extracellular interactions partners have been generally scarce, intracellular interactors are more developed. The 4.1B binding site, via its interaction with Protein 4.1B[123], is essential for clustering potassium channels (Kv1 family) at the juxtaparanodes areas of myelinated nerves[124]. This may be in response to upstream extracellular interactors like TAG-1, but this idea has not been explored fully. The PDZ binding site scaffolds a wide array of PDZ proteins, including DLGs, MAGUKs, and MUPP1 [125-127]. Thus far, it has been shown that the PDZ binding site can bring MAGUKs to the membrane surface[126] but is also responsible for enriching CNTNAP2 at the axon initial segment, along with the recruitment of MPP2 to the same position[128].

The presence of several ICD phosphorylation sites suggest the C-terminus is involved with protein signaling. The only characterized site is a threonine at 1292 – a protein kinase C target responsible for selective endocytosis and sorting of CNTNAP2 between the axon and dendrite[129]. Proteomic searches reveal phosphorylation at serines 1303 and 1306 as well[130], but their functions are unknown.

### 1.5.5. CNTNAP2's role in E/I balance

Recent evidence suggests CNTNAP2 regulates neural networks through E/I balance. CNTNAP2 knockdown led to decreases in dendrite arborization, impaired excitatory and inhibitory transmission in mouse cortical neurons, and impaired spine size[131]. *Cntnap2* KO mice have reduced numbers of PV+ GABAergic interneurons, as well as neuronal synchrony defects, epileptic seizures, and altered social behavior[110]. Similarly, Drosophila with *NrxnIV* (homologue of *CNTNAP2*) KO have axon path-finding defects[98], while a zebrafish KO model also showed strict changes in GABAergic, but not glutamatergic neurons[132]. Thus, CNTNAP2 loss may lead to specific impairments in excitatory synapses as well as focused reductions in the interneuron population, particularly the PV+ subtype, resulting in a hyper-excitable network that promotes downstream epileptic symptoms and behavioral abnormalities. Interestingly, the mouse's social deficits can be rescued with optogenetic stimulation of PV+ interneurons[133] while Vogt et al. has shown the decreased KO PV density is due to a maturation problem rather than a migration one[134]. Thus further work needs to be done to dissect the relationships of these phenotypes to one another as well as to further tease apart the cellular and neurobiological effects of CNTNAP2 loss on neural network.

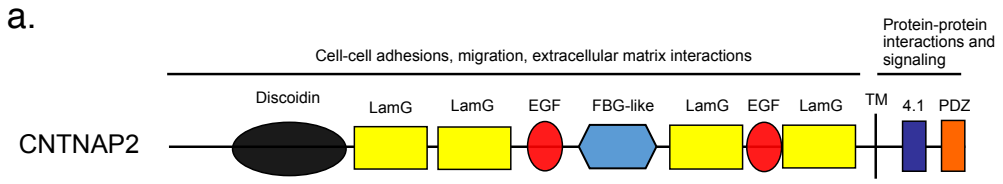


**Figure 1.3. Domain structure of the CNTNAP2 protein.** (a) CNTNAP2 is a single-pass transmembrane CAM. Most of the CNTNAP2 protein is located extracellularly, consisting of four LamG domains, two EGF domains, one Discoidin homology domain, and one FBG-like domain. These sites are predicted to be critical for CAM-to-CAM adhesions, migration, and extracellular matrix interactions. The small intracellular tail has a 4.1B (4.1) binding region and a type II PDZ-binding (PDZ) region at the tail end of the C-terminus, predicted to be involved with protein-protein interactions and signal transduction.

# CHAPTER 2: Characterization of CNTNAP2 interactors

## 2.1. Background

CNTNAP2 is a CAM highly expressed in both the central and peripheral nervous system. Structurally, it is a single-pass CAM, with a large extracellular region (94.6% of the whole protein) predicted to be involved with cell-to-cell adhesions[106] (Figure 1.3). Intracellularly, CNTNAP2 has a small C-terminus harboring a 4.1B and a PDZ-type II binding site, with the former likely to be involved in actin cross-linking[123, 135] and the latter with MAGUK protein recruitment[126, 136]. Surprisingly, despite CNTNAP2's association with a multitude of neuropsychiatric diseases, mechanistic studies are relatively lacking, likely because the largely extracellular topography makes functional investigations difficult. Several proteomic studies, however, have been performed but with no follow-up investigations[125, 137].

From the few molecular studies available, it appears CNTNAP2's extracellular and intracellular interactions are tightly connected to regulate function. For example, CNTNAP2's axon distribution patterns are determined via a region involving the second laminin G/first EGF domains as well as via its C-terminal PDZ-binding domain[136]. Similarly, axonal targeting is influenced by phosphorylation of its cytoplasmic tail by protein kinase C[129], and a ASD-associated mutation (D1129H) of a conserved extracellular amino acid abrogates surface trafficking[105]. Once at the axon, CNTNAP2 interacts with extracellularly with TAG-1 at the axon juxtaparanodes, an association that leads to the recruitment of potassium channels[115] via intracellular recruitment of the cytoskeletal structural protein 4.1B[137].

Here, we add to the burgeoning CNTNAP2 interactome by performing yeast-two hybrid to determine and validate candidate CNTNAP2 interactors. Our work may improve the underlying

comprehension of CNTNAP2 physiology, which will be critical for understanding its molecular mechanism in physiological and pathophysiological states.

2.2. Validation of CNTNAP2 C-terminal bait for yeast-two hybrid

We performed a yeast two-hybrid screen with the entire CNTNAP2 intracellular C-terminus domain (ICD) as bait (amino acids 1284-1331) to find potential intracellular interactors (Figure 2.1a; black line). We chose this region because it is the only intracellular part of the CNTNAP2 protein. After cloning the CNTNAP2 ICD into the pGBTK7 bait vector, we tested its expression in yeast by probing western blots of transformed yeast lysates with both the C-terminal (Millipore) and N-terminal (Neuromab) CNTNAP2 antibodies. The C-terminal, but not the N-terminal, antibody specifically detected a band of the appropriate size in the pGBKT7-ICD lane. Neither antibody gave a signal with yeast lysates transformed with other negative controls (pGBKT7-p53, empty vector, and non-transfected) (Figure 2.1b), suggesting specific in-frame expression.

We then tested the construct for toxicity by plating transformed yeast on SD-Trp plates, which is selective for yeast expressing pGBTK7 vector (contains a Trp-synthesizing cassette). After 4 days of expression, pGBKT7-ICD yeast colonies did not have noticeable morphological differences from yeast expressing pGBKT7-empty or pGBKT7-p53 colonies, providing evidence the CNTNAP2 ICD bait is not toxic to yeast (Figure 2.1c).

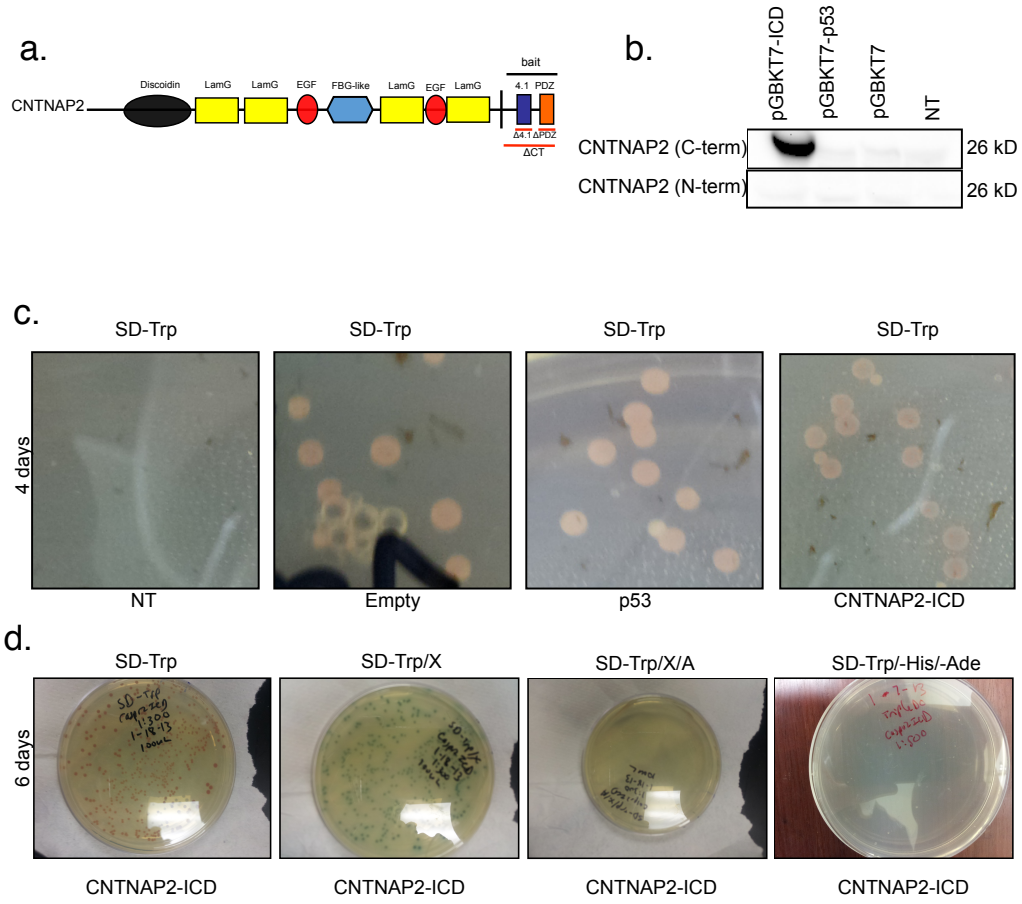


**2.1. Quality control tests for CNTNAP2 ICD bait.** (a) Schematic cartoon of CNTNAP2 domains. Black line indicates the bait region in yeast two-hybrid screening, while red lines indicate the various CNTNAP2 truncations used for domain mapping experiments. (b) Western blotting of yeast lysate expressing CNTNAP2 ICD (pGBKT7-ICD). Probing with a CNTNAP2 C-terminal antibody, but not an N-terminal antibody, reveals a positive band of the appropriate size only for the pGBKT7-ICD samples, but not for another bait (pGBKT7-p53), empty vector (pGBKT7), or non-transfected controls (NT). (c) Yeast transformed with pGBKT7-ICD grown for 4 days on SD-Trp plates revealed no morphological abnormalities relative to yeast transformed with pGBKT7-p53 or pGBKT7 alone. (d) Yeast transformed with pGBKT7-ICD grown for 6 days in SD-Trp/X plates revealed blue colonies, suggesting X-gal auto-activity. Growth on higher stringency plates (SD-Trp/X/A and SD-Trp/-His/-Ade), however, inhibited growth completely.

Finally, we tested for pGBKT7-ICD auto-activity by growing transformed pGBKT7-ICD yeast on selection plates of varying stringencies, all of which require a genuine bait-prey interaction for normal growth. After 6 days of expression, we found pGBKT7-ICD transformed yeast colonies turned blue when grown in X-α-galactosidase media (SD-Trp/X), suggesting the ICD bait has auto α-galactosidase activity. We also checked other types of auto-activity by growing yeast transformed with pGBKT7-ICD onto X-α-galactosidase and aurobasidin-A spiked media (SD-Trp/X/A) or high stringency triple dropout media (SD-Trp/-His/-Ade), neither of which resulted in the growth of any colonies (Figure 2.1d). Taken together, this suggests pGBKT7-ICD transformed yeast is not toxic and does not display auto-activation in the highest stringency conditions required for determining genuine bait-prey interactions, making the construct suitable for the subsequent screen.

## 2.3. List of CNTNAP2 interactors

We mated pGBKT7-ICD yeast with a prey mouse cDNA brain library (Clontech), allowing for the screening of three million candidates. From the screen, we derived 41 unique in-frame prey (Figure 2.2) that, when co-expressed with bait, successfully grew on the highest stringency plates (-Trp/-Leu/-His/-Ade + X-α-Gal + aurobasidin-A, or QDO/X/A). In an effort to find the best candidates for further study, we used several criteria to rate the confidence of each hit: 1). number of duplicates 2). likelihood of being a common proteomic contaminant (i.e. ribosomes)[138], 3). rationality of the interaction (i.e. proteins not found in the membrane or cytosol were disregarded, while the presence of either FERM or PDZ domains[123, 139] were preferred). From these considerations, we thus decided to focus specifically on three PDZ-domain candidates: PARD3, CASK, and MPP6. While HtRA1 also had a PDZ domain and was

highly represented in the screen, we did not deem it a logical candidate to study because multiple reports suggested it is a secreted protease and thereby highly unlikely to have a stable intracellular relationship with CNTNAP2[140, 141].

2.4. Validation of CASK as a CNTNAP2 interactor

CASK is a MAGUK molecule that is highly expressed in the brain and is involved with multiple neuronal functions, including dendritic spine maintenance, transcription, cargo transport, and presynaptic release[142]. CASK has a CaMK-like domain, two L27 domains, a PDZ domain, a SH3 domain, and a GK domain, while a 4.1B hook motif lies between the latter two (Figure 2.3a). Like other traditional MAGUKs, the L27 and PDZ domains serve as the primary sites for protein recruitment[143, 144]. However, CASK also has some peculiar functions not observed in other MAGUK members: the ability to traverse to the nucleus via the GK domain[145] and ion-sensitive kinase activity with the CaMK-like domain[146]. Genetically, CASK is associated with X-linked mental retardation[142], with its ablation being embryonically lethal in mouse models[147], thus making it an interesting, disease-relevant molecule to study.

To validate the yeast data, we tested whether CNTNAP2 and CASK participated in common protein complexes in native mouse brain tissue by co-immunoprecipitating and reverse co-immunoprecipitating CNTNAP2 with CASK (Figure 2.3b-c). To determine the domains of each protein involved in the interaction, we co-expressed individual domain truncations of CNTNAP2 with CASK in HEK293T cells and performed co-immunoprecipitations. We found that the C-terminal PDZ-binding motif of CNTNAP2 interacted with CASK, as the deletion mutant could

| Gene | Function | Hits |
|---|---|---|
| ATP1B1 | Na+/K+ Pump | 20+ |
| BCR | GTPase | 1 |
| BPGM | Controls oxygen affinity in RBCs | 1 |
| CACYBP | Calcium-dependent ubiquitination | 1 |
| CASK | MAGUK | 4 |
| CIRBP | Cellular stress response | 1 |
| CKAP5 | Spindle formation | 2 |
| CNOT7 | Cell proliferation | 2 |
| CNRIP1 | Cannabinoid signaling | 6 |
| COPS5 | Ubiquitination regulation | 3 |
| CUL1 | Uibiquitination regulation | 1 |
| DUS4L | tRNA synthesis | 1 |
| EPRS | tRNA synthesis | 3 |
| FARSB | tRNA synthesis | 2 |
| FLNB | Actin cytoskeleton network | 1 |
| HNRPLL | T-cell development | 1 |
| HSPA5 | Heat shock response | 1 |
| HTRA1 | Serine protease | 20+ |
| IMMT | Mitochondria morphology | 1 |
| KAL1 | Neuronal cell-adhesion | 1 |
| KIAA0528 | Glucose transport | 1 |
| KIAA1755 | Unknown function, has Sec14 domain | 1 |
| KRT222 | Unknown function | 2 |
| LYSMD2 | Unknown function | 2 |
| MARCKSL1 | Protein kinase C signaling | 1 |
| MPP6 | MAGUK | 4 |
| N4BP2L2 | Unknown function | 1 |
| PARD3 | Polarized growth | 1 |
| PCCA | Metabolism | 1 |
| PCNA | DNA replication | 2 |
| PGM1 | Metabolism | 7 |
| POLR2B | RNA synthesis | 2 |
| POMP | Degradation | 3 |
| PRRG3 | Function unknown | 1 |
| RPRD2 | RNA processing | 1 |
| RPS20 | Ribosome function | 2 |
| RSL24D1 | Ribosome function | 3 |
| STX8 | SNARE complex | 1 |
| TCTN1 | Embryonic development | 1 |
| ZNF410 | Transcripton factor | 1 |

**Figure 2.2. List of hits from the Yeast two-hybrid screen.** Table displaying all of the unique prey that, when co-expressed with the CNTNAP2 ICD bait in yeast, resulted in the formation of blue-colored colonies on the highest stringency media plates (SD-Leu/-Trp/-His/-Ade/X/A). Gene identity, protein function, and number of duplicate clones for each prey are listed. The prey highlighted in red indicate ones containing PDZ domains.

not immunoprecipitate CASK (Figure 2.3d). Reverse co-immunoprecipitations using CASK truncations were unsuccessful (data not shown), so we used PLA, a recently-developed antibody and DNA-based technique that produces fluorescence signal only when two target proteins are within close proximity (<40 nm) of each other (Figure 2.3e). We found that CNTNAP2 and CASK interacted near the plasma membrane when co-expressed in HEK293T cells; this interaction was dependent on CASK's PDZ domain (Figure 2.3f), as deletion of this region caused a significant reduction of PLA signal area (CNTNAP2 + CASK: 0.2713 ± 0.04 $\mu m^2$ vs. CNTNAP2 + CASKΔPDZ: 0.1586 ± 0.02 $\mu m^2$; Figure 2.3f).

2.5. Validation of PARD3 as a CNTNAP2 interactor

PARD3, along with PARD6 and aPKC, form a conserved protein complex that controls cell polarity by serving as a positional landmark to spatially regulate guanine nucleotide exchange factors (GEFs) like TIAM1 to control small GTPase signaling. This process has been shown to be critical for axon specification, synaptogenesis, polarized astrocyte migration, asymmetric cell division, and the establishment of apical-basal polarity in epithelial cells[148]. PARD3 contains a CR1 domain, three PDZ domains, and an aPKC binding site.

The PARD3 prey's insert sequence comprises the entire second and two-thirds of the third PDZ domain, suggesting a PDZ interaction with CNTNAP2 ICD (Figure 2.4a; black lines). To validate this hypothesis, we first confirmed that CNTNAP2 and PARD3 are in the same protein complex *in vivo* by co-immunoprecipitation experiments in mouse cortices (Figure 2.4b). We then co-expressed myc-PARD3 with either full-length FLAG-CNTNAP2 or various truncations (see Figure 2.1a; red lines for truncations) in HEK293T cells and performed a co-

a.

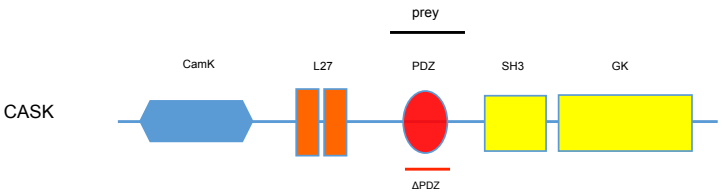
prey
CamK
L27
PDZ
SH3
GK
CASK
ΔPDZ

b.

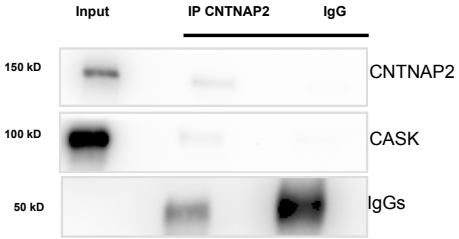
Input
IP CNTNAP2
IgG
150 kD
CNTNAP2
100 kD
CASK
50 kD
IgGs

c.

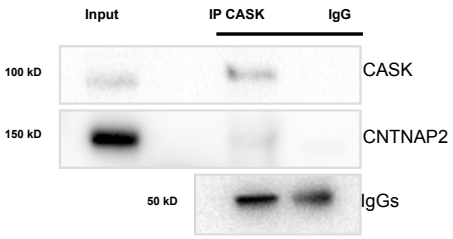
Input
IP CASK
IgG
100 kD
CASK
150 kD
CNTNAP2
50 kD
IgGs

d.

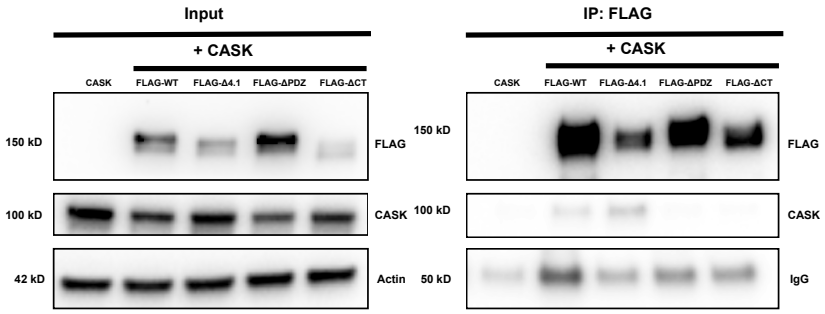
Input
+ CASK
CASK
FLAG-WT
FLAG-Δ4.1
FLAG-ΔPDZ
FLAG-ΔCT
150 kD
FLAG
100 kD
CASK
42 kD
Actin
IP: FLAG
+ CASK
CASK
FLAG-WT
FLAG-Δ4.1
FLAG-ΔPDZ
FLAG-ΔCT
150 kD
FLAG
100 kD
CASK
50 kD
IgG

e.

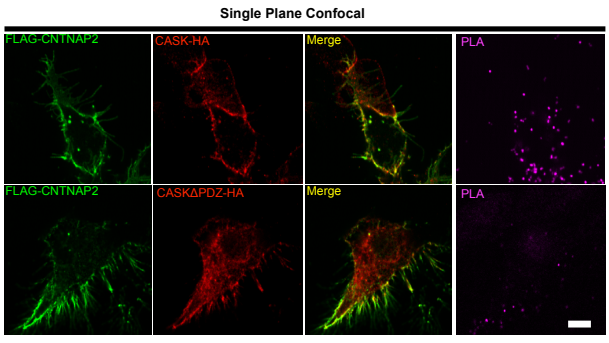
Single Plane Confocal
FLAG-CNTNAP2
CASK-HA
Merge
PLA
FLAG-CNTNAP2
CASKΔPDZ-HA
Merge
PLA

f.

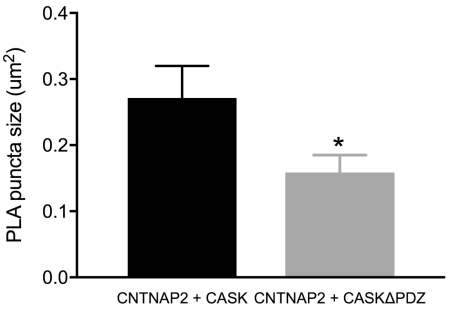
PLA puncta size (um2)
0.4
0.3
0.2
0.1
0.0
*
CNTNAP2 + CASK
CNTNAP2 + CASKΔPDZ

**Figure 2.3. Characterization of CNTNAP2-CASK interaction.** (a) Schematic cartoon of CASK domains. Black line indicates region encoded by the prey clone while the red line indicates the truncation mutant used for interaction verification. (b-c) Cropped western blots of co-immunoprecipitation experiments with CASK and CNTNAP2 in mouse cortex. (d) Cropped western blots showing co-immunoprecipitation of various FLAG-CNTNAP2 truncation mutants (2.1a; red lines) with untagged, full-length CASK in HEK293T cells. (e) Co-expression of FLAG-CNTNAP2 and CASK-HA or CASKΔPDZ-HA in HEK293T cells and the resulting PLA interaction profiles (scale bar = 5 μm). (f) Quantification of (e) for PLA puncta size (CNTNAP2 + CASK: n = 19 cells from 3 independent experiments; CNTNAP2 + CASKΔPDZ: n = 16 cells from 3 independent experiments). Values are means ± SEM. * P≤0.05; Mann-Whitney test (f).

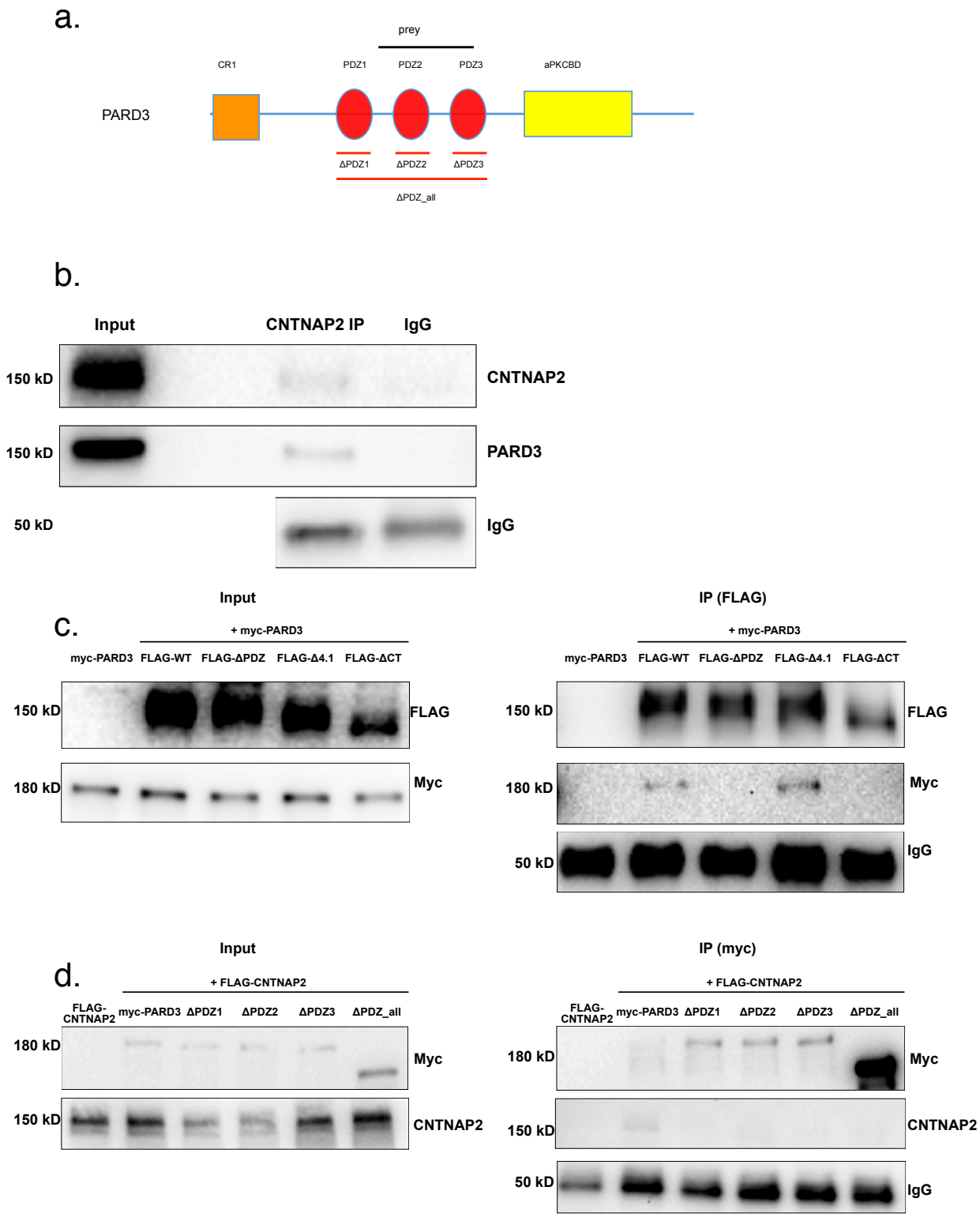
a.
prey
CR1
PDZ1
PDZ2
PDZ3
aPKCBD
PARD3
ΔPDZ1
ΔPDZ2
ΔPDZ3
ΔPDZ_all
b.
Input
CNTNAP2 IP
IgG
150 kD
CNTNAP2
150 kD
PARD3
50 kD
IgG
c.
Input
IP (FLAG)
+ myc-PARD3
myc-PARD3
FLAG-WT
FLAG-ΔPDZ
FLAG-Δ4.1
FLAG-ΔCT
150 kD
FLAG
180 kD
Myc
50 kD
IgG
d.
Input
IP (myc)
+ FLAG-CNTNAP2
FLAG-CNTNAP2
myc-PARD3
ΔPDZ1
ΔPDZ2
ΔPDZ3
ΔPDZ_all
180 kD
Myc
150 kD
CNTNAP2
50 kD
IgG

**Figure 2.4. Characterization of CNTNAP2-PARD3 interaction.** (a) Schematic cartoon of PARD3 domains. Black line indicates region encoded by the prey clone while the red line indicates the truncation mutant used for interaction verification. (b) Representative western blot demonstrating PARD3 co-immunoprecipitation with CNTNAP2 in mouse cortex. (c) Western blots showing co-immunoprecipitation of various FLAG-CNTNAP2 truncation mutants with myc-tagged full-length PARD3 in HEK293T cells. (d) Western blots showing co-immunoprecipitation of various myc-PARD3 truncation mutants with FLAG-tagged full-length CNTNAP2 in HEK293T cells.

immunoprecipitation experiment. We showed that while CNTNAP2 full-length and Δ4.1B co-immunoprecipitated with PARD3, ΔPDZ and ΔCT mutants did not (Figure 2.4c). Conversely, ablation of any or all of PARD3's three PDZ domains (Figure 2.4a; red lines) surprisingly resulted in a reduction of CNTNAP2 co-immunoprecipitation efficiency (Figure 2.4d). From this result, we concluded that CNTNAP2's PDZ-binding domain can interact with multiple PARD3 PDZ domains[149]. These data suggest PARD3 is a genuine CNTNAP2 interactor, and that this interaction occurs through PDZ binding.

## 2.6. Validation of MPP6 as a CNTNAP2 interactor

MPP6 is a MAGUK known to be targeted to the peripheral membrane by protein 4.1G in myelinated nerves[150], where it interacts with and localizes the kinase Src[151]. In addition, MPP6 can interact with Veli-[152], an adaptor protein responsible for basolateral localization of LET-23 kinase receptor[153]. MPP6 has two L27, a PDZ, a SH3, and a GK domain, with the prey's insert falling conveniently within the PDZ domain (Figure 2.5a, black lines)

Because the literature on MPP6 was scarce, we only validated that CNTNAP2 and MPP6 participated in common protein complexes in native mouse brain tissue by co-immunoprecipitating CNTNAP2 with MPP6 (Figure 2.5b).

## 2.7. Discussion

The cytosolic C-terminus of CAMs are critical for transducing extracellular events into intracellular signaling and thus play an important role in function[154]. Despite being linked to multiple neuropsychiatric disorders, CNTNAP2's molecular mechanisms have not been well

characterized. Here, we use yeast-two hybrid to expand upon the interaction network for CNTNAP2's ICD. Our results show the CNTNAP2 ICD interacts mainly with adaptor scaffolds responsible for organizing protein-protein interactions. This idea is further supported by several proteomic studies demonstrating CNTNAP2 forming complexes with MAGUKs (DLGs and MPPs) and LGI family members[125]. Our results suggest interaction with multiple PDZ proteins may be localizing different scaffolds, and in turn different downstream signaling modules, to the plasma membrane surface. For example, PARD3 is part of PAR polarity complex, and can localize Rac and Cdc42 signaling through TIAM1 and PARD6 respectively[155, 156]. Thus, with CNTNAP2's abundance in synapses[157], plasma membrane[126], and lipid rafts[125], CNTNAP2 may be spatially restricting Rac/Cdc42 signaling to specific surface locations within the cell, a precise process necessary for proper development[148].

CNTNAP2's recruitment of PARD3-TIAM1/PARD6 is also topologically feasible; CNTNAP2 binds PARD3 via the PDZ domains (Figure 2.4), while PARD3 binds directly to TIAM1 via its carboxy-terminal region[158] and to PARD6 through its conserved N-terminal region[156]. Similarly, other CAMs have been predicted to bind PARD3[159, 160], while their knockdown has been shown to dysregulate PARD3 and TIAM1[159], while disruption of these processes ultimately disrupt Rac/Cdc42 signaling[155, 156, 159, 161]. The rational next step, therefore, would be first to explore the localization relationship between CNTNAP2 and PARD3, and second, to determine if CNTNAP2 can regulate Rac/Cdc42 through PARD3-TIAM1. Our preliminary data shows that CNTNAP2 can co-immunoprecipitate TIAM1 in HEK293T cells; CNTNAP2 overexpression can also induce the formation of filopodia in COS7 cells (data not shown). Rac/Cdc42 activity assays and phallodin-staining, as well as PARD3/TIAM1 knockdown

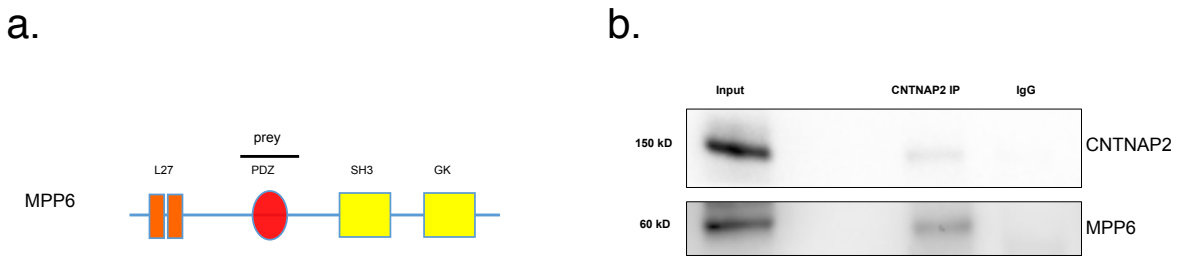


**Figure 2.5. Characterization of CNTNAP2-MPP6 interaction.** (a) Schematic cartoon of MPP6 domains. Black line indicates region encoded by the prey clone. (b) Cropped western blots of co-immunoprecipitation experiments with MPP6 and CNTNAP2 in mouse cortex.

experiments would be critical to determine if these results are linked to a PARD3-associated pathway.

CASK has been documented to interact with SAP97 via L27 binding to transport NMDARs and AMPARs to the cell surface[144, 162, 163], while SAP97 has been shown to affect dendrite arborization through GluA1[164]. Moreover, CASK's C-terminus can bind to protein 4.1N and translocate to the nucleus, leading to cytoskeletal stability and gene transcription regulation respectively [135, 145]. Interestingly, perturbation of CNTNAP2 has been shown to cause AMPAR trafficking deficits[157] and simplified dendritic branching deficits in pyramidal neurons[131]. Collectively, CASK, as a multi-purpose scaffold, may be the downstream molecule responsible for several of these characteristics in CNTNAP2-deficient neurons. Thus, spatiotemporal control of CNTNAP2's ICD interactions may result in downstream events with different consequences.

Mutations in *CASK* and *PARD3* have been intimately linked with several neuropsychiatric disorders, including autism[165, 166], epilepsy[167], and mental retardation[142, 168]. Hence, elucidation of pathway functionality behind these interactions may uncover shared pathophysiological mechanisms in different diseases.

# CHAPTER 3: CNTNAP2 stabilizes interneuron dendritic arbors through CASK

## 3.1. Background

GABAergic interneurons comprise only 20-30% of the entire cortical neuron population but play crucial roles in fine-tuning cortical circuit function through their abilities to control excitatory neuron activity[27]. As such, interneuron dysfunction has gained a prominent role in the pathogenesis of several neurodevelopmental diseases, such as ASD, SCZ, ID, and epilepsy. Indeed, post-mortem, electrophysiological, and cellular studies have all reported inhibitory-related structural and functional perturbations in these diseases[169]. Several alterations could account for these observations, including reduced interneuron cell density, impaired input/output function, and changes in dendritic arborization. While studies on the former two are abundant[88], interneuron morphology has not been carefully studied despite its necessity for proper brain function. Dendrites determine the extent of the cell's synaptic field, impact how it processes information, and ultimately are critical determinants of neural circuit integrity[170]; conversely, abnormal dendritic architecture can impact circuit function and contribute to pathogenesis[171]. The literature, albeit scarce at this point, provides some evidence of altered interneuron morphology in some neurodevelopmental disorders, including SCZ[172], epilepsy[173], and ID[174]. Cellular knowledge about interneuron dendrite morphogenesis is equally sparse, with only a handful of molecules documented as having roles in this process[175-178].

Gene dosage, rare mutations, and common variation in *CNTNAP2* have been associated with a range of neurodevelopmental disorders, including ID[98, 101], ASD[89, 90, 92, 111, 179], and SCZ[93, 94, 180], with afflicted patients often sharing features of mental retardation, autistic traits, seizures, and language impairment[106]. Additionally, homozygous loss-of-function in *CNTNAP2* via compound mutations/copy number variations (CNVs) is causative for CDFE, a syndrome involving epilepsy

and ID – both symptoms of chronic E/I imbalance[104, 107, 181]. These observations suggest that CNTNAP2 may be implicated in molecular and cellular pathways that regulate interneurons.

A role for CNTNAP2 in inhibitory neurobiological processes is supported by the presence of spontaneous seizures in *Cntnap2* KO mice beginning at 6 months[110]. Even before seizure onset, these mice show decreased GABAergic interneuron density[110], as well as alterations of synaptic function, abnormal network activity, and reduced inhibition[134, 182, 183]. Likewise, network analysis maps CNTNAP2 to modules involved in inhibitory transmission[110]. Moreover, CNTNAP2 auto-antibodies, which are present in autoimmune neurological disorders with seizures[184, 185], preferentially target inhibitory neurons[136]. While CNTNAP2 was first identified in the peripheral nervous system, where it clusters potassium channels at juxtaparanodes[124], it is also abundant in the brain and is embryonically expressed in the ganglionic eminences of the ventral telencephalon – the interneuronal birthplace[110]. These data are consistent with a role in interneuron development. Despite this, it is unclear how CNTNAP2 loss can alter inhibitory circuits.

Here we show that cultured *Cntnap2* KO mouse neurons exhibit an interneuron-specific simplification of the dendritic tree. SIM and STED super-resolution imaging techniques uncovered a novel correlation between nanoscale CNTNAP2 protein localization and dendrite arborization patterns. We show that these effects are mediated by the interaction of the CNTNAP2 C-terminus with CASK at the plasma membrane. Finally, we show that mature *Cntnap2* KO mice have reduced interneuron dendritic length/branching in specific brain regions and a decrease of CASK levels at the membrane. Our data reveal an interneuron-specific mechanism for dendrite stability mediated by the convergence between two ASD/ID risk genes, establish a previously undescribed

relationship between nanoscale protein localization and dendrite architecture, and provide a cellular mechanism for inhibitory circuit dysfunction in *CNTNAP2*-related disorders.

3.2. Mature *Cntnap2* KO neurons have an interneuron-specific deficit in dendrite arborization While behavioral deficits of *Cntnap2* KO mice have been thoroughly characterized, the cellular and molecular substrates underlying these deficits are less clear. To gain insight into the cellular roles of CNTNAP2, we employed *Cntnap2* KO neuronal cultures. To determine the optimal time-point for analysis, we examined CNTNAP2 protein levels in WT neuronal cultures. CNTNAP2 increased over 12-fold at 4 weeks compared to 1 week (1 week: 1 ± 0.3 vs. 4 weeks: 12.8 ± 2.8; Figure 3.1a-b). As this suggested a prominent role for CNTNAP2 later in postnatal development, we investigated its role at 4 weeks. Because dendrites constitute the receptive fields of neurons and are altered in multiple neurodevelopmental disorders[88], we compared dendritic architecture in *Cntnap2* WT vs. KO neurons. We transiently expressed GFP and used a GABA antibody as a marker to identify interneurons (Figure 3.1c). We found that KO interneurons had reduced total dendritic length (WT: 2144 ± 149.1 μm vs. KO: 1559 ± 111.1 μm) and arborization compared to WT (Figure 3.1d-e) at 4 weeks. Surprisingly, pyramidal dendrites were unaffected (WT: 3269 ± 110.8 μm vs. KO: 3307 ± 111.7 μm; Figure 3.1h-i). CNTNAP2 overexpression reversed this phenotype in interneurons (KO: 1564 ± 82.2 μm vs. KO + CNTNAP2 Ox: 1938 ± 89.7 μm; Figure 3.1f-g), while having no effect on pyramidal neurons (KO: 3038 ± 121.9 μm vs. KO + CNTNAP2 Ox: 2949 ± 115.9 μm; Figure 3.1j-k).

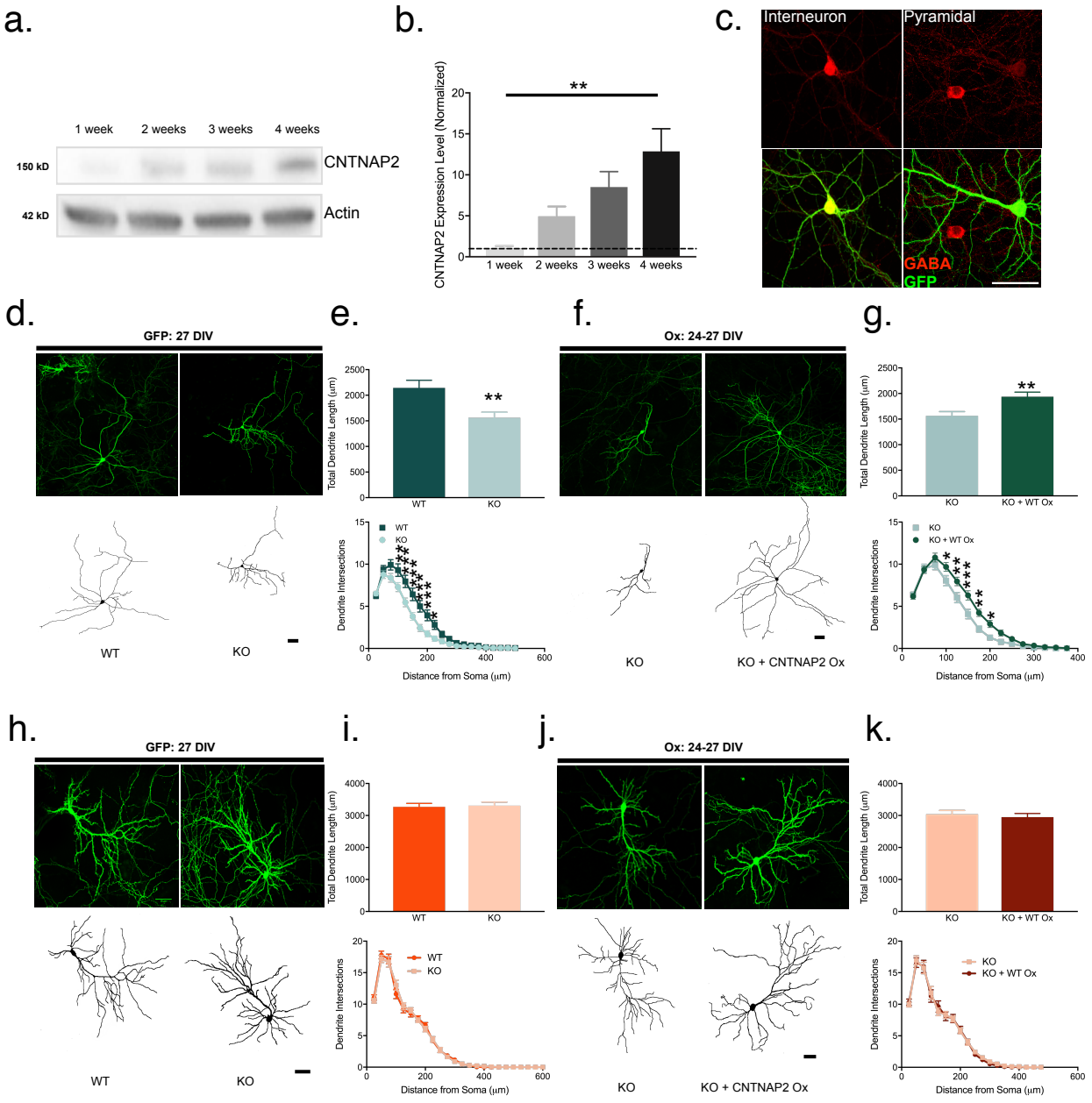
a.
1 week
2 weeks
3 weeks
4 weeks
150 kD
CNTNAP2
42 kD
Actin
b.
CNTNAP2 Expression Level (Normalized)
**
1 week
2 weeks
3 weeks
4 weeks
c.
Interneuron
Pyramidal
GABA
GFP
d.
GFP: 27 DIV
WT
KO
e.
Total Dendrite Length (μm)
**
WT
KO
Dendrite Intersections
Distance from Soma (μm)
f.
Ox: 24-27 DIV
KO
KO + CNTNAP2 Ox
g.
Total Dendrite Length (μm)
**
KO
KO + WT Ox
Dendrite Intersections
Distance from Soma (μm)
h.
GFP: 27 DIV
WT
KO
i.
Total Dendrite Length (μm)
WT
KO
Dendrite Intersections
Distance from Soma (μm)
j.
Ox: 24-27 DIV
KO
KO + CNTNAP2 Ox
k.
Total Dendrite Length (μm)
KO
KO + WT Ox
Dendrite Intersections
Distance from Soma (μm)

**Figure 3.1. *Cntnap2* KO interneurons have a cell-autonomous deficit in dendrite maintenance.** (a) Representative cropped western blot showing developmental time course of CNTNAP2 expression in cultured cortical neurons and (b) quantification (n = 3 independent experiments for each time point). (c) Immunostaining with a GABA antibody identifies inhibitory cells (left) but not pyramidal cells (right) (scale bar = 50 $\mu$m). (d) Representative images of GFP-expressing WT or KO mouse interneurons at 27 DIV (scale bar = 50 $\mu$m) and (e) quantification of total dendrite length and Sholl (WT: n = 43 cells from 5 cultures; KO: n = 55 cells from 6 cultures). (f) Representative images of 27 DIV KO mouse interneurons transfected (24-27 DIV) with GFP + pCS2-FLAG (KO) or GFP + FLAG-CNTNAP2 (KO + CNTNAP2 Ox) (scale bar = 50 $\mu$m) and (g) quantification of total dendrite length and Sholl (KO: n = 49 cells from 6 cultures; KO + CNTNAP2 Ox: n = 47 cells from 6 cultures). (h) Representative images of GFP-expressing WT and KO mouse pyramidal neurons at 27 DIV (scale bar = 50 $\mu$m), with (i) quantification of total dendrite length and Sholl (WT: n = 49 cells from 6 cultures; KO: n = 50 cells from 6 cultures). (j) Representative images of 27 DIV KO mouse pyramidal cells transfected (24-27 DIV) with GFP + pCS2-FLAG (KO) or GFP + FLAG-CNTNAP2 (KO + CNTNAP2 Ox) (scale bar = 50 $\mu$m) and (k) quantification (KO: n = 36 cells from 5 cultures; KO + CNTNAP2 Ox: n = 30 cells from 5 cultures). Values are means $\pm$ SEM. * P≤0.05, ** P≤0.01, *** P≤0.001; one-way ANOVA with Bonferroni's correction (b), Student's *t*-test (total dendrite length; k), Mann-Whitney test (total dendrite length; e, g, i), and two-way ANOVA with Bonferroni's correction (Sholl; e, g, i, k).

3.3. *Cntnap2* KO neurons show no defects in dendrite outgrowth

Such alterations in dendritic architecture could be caused by abnormal dendrite stabilization in mature neurons or impaired dendritic outgrowth in young neurons[186]. To distinguish between these alternatives, we analyzed dendrites in young neurons. We found no differences in dendrite length or arborization in inhibitory (WT: 891.8 ± 53.7 μm vs. KO: 987.9 ± 46.8 μm; Figure 3.2a-b) or excitatory neurons (WT: 935 ± 36.8 μm vs. KO: 880.9 ± 38.5 μm; Figure 3.2c-d) between WT and KO at this time. This suggests that absence of CNTNAP2 preferentially affects dendrite stabilization in more mature interneurons, and not dendrite outgrowth in young neurons.

3.4. CNTNAP2 Antibody and shRNA validation

To further test this hypothesis, and to determine whether the effects of CNTNAP2 loss were cell-autonomous, we decided to use shRNA. However, before any experiments could be performed, we first validated the efficacy of two commercial antibodies (mouse antibody from Neuromab and rabbit antibody from Millipore; see Methods) used in this study by staining *Cntnap2* WT and KO neurons. We found that staining intensity significantly decreased in the soma, dendrite, and axon in the KO neurons relative to the KO for both antibodies (Figure 3.3a-d). Both antibodies also successfully recognize full-length CNTNAP2 protein via western blotting in WT but not KO brain lysates (Figure 3.3e-f).

We then tested the knockdown strength of four CNTNAP2 shRNA hairpins by co-expressing them with full-length CNTNAP2 in HEK293T cells. Hairpin 1 (shRNA-1) led to the most robust decrease in CNTNAP2 protein levels (Figure 3.4a). Transfection of shRNA-1 into neuronal cells

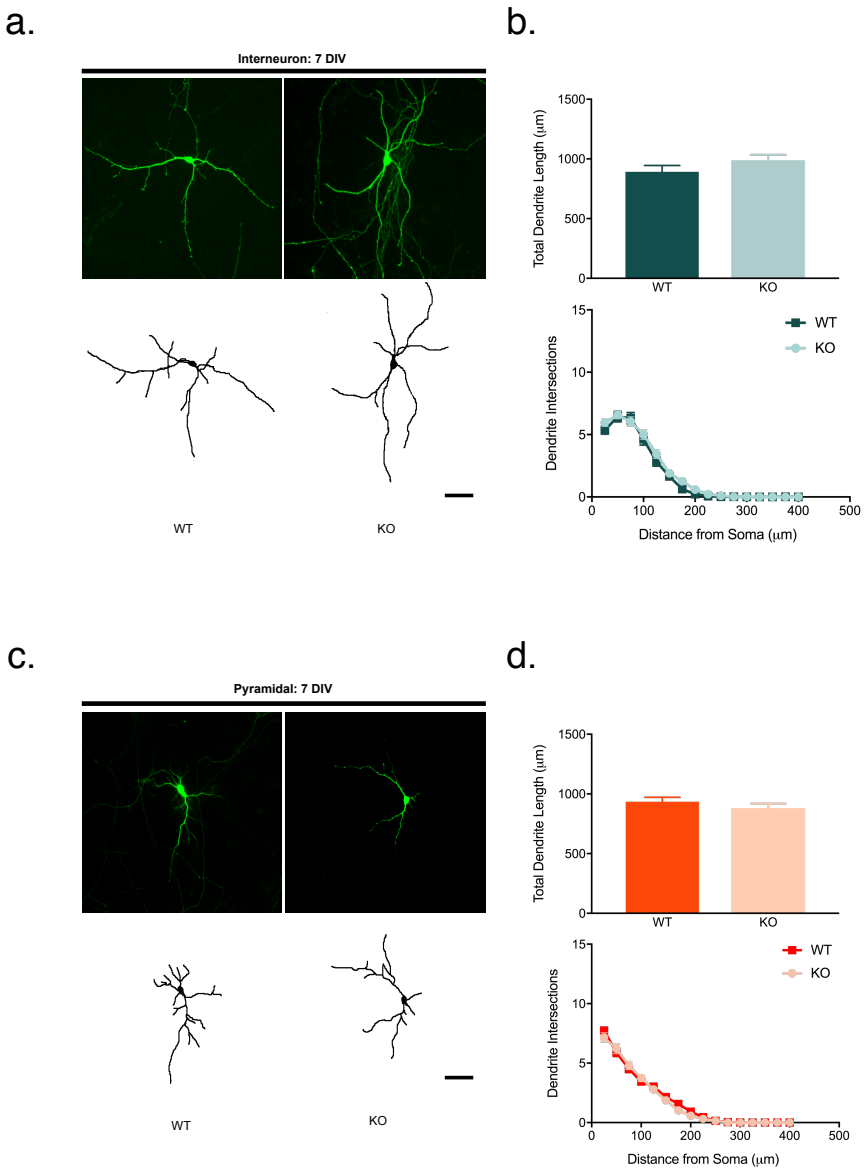


**Figure 3.2. *Cntnap2* KO neurons show no defects in dendrite outgrowth.** (a) Representative images of GFP-transfected WT or KO mouse interneurons at 7 DIV (scale bar = 50 $\mu$m) and (b) quantification of total dendrite length and Sholl (WT: n = 49 cells from 3 cultures; KO: n = 48 cells from 3 cultures). (c) Representative images of GFP-transfected WT or KO mouse pyramidal neurons at 7 DIV (scale bar = 50 $\mu$m) and (d) respective quantification of total dendrite length and Sholl (WT: n = 48 cells from 4 cultures; KO: n = 50 cells from 4 cultures). Values are means ± SEM; Student's *t*-test (total dendrite length; b, d) and two-way ANOVA with Bonferroni's correction (Sholl; b, d).

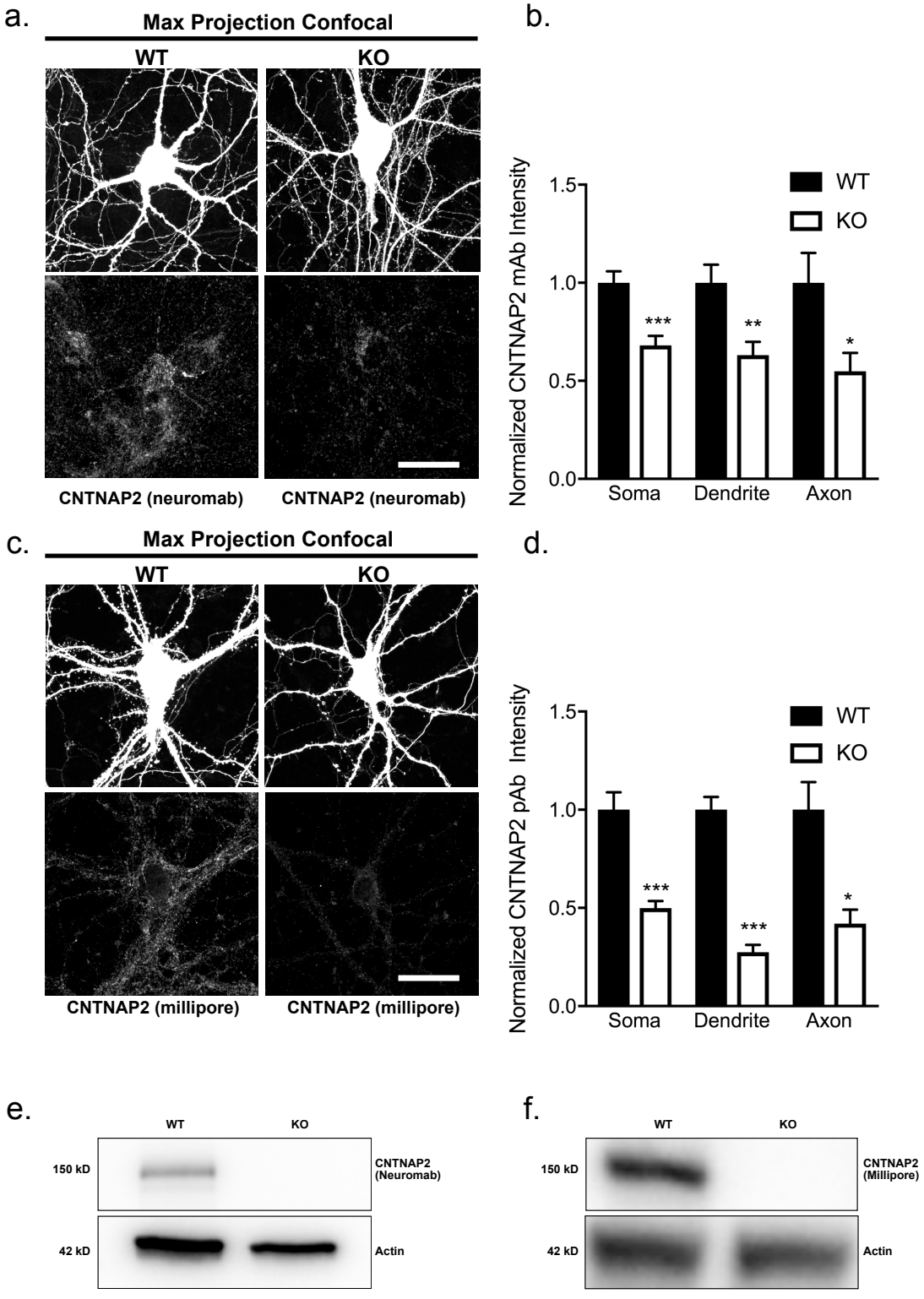
a.
Max Projection Confocal
WT
KO
CNTNAP2 (neuromab)
CNTNAP2 (neuromab)
b.
Normalized CNTNAP2 mAb Intensity
1.5
1.0
0.5
0.0
WT
KO
***
**
*
Soma
Dendrite
Axon
c.
Max Projection Confocal
WT
KO
CNTNAP2 (millipore)
CNTNAP2 (millipore)
d.
Normalized CNTNAP2 pAb Intensity
1.5
1.0
0.5
0.0
WT
KO
***
***
*
Soma
Dendrite
Axon
e.
WT
KO
150 kD
CNTNAP2
(Neuromab)
42 kD
Actin
f.
WT
KO
150 kD
CNTNAP2
(Millipore)
42 kD
Actin

**Figure 3.3. Antibody validation.** (a) Immunostaining of GFP-transfected WT or KO mouse neurons at 27 DIV with the mouse CNTNAP2 antibody (Neuromab) (scale bar = 25 μm) and (b) resulting quantification of CNTNAP2 intensity in soma/dendrite/axon (WT: n = 17 somas, 17 dendrites, and 14 axons from 2 cultures; KO: n = 19 somas, 19 dendrites, and 18 axons from 2 cultures). (c) Immunostaining of GFP-expressing WT or KO neurons at 27 DIV with the rabbit CNTNAP2 antibody (Millipore) (scale bar = 25 μm) and (d) resulting quantification of CNTNAP2 intensity in soma/dendrite/axon (WT: n = 17 somas, 17 dendrites, and 14 axons from 2 cultures; KO: n = 18 somas, 18 dendrites, and 16 axons from 2 cultures). (e-f) Representative cropped western blots demonstrating antibody specificity. Values are means ± SEM. * P≤0.05, ** P≤0.01, *** P≤0.001; Student's *t*-test (soma, dendrite; b, d), Mann-Whitney test (axon; b, d).

a.

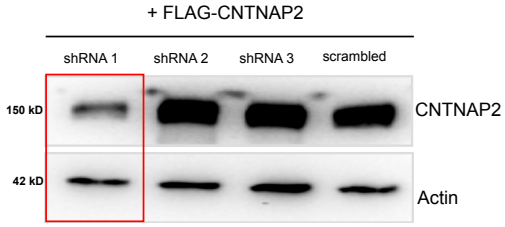
+ FLAG-CNTNAP2
shRNA 1
shRNA 2
shRNA 3
scrambled
150 kD
CNTNAP2
42 kD
Actin

b.

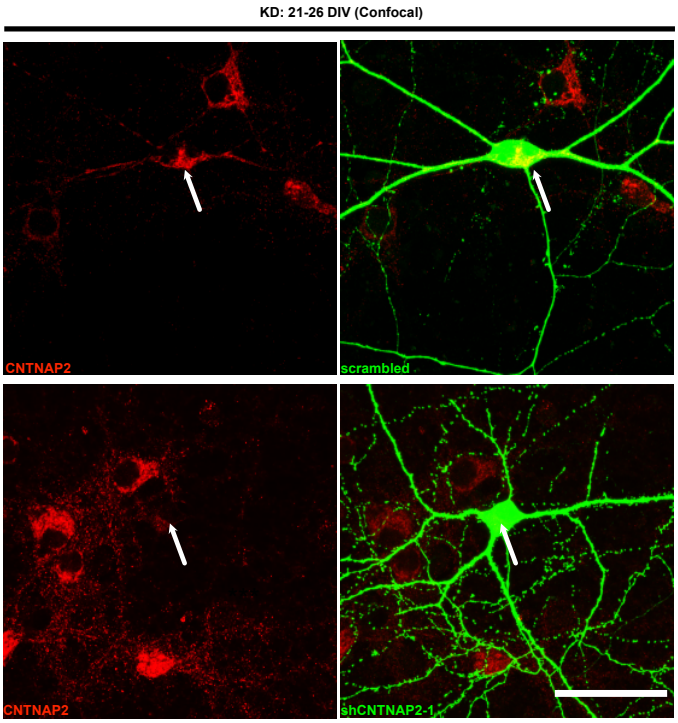
KD: 21-26 DIV (Confocal)
CNTNAP2
scrambled
CNTNAP2
shCNTNAP2-1

c.

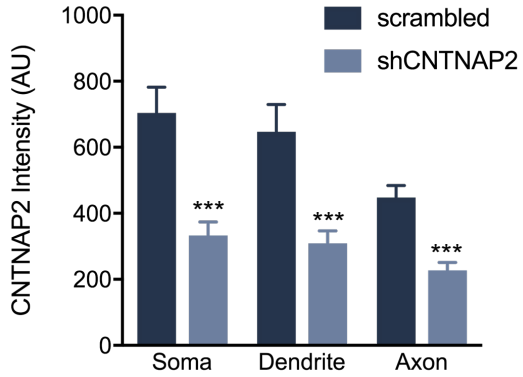
CNTNAP2 Intensity (AU)
1000
800
600
400
200
0
scrambled
shCNTNAP2
***
***
***
Soma
Dendrite
Axon

d.

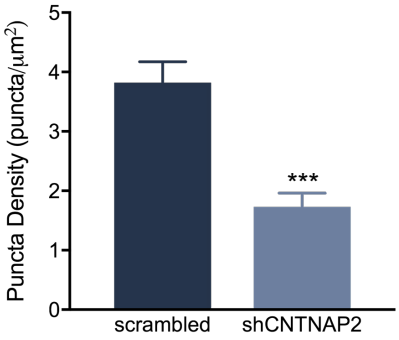
Puncta Density (puncta/μm²)
5
4
3
2
1
0
***
scrambled
shCNTNAP2

e.

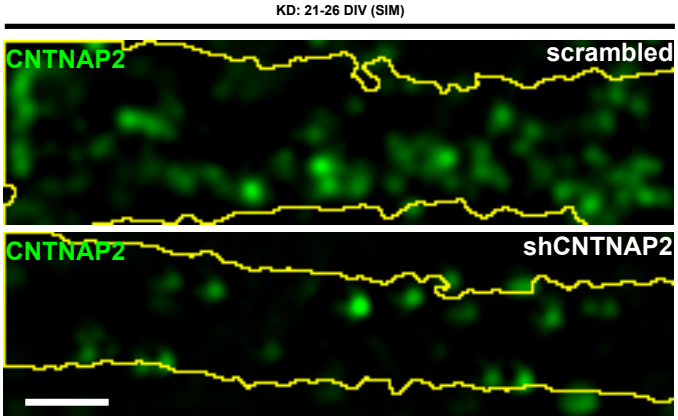
KD: 21-26 DIV (SIM)
CNTNAP2
scrambled
CNTNAP2
shCNTNAP2

**Figure 3.4**. **CNTNAP2 shRNA validation.** (a) Cropped western blot showing the efficacy of several shCNTNAP2 hairpins on the expression of a FLAG-CNTNAP2 plasmid in HEK293T cells, with shRNA-1 (the shRNA used for all knockdown experiments in this manuscript) being the most potent (red box). (b) Representative confocal images demonstrating how scrambled or shCNTNAP2 transfected (21-26 DIV) plasmids (arrows delineate transfected cell soma) affect endogenous CNTNAP2 expression in mature rat interneurons (scale bar = 50 $\mu$m) with (c) soma/dendrite/axon quantification (scrambled: n = 14 somas, 18 dendrites, and 11 axons from 3 cultures; shCNTNAP2: n = 12 somas, 16 dendrites, and 10 axons from 3 cultures). (d-e) Representative SIM images of mature scrambled or shCNTNAP2-treated interneurons endogenously stained for CNTNAP2 and respective analysis of CNTNAP2 dendrite puncta density (scale bar = 1μm; scrambled: n = 16 branches from 3 cultures; shCNTNAP2: n = 17 branches from 3 cultures). Values are means ± SEM; *** P≤0.001; Student's *t*-test (d, soma and axon; c). Mann-Whitney test (dendrite; c).

also resulted in a significant decrease of endogenous CNTNAP2 expression, as seen by confocal (Figure 3.4b-c) and high resolution SIM (Figure 3.4d-e) imaging. From these tests, we decided to use the shRNA-1 hairpin for all of our subsequent studies (and hereby will refer to this construct as "shCNTNAP2").

### 3.5. CNTNAP2 knockdown during the dendritic stabilization period affects interneuronal branching

We acutely knocked down CNTNAP2 in mature and in young interneurons using RNAi. Consistent with the KO, CNTNAP2-silenced mature interneurons displayed reduced length and complexity, which was partially rescued by overexpression of RNAi-resistant CNTNAP2 (scrambled: 3206 ± 142.6 μm vs. shCNTNAP2: 1640 ± 134.6 μm vs. shCNTNAP2 + rescue: 2286 ± 150.6 μm; Figure 3.5a-c). On the contrary, CNTNAP2 knockdown in young neurons had no effect on interneuron arborization (scrambled: 641.4 ± 43.8 μm vs. shCNTNAP2: 685.9 ± 52.8 μm; Figure 3.5d-e). Taken together, these data suggest that CNTNAP2 has an important role in the stabilization of interneuronal dendritic arbors in later stages of postnatal development.

### 3.6. CNTNAP2 is more highly expressed in interneurons relative to pyramidal cells

To understand why CNTNAP2 loss has different effects on different neuron types, we analyzed CNTNAP2 endogenous expression levels in cultured *Cntnap2* WT inhibitory and excitatory cells. Consistent with previous data, immunofluorescence analysis with a CNTNAP2 antibody (Figure 3.3c-d, f) revealed a higher abundance of CNTNAP2 protein in inhibitory compared to excitatory neurons in soma, dendrites, and axons (Figure 3.6a-c), similar to a published cell-specific RNA-

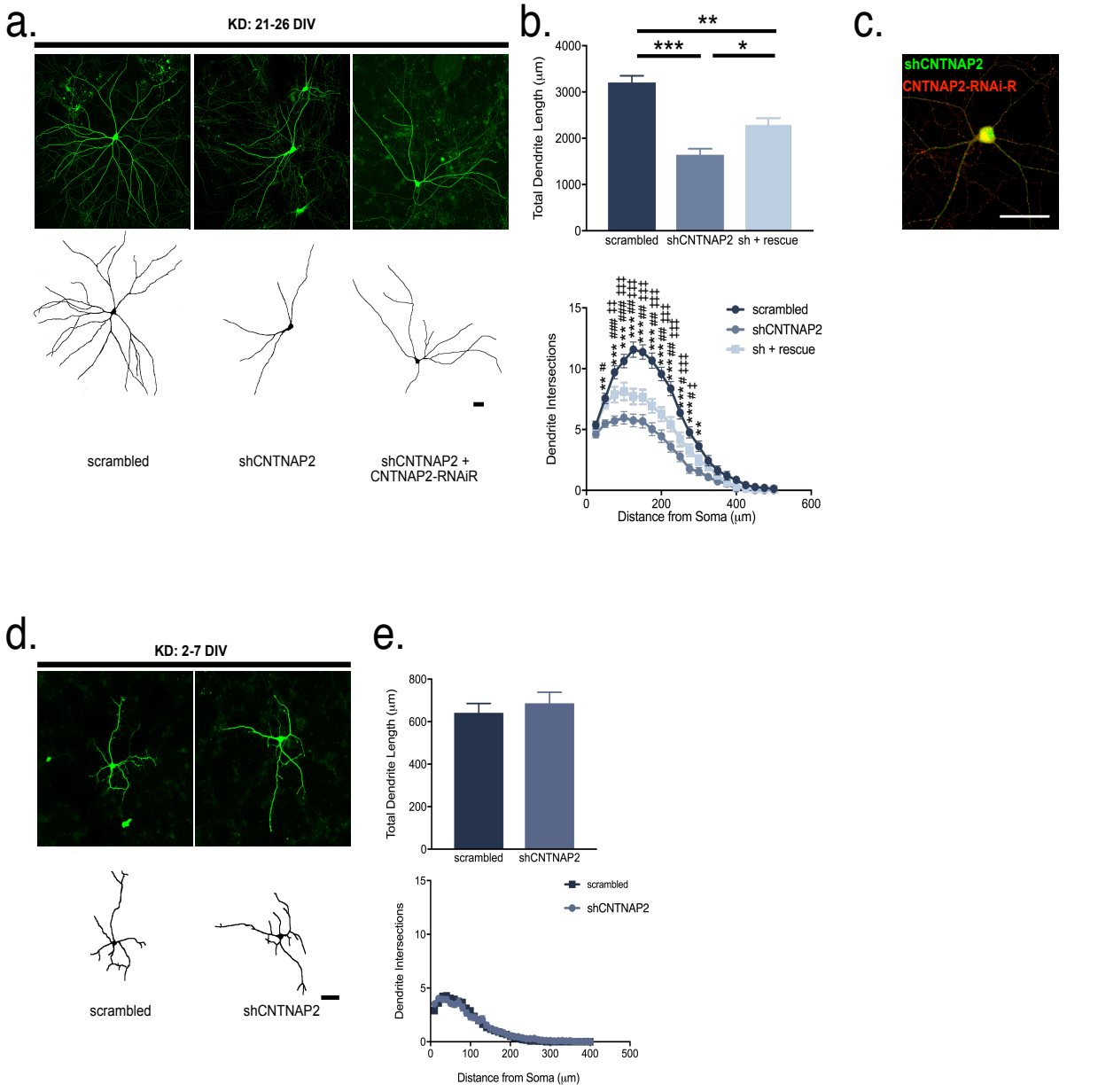
a.
KD: 21-26 DIV
scrambled
shCNTNAP2
shCNTNAP2 +
CNTNAP2-RNAiR
b.
**
***
*
Total Dendrite Length (μm)
4000
3000
2000
1000
0
scrambled
shCNTNAP2
sh + rescue
Dendrite Intersections
15
10
5
0
0
200
400
600
Distance from Soma (μm)
scrambled
shCNTNAP2
sh + rescue
c.
shCNTNAP2
CNTNAP2-RNAi-R
d.
KD: 2-7 DIV
scrambled
shCNTNAP2
e.
Total Dendrite Length (μm)
800
600
400
200
0
scrambled
shCNTNAP2
Dendrite Intersections
15
10
5
0
0
100
200
300
400
500
Distance from Soma (μm)
scrambled
shCNTNAP2

**Figure 3.5. CNTNAP2 knockdown during the dendritic stabilization period affects interneuronal branching.** (a) Representative images of 26 DIV rat interneurons treated (21-26 DIV) with either scrambled, shCNTNAP2, or shCNTNAP2 + RNAi-resistant CNTNAP2 (scale bar = 50 $\mu$m) and (b) quantification of total dendrite length and Sholl for the respective populations (scrambled: n = 30 cells from 4 cultures; shCNTNAP2: n = 31 cells from 4 cultures; shCNTNAP2 + RNAi-resistant CNTNAP2: n = 31 cells from 4 cultures; for Sholl, * compares scrambled vs. shCNTNAP2, # compares shCNTNAP2 + rescue vs. shCNTNAP2, ‡ compares shCNTNAP2 + rescue vs. scrambled). (c) Representative image of a shCNTNAP2 interneuron overexpressing RNAi-resistant CNTNAP2 (scale bar = 50 $\mu$m). (d) Representative images of 7 DIV rat interneurons treated (2-7 DIV) with either scrambled or shCNTNAP2 (scale bar = 50 $\mu$m) and (e) quantification of total dendrite length and Sholl (scrambled: n = 50 cells from 6 cultures; shCNTNAP2: n = 46 cells from 6 cultures). Values are means ± SEM; * P≤0.05, ** P≤0.01, *** P≤0.001 (also applies for # and ‡); Mann-Whitney test (total dendrite length; e), Kruskal-Wallis test with Dunn's correction (total dendrite length; b), Two-way ANOVA with Bonferroni's correction (Sholl; b, e).

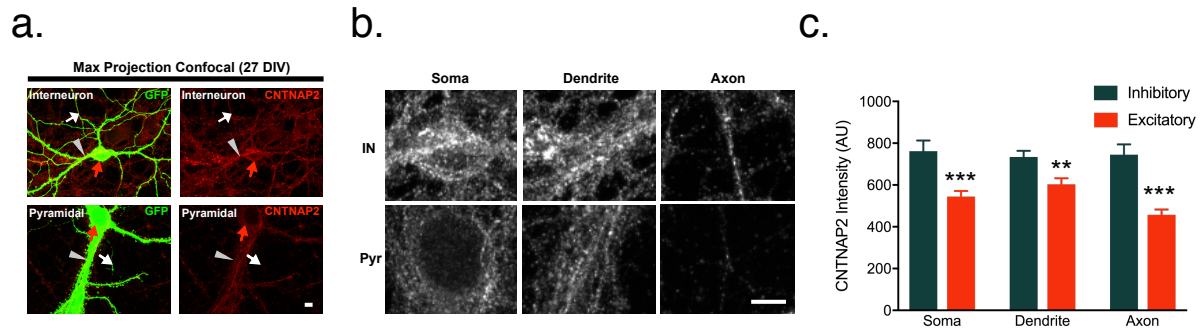


**Figure 3.6. CNTNAP2 is more highly expressed in interneurons relative to pyramidal cells.** (a) Representative images (scale bar = 5 µm) of GFP-transfected inhibitory and excitatory WT mouse neurons at 27 DIV, with soma (red arrow), dendrites (arrowhead), and axons (white arrow) highlighted. (b) Magnification of structures from (a) (scale bar = 5 µm) and (c) respective quantification (Inhibitory: n = 22 somas, 37 dendrites, and 19 axons from 3 cultures; Excitatory: n = 19 somas, 29 dendrites, and 13 axons from 3 cultures). Values are means ± SEM. * P≤0.05, ** P ≤0.01, *** P ≤0.001; Student's *t*-test (c).

Seq database[187]. Taken together, our data suggests the different impact of CNTNAP2 loss on neuronal types may be due to its differential expression levels in interneurons vs. pyramidal neurons.

3.7. CNTNAP2 has spatially distinct localization patterns in inhibitory neuronal dendrites

Because of CNTNAP2's role in interneurons, we used different microscopy approaches to examine its subcellular distribution in interneuronal dendritic trees. Confocal imaging with a CNTNAP2 antibody (Figure 3.3a-b, e), along with MAP2 as a dendritic marker and a GABA antibody as an interneuron marker, revealed that CNTNAP2 was abundant in punctate clusters throughout interneuronal dendrites at 27 DIV (Figure 3.7a). Further analysis revealed a CNTNAP2 spatial localization gradient, with puncta intensity (primary: 556.1 ± 42.5 AU vs. secondary: 418.5 ± 30.1 AU vs. tertiary: 377 ± 35.2 AU; Figure 3.7b-c) and puncta size (primary: 0.26 ± 0.03 $\mu m^2$ vs. secondary: 0.14 ± 0.02 $\mu m^2$ vs. tertiary: 0.097 ± 0.01 $\mu m^2$; Figure 3.7b-c) higher in primary dendrites while tapering off in secondary and tertiary branches. Meanwhile, CNTNAP2 puncta density was not affected by branch region (primary: 0.59 ± 0.03 puncta/$\mu m^2$ vs. secondary: 0.57 ± 0.05 puncta/$\mu m^2$ vs. tertiary: 0.56 ± 0.07 puncta/$\mu m^2$; Figure 3.7b-c). This suggests that CNTNAP2 cluster size, but not number, have a dendrite order-sensitive spatial distribution.

3.8. High resolution imaging reveals unique CNTNAP2 nanodomains in interneuron dendrites

Because of the limited resolution of confocal microscopy, we used SIM, a super-resolution technique that increases lateral resolution two-fold over confocal[188], to visualize ultrastructural profiles of CNTNAP2 distribution. We found CNTNAP2 to be frequently positioned in linear,

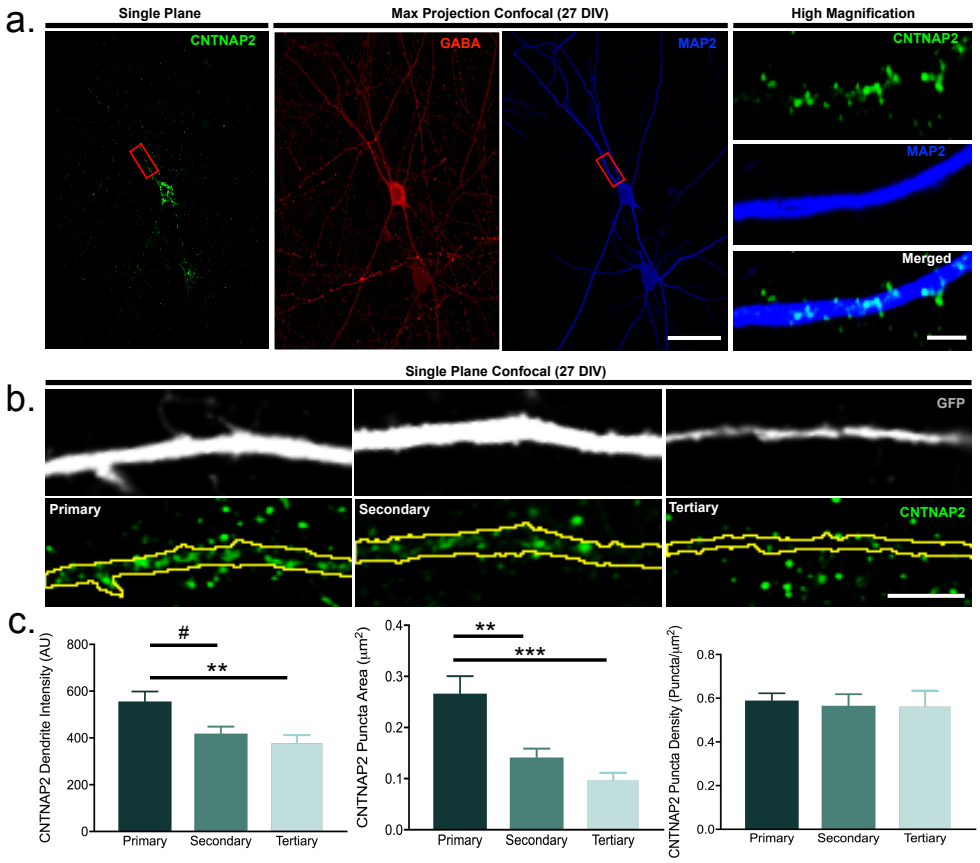


**Figure 3.7. CNTNAP2 has spatially distinct localization patterns in inhibitory neuronal dendrites.** (a) Confocal images of GABA-positive rat interneurons at 27 DIV co-stained with endogenous CNTNAP2 and the dendrite marker MAP2 (scale bar = 50 $\mu$m). Inset shows magnification of region around red box. (Scale bar = 5 $\mu$m). (b) Confocal imaging reveals general CNTNAP2 expression patterns in GFP-transfected primary, secondary, and tertiary dendritic branches (scale bar = 5 $\mu$m), with (c) quantification of intensity, puncta area, and puncta density (intensity: n = 28 primary, 28 secondary, and 25 tertiary branches from 4 cultures; puncta area/density: n = 20 primary, 20 secondary, and 18 tertiary branches from 3 cultures). Values are means $\pm$ SEM. # P=0.07, ** P≤0.01, *** P≤0.001; Kruskal-Wallis test with Dunn's correction (intensity and puncta size; c), one way-ANOVA with Bonferroni's correction (puncta density; c).

bead-like configurations along dendrites (Figure 3.8a), which were not resolvable by confocal (Figure 3.7b). Three-dimensional reconstruction of stacked SIM images revealed these structures to be near the peripheral edge, suggesting membrane proximity (Figure 3.8b). To validate the existence of these structures using a different super-resolution method, we used STED microscopy, a point-scanning imaging technique that can further enhance lateral resolution to 35 nm[189]. STED also detected CNTNAP2 nanostructures in primary dendrites indicating that they were not an artefact of SIM imaging (Figure 3.8c).

To determine the relationship between nanostructures and dendrite branch length, we used RNAi to knock down CNTNAP2 in mature interneurons (Figure 3.4d-e) and quantitatively analyzed nanostructure distribution along multiple dendrite regions. Nanostructures were present most frequently in primary compared to secondary and tertiary branches, with RNAi strongly reducing their abundance in secondary and tertiary dendrites (scrambled: 58% primary vs. 30% secondary vs. 33.3% tertiary; shCNTNAP2: 26% primary vs. 8% secondary vs. 12% tertiary; Figure 3.8d-e). Analysis of RNAi-expressing interneurons also revealed a surprising stability of primary, but significant decrease of distal branch length (primary scrambled: 301.4 ± 26.1 μm vs. primary shCNTNAP2: 398.8 ± 36.8 μm; secondary scrambled: 838.8 ± 57.8 μm vs. secondary shCNTNAP2: 632.5 ± 48.3 μm; tertiary scrambled: 876.3 ± 65.0 μm vs. tertiary shCNTNAP2: 622.9 ± 50.7 μm; Figure 3.8f), which correlated with the abundance of residual nanostructures (Figure 3.8d-e). Taken together, these data indicate that CNTNAP2 distribution correlates with interneuronal dendrite branch stability.

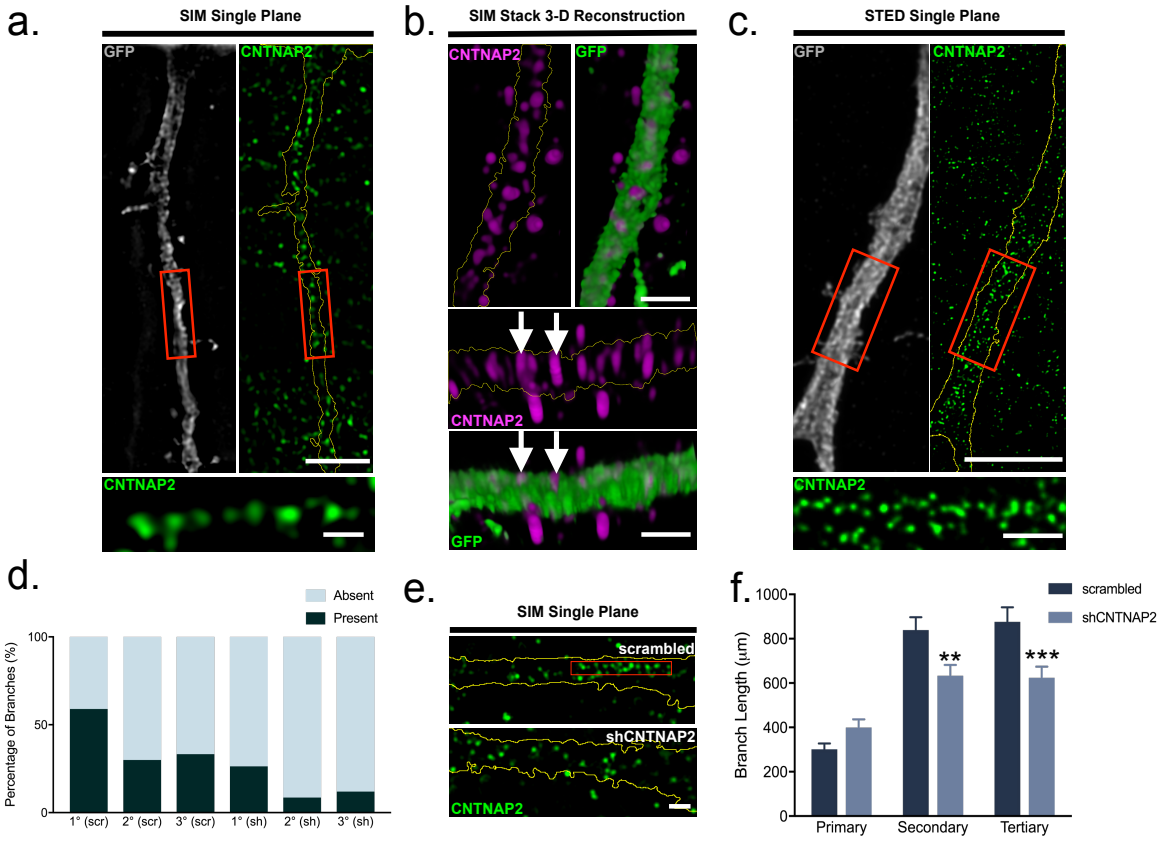


**3.8. High resolution imaging reveals unique CNTNAP2 nanodomains in interneuron dendrites.** (a) High resolution SIM imaging detects the presence of linear "bead"-like CNTNAP2 nanostructures in GFP-expressing dendrites of rat interneurons. Inset shows magnification of region around red box (scale bar = 5 $\mu$m and 1 $\mu$m respectively). (b) Top and side angles of a 3D reconstructed SIM image stack showing CNTNAP2 "beads" either alone or with GFP overlay (scale bars = 1 $\mu$m). White arrows point to nanostructures near the membrane surface. (c) STED imaging confirms CNTNAP2 nanostructures in interneuron primary dendrites, with inset showing magnification of region around the red box (scale bar = 5 $\mu$m and 1 $\mu$m respectively). (d) CNTNAP2 nanostructure distribution in primary, secondary, and tertiary dendrites in mature scrambled or shCNTNAP2-treated (21-26 DIV) rat interneurons (scrambled: n = 39 primary branches, 40 secondary branches, and 36 tertiary branches from 3 cultures; shCNTNAP2: n = 38 primary branches, 35 secondary branches, and 25 tertiary branches from 3 cultures). (e) Representative SIM images of CNTNAP2 endogenous staining in scrambled or shCNTNAP2-

treated rat interneuron branches (scale bar = 1 $\mu$m). (f) Quantification of primary, secondary, and tertiary branch lengths in scrambled or shCNTNAP2-treated (21-26 DIV) mature rat interneurons (scrambled: n = 57 cells from 5 cultures; shCNTNAP2: n = 68 cells from 5 cultures). Values are means ± SEM. ** P≤0.01, *** P≤0.001; two-way ANOVA with Bonferroni's correction (f).

3.9. CNTNAP2 recruits CASK to the plasma membrane in HEK293T cells

We next investigated the mechanisms of CNTNAP2-dependent dendrite stabilization. Because the effects of CNTNAP2 knockdown were cell-autonomous, and because CAMs often utilize C-termini for intracellular signaling and protein-protein interactions[190], we performed a yeast two-hybrid screen of a mouse brain cDNA library with the entire CNTNAP2 C-terminus as bait (amino acids 1284-1331) to find intracellular interactors. We identified 41 unique clones (Figure 2.2) of which the scaffold protein CASK was one of the most highly represented. To determine the function of this interaction, we fractionated HEK293T cell homogenates and observed co-expression of CNTNAP2 and CASK, but not CASKΔPDZ, increased CASK in the membrane fraction (CASK: 41.1 ± 1.9% vs. CNTNAP2 + CASK: 51.8 ± 0.7% vs. CNTNAP2 + CASKΔPDZ: 35.2±2.1%; Figure 3.9a), consistent with immunocytochemistry (Figure 2.3e). On the other hand, CNTNAP2's localization to the membrane was not affected when co-expressed either with CASK or CASKΔPDZ (CNTNAP2 + CASK: 84.9 ± 2.2% vs. CNTNAP2 + CASKΔPDZ: 85.7 ± 2.9%; Figure 3.9b). Finally, CASK's membrane localization was unaffected when either CASK or CASKΔPDZ was expressed alone (CASK: 44.4±1.5% vs. CASKΔPDZ: 43.3±2.3%) (Figure 3.9c). Taken together, our results suggest CNTNAP2 is upstream of CASK and has the ability to recruit CASK to the membrane.

3.10. CNTNAP2 interacts with CASK at the plasma membrane in cortical GABAergic interneurons

We next investigated the relative spatial localization of CNTNAP2 and CASK. To determine where the CNTNAP2 and CASK interaction was spatially localized, we imaged endogenous proteins with SIM. Co-localization occurred frequently near the lateral edge (48.1% and 45.7% of

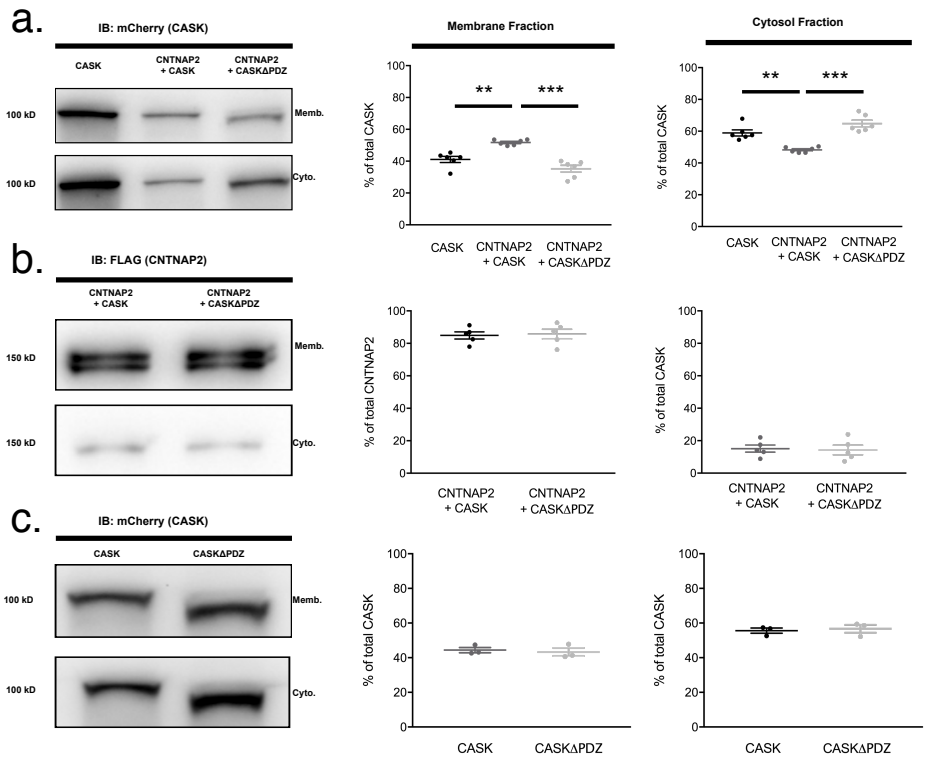


**Figure 3.9. CNTNAP2 recruits CASK to the plasma membrane in HEK293T cells.** (a-c) Representative cropped western blots of membrane/cytosol fractions of HEK293T cells expressing pCS2-FLAG + CASK-mCherry (CASK), FLAG-CNTNAP2 + CASK-mCherry (CNTNAP2 + CASK), or FLAG-CNTNAP2 + CASKΔPDZ-mCherry (CNTNAP2 + CASKΔPDZ) and subsequent quantification of protein localization (CASK vs. CNTNAP2 + CASK vs. CNTNAP2 + CASKΔPDZ: 5-6 independent experiments; CASK alone vs. CASKΔPDZ alone: 3 independent experiments). Percentages were calculated by dividing the densitometry value of CASK/CNTNAP2 in either membrane or cytosol fraction by the summation of both. Values are means ± SEM. * P≤0.05, ** P≤0.01, *** P≤0.001; one-way ANOVA with Bonferroni's correction (a). Student's *t*-test (b, c).

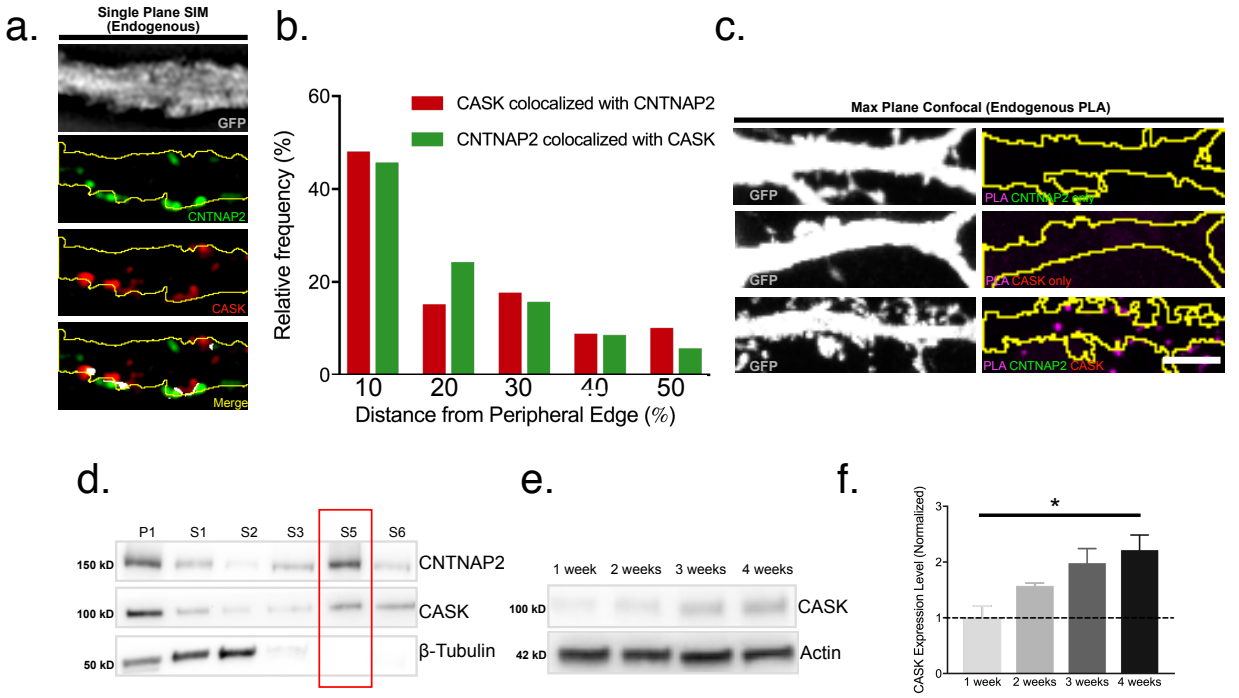


**Figure 3.10. CNTNAP2 interacts with CASK at the plasma membrane in cortical GABAergic interneurons.** (a) Representative SIM image of endogenous CNTNAP2 and CASK co-localization (white) on a GFP-transfected interneuronal dendrite (scale bar = 1 μm). (b) Histogram showing distribution of CASK/CNTNAP2 co-localized puncta relative to the dendrite's lateral edge from (a) (CASK colocalized with CNTNAP2: n = 79 puncta from 3 cultures; CNTNAP2 colocalized with CASK: n = 70 puncta from 3 cultures). (c) Representative confocal image showing PLA signal from endogenous CASK/CNTNAP2 staining, which occurs only when CASK and CNTNAP2 primary antibodies are both applied (scale bar = 5 μm). (d) Cropped immunoblots of subcellular fractionations from adult mouse forebrain probed with CNTNAP2, CASK, and β-tubulin. CNTNAP2 and CASK, but not β-tubulin, are found in the washed membrane fraction (S5; red box). (e) Cropped western blot of time course and (f) quantification of CASK expression in cultured cortical neurons (n = 3 independent experiments). Values are means ± SEM. * P≤0.05; one-way ANOVA with Bonferroni's correction (f).

total co-localized CASK and CNTNAP2 were respectively within 10% of the peripheral edge; Figure 3.10a-b), suggesting CASK binds to CNTNAP2 near the plasma membrane. We validated this using PLA, which showed both molecules (Figure 3.10c, Figure 2.3e) often interacted *in situ* near the dendrite's peripheral edge. By subcellular fractionation and salt/detergent solubilization of mouse brain homogenates (Figure 3.10d) we found both CNTNAP2 and CASK were highly abundant in the washed membrane fraction (S5), consistent with previous publications[191, 192]; notably, CASK was not removed from the membrane even by stringent wash conditions (see Methods). This suggests that CASK interacts with high affinity with CNTNAP2 and other transmembrane proteins. Lastly, CASK protein levels increased with age in cultured cortical neurons, in a similar pattern as CNTNAP2 (Figure 3.10e-f)[193], supporting functional roles later in postnatal development[194]. In summary, CNTNAP2 recruits CASK to the plasma membrane through the interaction of its C-terminal PDZ-binding motif with the PDZ domain of CASK.

3.11. CNTNAP2 regulates CASK stability in interneurons in a unidirectional manner

To understand the mechanistic significance of the CNTNAP2-CASK interaction, we tested the impact of their reciprocal knockdowns on each other. CNTNAP2 knockdown resulted in a reduction of average CASK fluorescence intensity (scrambled: 1288 ± 100.3 AU vs. shCNTNAP2: 899.6 ± 61.8 AU) and puncta size (scrambled: 0.92 ± 0.2 $\mu m^2$ vs. shCNTNAP2: 0.26 ± 0.06 $\mu m^2$) in interneuronal dendrites (Figure 3.11a-b) and somas (scrambled: 1214 ± 110 AU vs. shCNTNAP2: 738.9 ± 89.9 AU; Figure 3.11c-d), suggesting an effect on overall CASK protein levels. On the contrary, CASK knockdown (Figure 3.14e) did not affect CNTNAP2 intensity (scrambled: 793.4 ± 91.9 AU vs. shCASK: 685.9 ± 57.4 AU) or puncta size (scrambled: 0.33 ±

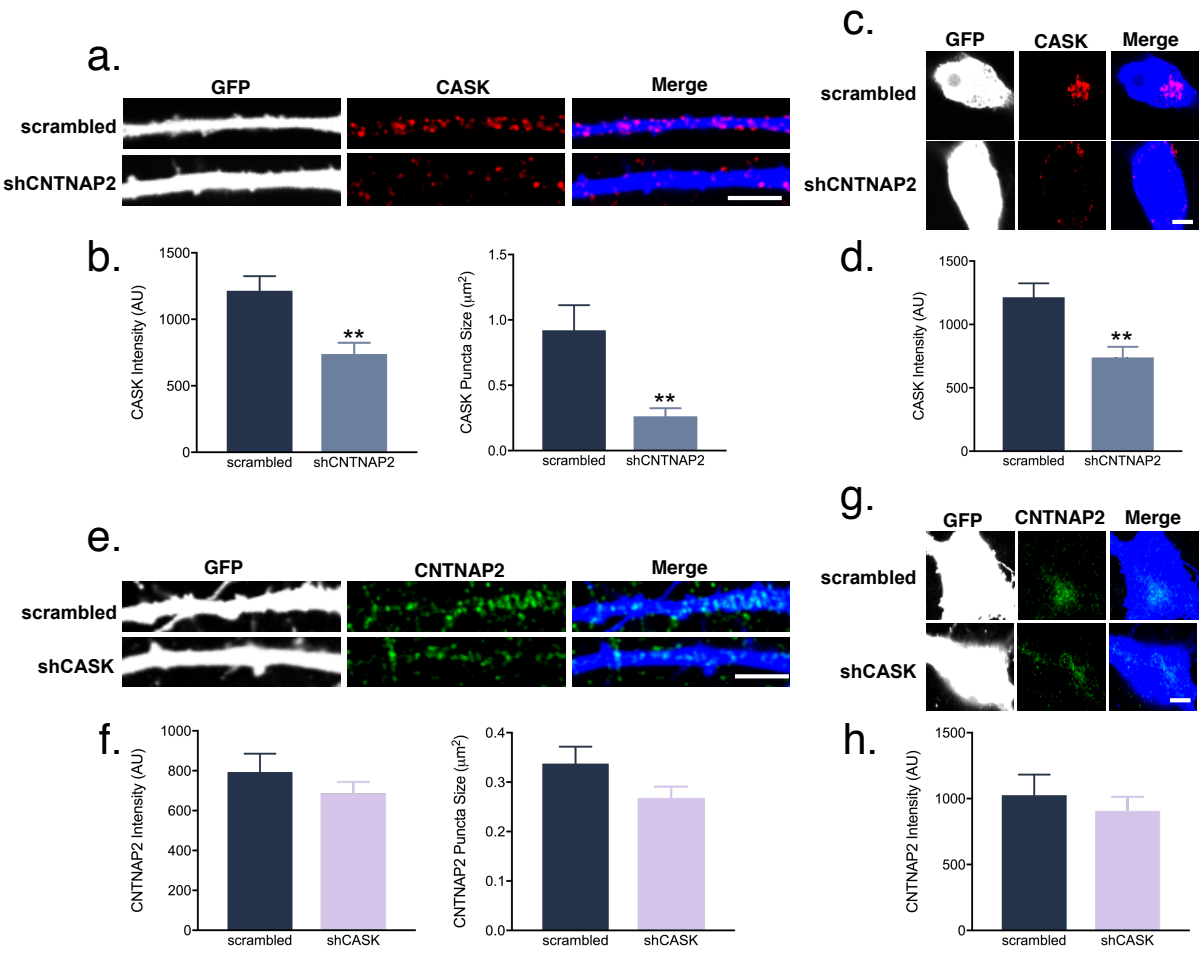


**Figure 3.11. CNTNAP2 regulates CASK stability in interneurons.** (a) Representative confocal images and (b) quantification of CASK average intensity and puncta area in scrambled or shCNTNAP2-treated (21-26 DIV) rat interneuron dendrites at 26 DIV (scale bar = 5 $\mu$m; scrambled: n = 42 branches for intensity and n = 37 branches for puncta area from 3 cultures; shCNTNAP2: n = 43 branches for intensity and n = 37 branches for puncta area from 3 cultures). (c) Representative confocal images and (d) quantification of CASK average intensity in scrambled or shCNTNAP2 interneuron somas (scale bar = 5 $\mu$m; scrambled: n = 23 cells from 3 cultures; shCNTNAP2: n = 24 cells from 3 cultures). (e) Representative confocal images and (f) quantification of CNTNAP2 average intensity and puncta area in scrambled or shCASK-treated (21-26 DIV) rat interneuron dendrites at 26 DIV (scale bar = 5 $\mu$m; scrambled: n = 49 branches for intensity and n = 57 branches for puncta area from 4 cultures; shCASK: n = 52 branches for intensity and n = 47 branches for puncta area from 4 cultures) and (g-h) quantification of average

CNTNAP2 intensity in the somas of scrambled or shCASK interneurons (scale bar = 5 $\mu$m; scrambled: n = 24 cells from 4 cultures; shCASK: n = 29 cells from 4 cultures). Values are means $\pm$ SEM. **P≤0.01; Mann-Whitney test (b, d, f, h).

0.03 μm$^2$ vs. shCASK: 0.27 ± 0.02 μm$^2$) in dendrites (Figure 3.11e-f) or somas (scrambled: 1026 ± 156.6 AU vs. shCASK: 906.4 ± 106.9 AU; Figure 3.11g-h).

3.12. CNTNAP2 regulates CASK localization in interneurons in a unidirectional manner

To gain further insight into the spatial distribution of CASK or CNTNAP2 upon their reciprocal knockdown, we employed SIM. Consistent with confocal imaging, CASK puncta density was decreased in shCNTNAP2 interneurons (scrambled: 1.99 ± 0.12 puncta/μm$^2$ vs. shCNTNAP2: 1.41 ± 0.10 puncta/μm$^2$; Figure 3.12b), while CNTNAP2 puncta density remained unaltered in shCASK interneurons (scrambled: 2.77 ± 0.13 puncta/μm$^2$ vs. shCASK: 2.46 ± 0.11 puncta/μm$^2$; Figure 3.12e). However, CASK puncta in shCNTNAP2 dendrites were on average closer to the peripheral edge compared to scrambled (scrambled: 22.0 ± 0.7% vs. shCNTNAP2: 19.5 ± 0.8% away from periphery; Figure 3.12a, c), due primarily to changes in localization near the plasma membrane (scrambled: 28.4% vs. shCNTNAP2: 37.5% of all puncta within 10% of periphery; Figure 3.12g). Conversely, CASK knockdown did not alter CNTNAP2 distribution overall (scrambled: 25.8 ± 0.6% vs. shCASK: 25.2 ± 0.6% away from periphery; Figure 3.12d, f) or specifically near the plasma membrane (scrambled: 16.4% vs. shCASK: 17.5% of all puncta within 10% of periphery; Figure 3.12h).

3.13. CASK mediates CNTNAP2-dependent interneuron dendrite stabilization in *Cntnap2* KO and CNTNAP2 knockdown neurons

Next, we tested whether CASK functioned downstream of CNTNAP2 to regulate interneuron dendrite stability. We overexpressed CASK in mature *Cntnap2* KO neurons and analyzed the effects on both excitatory and inhibitory cell-types. Remarkably, while CASK overexpression in

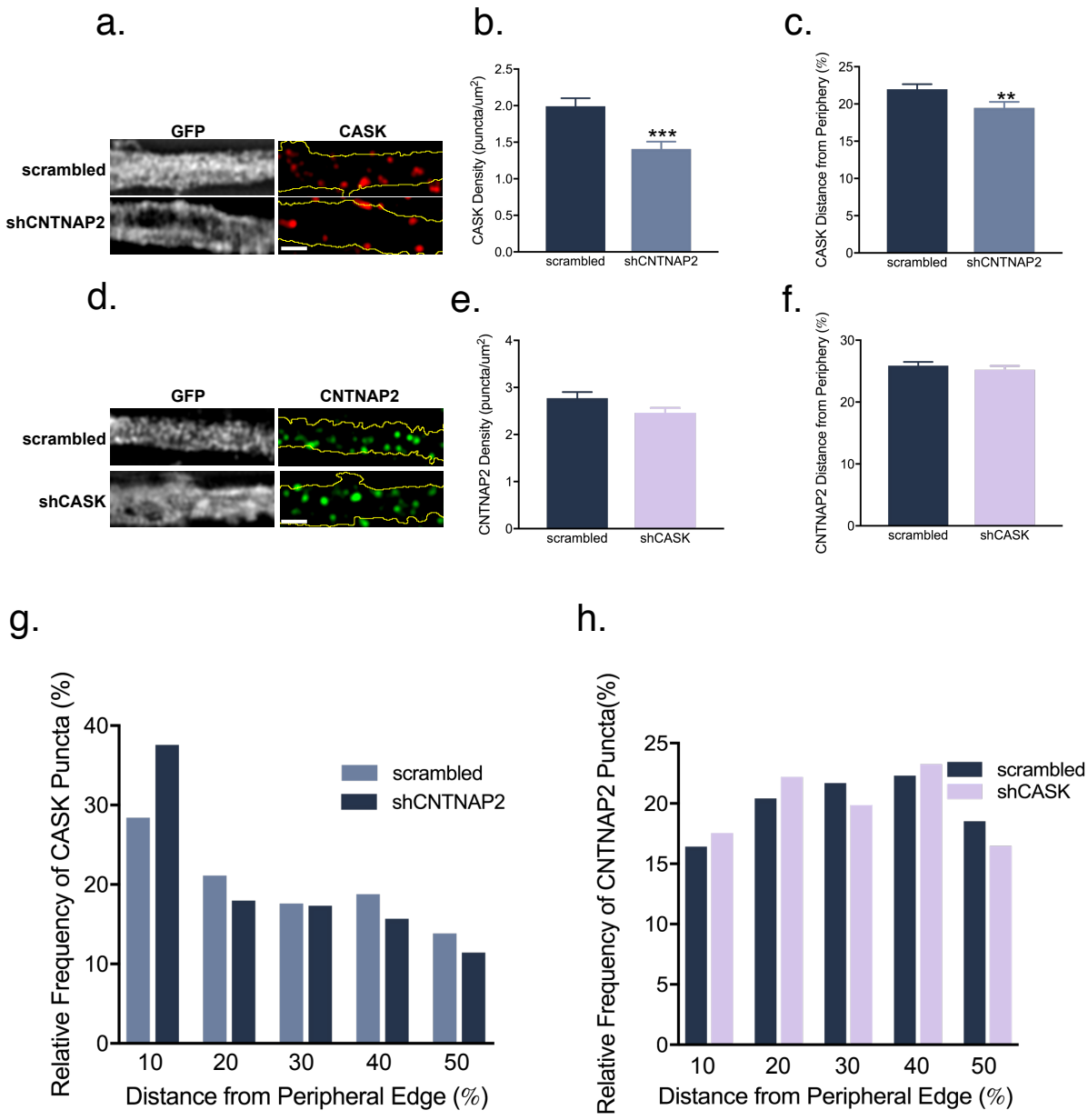


**Figure 3.12. CNTNAP2 regulates CASK localization in interneurons.** (a) High resolution SIM images of endogenous CASK in scrambled or shCNTNAP2 interneuron dendrites at 26 DIV (scale bar = 1 $\mu$m). (b) Analysis of CASK puncta density (scrambled: n = 31 branches from 5 cultures; shCNTNAP2: n = 26 branches from 5 cultures) and (c) average distance from peripheral edge (scrambled: n = 426 puncta from 5 cultures; shCNTNAP2: n = 306 puncta from 5 cultures) via SIM in scrambled or shCNTNAP2 interneurons. (d) High resolution SIM images

of endogenous CNTNAP2 in scrambled or shCASK interneuron dendrites at 26 DIV. (e) Analysis of CNTNAP2 puncta density (scrambled: n = 23 branches from 3 cultures; shCASK: n = 25 branches from 3 cultures) and (f) average distance from peripheral edge (scrambled: n = 475 puncta from 3 cultures; shCASK: n = 473 puncta from 3 cultures) via SIM in scrambled or shCASK interneurons. (g) Frequency distribution of CASK puncta (scrambled: n = 426 puncta from 5 cultures; shCNTNAP2: n = 306 puncta from 5 cultures) in scrambled and shCNTNAP2 treated (21-26 DIV) rat interneuron dendrites (21-26 DIV). (h) Frequency distribution of CNTNAP2 puncta (scrambled: n = 475 puncta from 3 cultures; shCASK: n = 473 puncta from 3 cultures) in scrambled and shCASK treated (21-26 DIV) rat interneuron dendrites. Bin widths in (g) and (h) are 10%, with the percentage value representing the distance of the puncta to the closest lateral edge divided by the total width of the dendrite at that point multiplied by 100. Same applies to distances in (c) and (f). Values are means ± SEM. **P≤0.01, ***P≤0.001; Mann-Whitney test (c, e, f), Student's *t*-test (b).

inhibitory KO neurons significantly increased total dendrite length (KO: 1498 ± 84.2 μm vs. KO + CASK: 2079 ± 110.4 μm; Figure 3.13a-b), it did not affect dendrite length in KO pyramidal neurons from the same coverslips (KO: 2693 ± 84.9 μm vs. KO+CASK: 2901 ± 98.7 μm; Figure 3.13c-d). Similarly, overexpression of CASK in mature CNTNAP2 knockdown neurons rescued dendrite alterations (scrambled: 3356 ± 137.2 μm vs. shCNTNAP2: 2010 ± 173.8 μm vs. sh+CASK: 3172±200.7μm; Figure 3.14a-b), but did not alter dendrite length or complexity in WT neurons (GFP: 3345 ± 204.4μm vs. GFP + CASK: 3014 ± 176.5μm; Figure 3.14c-d). Conversely, CASK knockdown in mature (scrambled: 2883 ± 136μm vs. shCASK: 2467 ± 153μm; Figure 3.14e-g) but not young (scrambled: 785.4 ± 82.6μm vs. shCASK: 871.3 ± 78.8μm; Figure 3.14h-i) interneurons resulted in simplified interneuronal arbors. Because we have shown that CASK's PDZ domain mediates its interaction with CNTNAP2 (Figure 2.3d), we examined the role of this domain on CNTNAP2-dependent dendrite stabilization. Overexpression of CASKΔPDZ in mature *Cntnap2* KO or CNTNAP2 knockdown interneurons did not fully reverse dendrite deficits, as compared to full-length CASK (KO: 1527 ± 52.8 μm vs. KO + CASK: 1919 ± 68.0 μm vs. KO + CASKΔPDZ: 1720 ± 68.4 μm; Figure 3.13e-f; shCNTNAP2: 1646 ± 97.5 μm vs. shCNTNAP2 + CASK: 2358 ± 118.5 μm vs. shCNTNAP2 + CASKΔPDZ: 1919 ± 95.3 μm; Figure 3.14j-k). In summary, these experiments indicate that CASK, through its PDZ domain, functions downstream of CNTNAP2 to mediate dendrite stabilization in interneurons.

3.14. Endogenous CASK levels are higher in interneurons relative to pyramidal cells in *Cntnap2* WT cultures but differences are reduced in KO cultures

If CNTNAP2 regulates CASK stability (Figure 3.11) and is more highly expressed in interneurons than pyramidal cells (Figure 3.6), we hypothesized that endogenous CASK levels

would also be discrepant between the two cell types; in addition, we reasoned that such differences may be lost with the KO. To test our theory, we transfected mature *Cntnap2* WT or KO cultures with GFP and stained for endogenous CASK via immunocytochemistry. We analyzed cell somas, as it is the region where most proteins are translated and therefore indicative of expression level. In line with our theory, we found CASK levels to be significantly upregulated in WT inhibitory cells compared to WT excitatory cells, with this difference being significantly reduced in the KO neurons as a result of reduced CASK levels in KO interneurons (WT Excitatory: 553.6 ± 15.4 AU vs. WT Inhibitory: 679.4 ± 25.6 AU vs. KO Excitatory: 519.2 ± 21.6 AU vs. KO Inhibitory: 600.9 ± 18.7 AU; Figure 3.15a). Taken together, our data provides further evidence that different abundances of CNTNAP2 in different cell types may cause differences in CASK-mediated pathways.

### 3.15. Domain mapping of CASK reveals key regions critical for interneuron dendrite maintenance

As PDZ domains play a key role in anchoring proteins to the plasma membrane, CASK's PDZ site likely involved with the protein's spatial localization. This suggests CASK's mechanism of dendrite maintenance may be multi-faceted, involving other domains that may be important for downstream signaling. To explore this possibility, we overexpressed other CASK truncation mutants (Figure 3.16a; red lines) in *Cntnap2* KO interneurons to further elucidate CASK's mechanism of rescue and found the region covering SH3, 4.1, and GK domains (exons 21-27) to also be critical for the effect. (Figure 3.16b-c) This suggests multiple CASK domains, each with a possibly different function, may work in synergy to control dendrite maintenance.

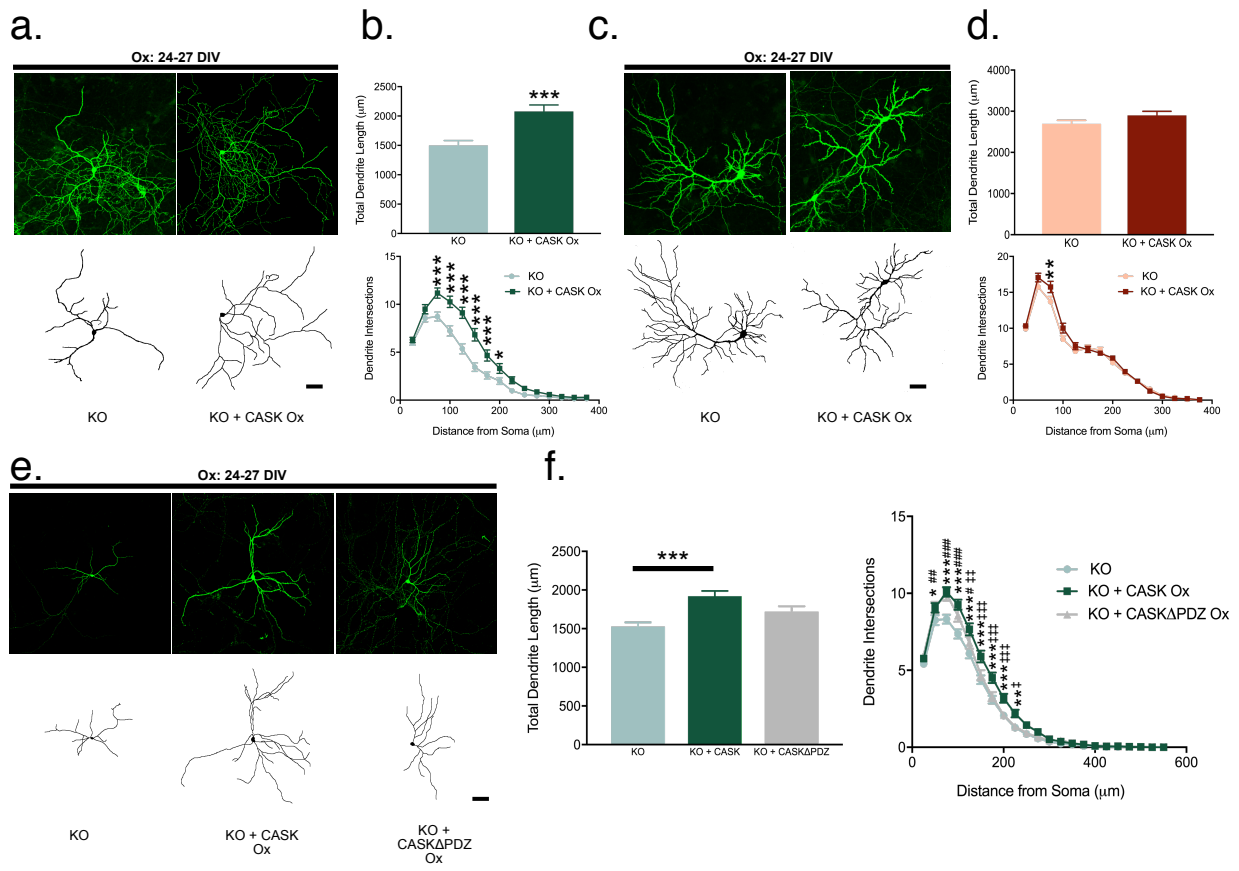


**Figure 3.13. CASK mediates CNTNAP2-dependent interneuron dendrite stabilization in *Cntnap2* KO neurons.** (a) Representative images of 27 DIV KO mouse interneurons transfected (24-27 DIV) with either GFP + mCherry (KO) or GFP + CASK-mCherry (KO + CASK Ox) (scale bar = 50 $\mu$m) and (b) respective quantification of total dendrite length and Sholl (KO: n = 57 cells from 4 cultures; KO + CASK Ox: 50 cells from 4 cultures). (c) Representation and (d) analysis of KO mouse pyramidal cells under the same conditions (scale bar = 50 $\mu$m; KO and KO + CASK Ox: n = 49 cells from 3 cultures). (e) Representative confocal images of 27 DIV KO mouse interneurons transfected (24-27 DIV) with GFP + mCherry (KO), GFP + CASK-mCherry (KO + CASK Ox), or GFP + CASKΔPDZ-mCherry (KO + CASKΔPDZ Ox) (scale bar = 50 $\mu$m). (f) Quantification of (e) using total dendrite length and Sholl (KO: n = 163 cells from 10 cultures; KO + CASK Ox: n = 144 cells from 10 cultures; KO + CASKΔPDZ Ox: n = 130 cells from 10 cultures; for Sholl, * compares KO vs KO + CASK Ox, # compares KO vs. KO +

CASKΔPDZ Ox and ‡ compares KO + CASK Ox vs. KO + CASKΔPDZ Ox). Values are means ± SEM; * P≤0.05, ** P≤0.01, *** P≤0.001 (also applies for # and ‡); Mann-Whitney test (total dendrite length; b), Student's *t*-test (total dendrite length; d), Kruskal-Wallis test with Dunn's correction (total dendrite length; f), Two-way ANOVA with Bonferroni's correction (Sholl; b, d, f).

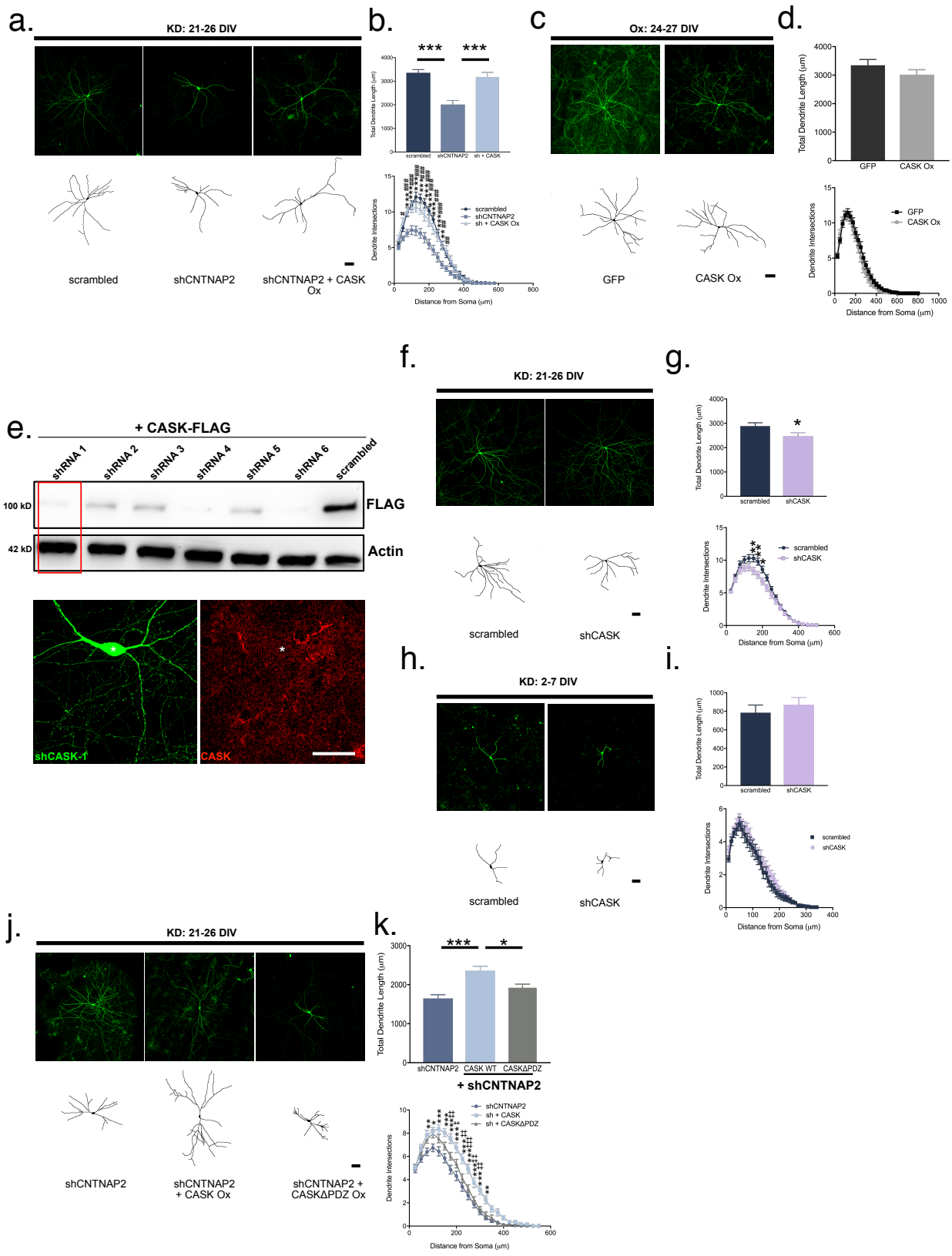
a.
KD: 21-26 DIV
scrambled
shCNTNAP2
shCNTNAP2 + CASK Ox
b.
***
***
Total Dendrite Length (μm)
scrambled
shCNTNAP2
sh + CASK
Dendrite Intersections
scrambled
shCNTNAP2
sh + CASK Ox
Distance from Soma (μm)
c
Ox: 24-27 DIV
GFP
CASK Ox
d.
Total Dendrite Length (μm)
GFP
CASK Ox
Dendrite Intersections
GFP
CASK Ox
Distance from Soma (μm)
e.
+ CASK-FLAG
shRNA 1
shRNA 2
shRNA 3
shRNA 4
shRNA 5
shRNA 6
scrambled
100 kD
FLAG
42 kD
Actin
shCASK-1
CASK
f.
KD: 21-26 DIV
scrambled
shCASK
g.
Total Dendrite Length (μm)
*
scrambled
shCASK
Dendrite Intersections
scrambled
shCASK
Distance from Soma (μm)
h.
KD: 2-7 DIV
scrambled
shCASK
i.
Total Dendrite Length (μm)
scrambled
shCASK
Dendrite Intersections
scrambled
shCASK
Distance from Soma (μm)
j.
KD: 21-26 DIV
shCNTNAP2
shCNTNAP2 + CASK Ox
shCNTNAP2 + CASKΔPDZ Ox
k.
***
*
Total Dendrite Length (μm)
shCNTNAP2
CASK WT
CASKΔPDZ
+ shCNTNAP2
Dendrite Intersections
shCNTNAP2
sh + CASK
sh + CASKΔPDZ
Distance from Soma (μm)

**Figure 3.14. CASK mediates CNTNAP2-dependent interneuron dendrite stabilization in shCNTNAP2 neurons.** (a) Representative images of rat interneurons transfected (21-26 DIV) with either scrambled + mCherry (scrambled), shCNTNAP2 + mCherry (shCNTNAP2), or shCNTNAP2 + CASK-mCherry (shCNTNAP2 + CASK Ox) at 26 DIV (scale bar = 50 $\mu$m) and (b) quantification of total dendrite length and Sholl in resulting conditions (scrambled: n = 30 cells from 4 cultures; shCNTNAP2: n = 34 cells from 4 cultures; shCNTNAP2 + CASK Ox: n = 31 cells from 4 cultures; for Sholl, * compares scrambled vs. shCNTNAP2, # compares shCNTNAP2 vs. shCTNAP2 + CASK Ox). (c) Representative images of rat interneurons transfected (24-27 DIV) either with GFP + mCherry (GFP) or GFP + CASK-mCherry (CASK Ox) at 27 DIV (scale bar = 50 $\mu$m) and (d) quantification (GFP: n = 28 cells from 3 cultures; CASK Ox: n = 34 cells from 3 cultures). (e) Cropped western blot (top) showing the efficacy of several shCASK hairpins on the expression of a CASK-FLAG plasmid in HEK293T cells, with shRNA-1 (the shRNA used for all knockdown experiments) being one of the most potent (red box). Representative image (bottom) demonstrating how transfected shCASK (21-26 DIV; asterisk delineates transfected cell soma) affects endogenous CASK expression in 26 DIV mature rat interneurons (scale bar = 25 $\mu$m). (f) Representative images of rat interneurons transfected (21-26 DIV) with either scrambled or shCASK at 26 DIV (scale bar = 50 $\mu$m) and (g) quantification of total dendrite length and Sholl in respective conditions (scrambled: n = 55 cells from 3 cultures; shCASK: n = 51 cells from 3 cultures). (h) Representative images of rat interneurons transfected (2-7 DIV) with either scrambled or shCASK at 7 DIV (scale bar = 50 μm) and (i) quantification of total dendrite length and Sholl in respective conditions (scrambled: n = 41 cells from 3 cultures; shCASK: n = 49 cells from 3 cultures). (j) Representative images of rat interneurons transfected (21-26 DIV) with either shCNTNAP2 + mCherry (shCNTNAP2), shCNTNAP2 + CASK-mCherry (shCNTNAP2 + CASK Ox), or shCNTNAP2 + CASKΔPDZ-mCherry (shCNTNAP2 + CASKΔPDZ Ox) at 26 DIV (scale bar = 50 $\mu$m) and (k) quantification of total dendrite length and Sholl in resulting conditions (shCNTNAP2: n = 57 cells from 3 cultures; shCNTNAP2 + CASK Ox: n = 52 cells from 3 cultures; shCNTNAP2 + CASKΔPDZ Ox: n = 53 cells from 3 cultures; for Sholl, * compares shCNTNAP2 vs. shCNTNAP2 + CASK, ‡ compares shCNTNAP2 + CASK vs. shCNTNAP2 + CASKΔPDZ). Values are means ± SEM; * P≤0.05, ** P≤0.01, *** P≤0.001 (also applies for ‡ and #); Kruskal-Wallis test with Dunn's

correction (total dendrite length; b), Student's *t*-test (total dendrite length; d, g), Mann-Whitney test (total dendrite length; i) one-way ANOVA with Bonferroni's correction (total dendrite length; k), Two-way ANOVA with Bonferroni's correction (Sholl; b, d, g, i, k).

a.

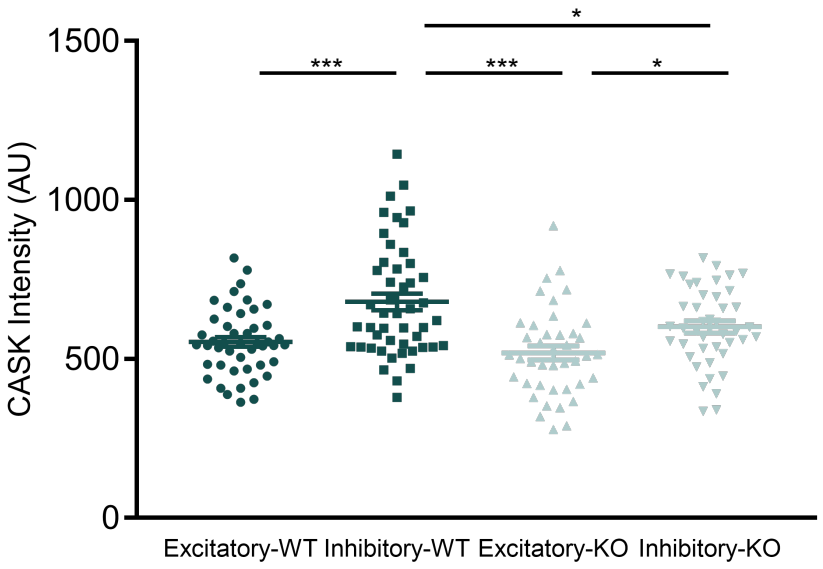


**3.15. Endogenous CASK levels of different cell types in *Cntnap2* WT and KO cultures.** (a) CASK intensity in the soma of pyramidal and inhibitory cells in *Cntnap2* WT and KO cultures (WT pyramidal: n = 46 cells from 3 experiments; WT inhibitory: n = 48 cells from 3 experiments; KO pyramidal: n = 41 cells from 3 experiments; KO inhibitory: n = 43 cells from 3 experiments). Values are means ± SEM; * P≤0.05, *** P≤0.001. One-way ANOVA with Bonferroni's correction (a).

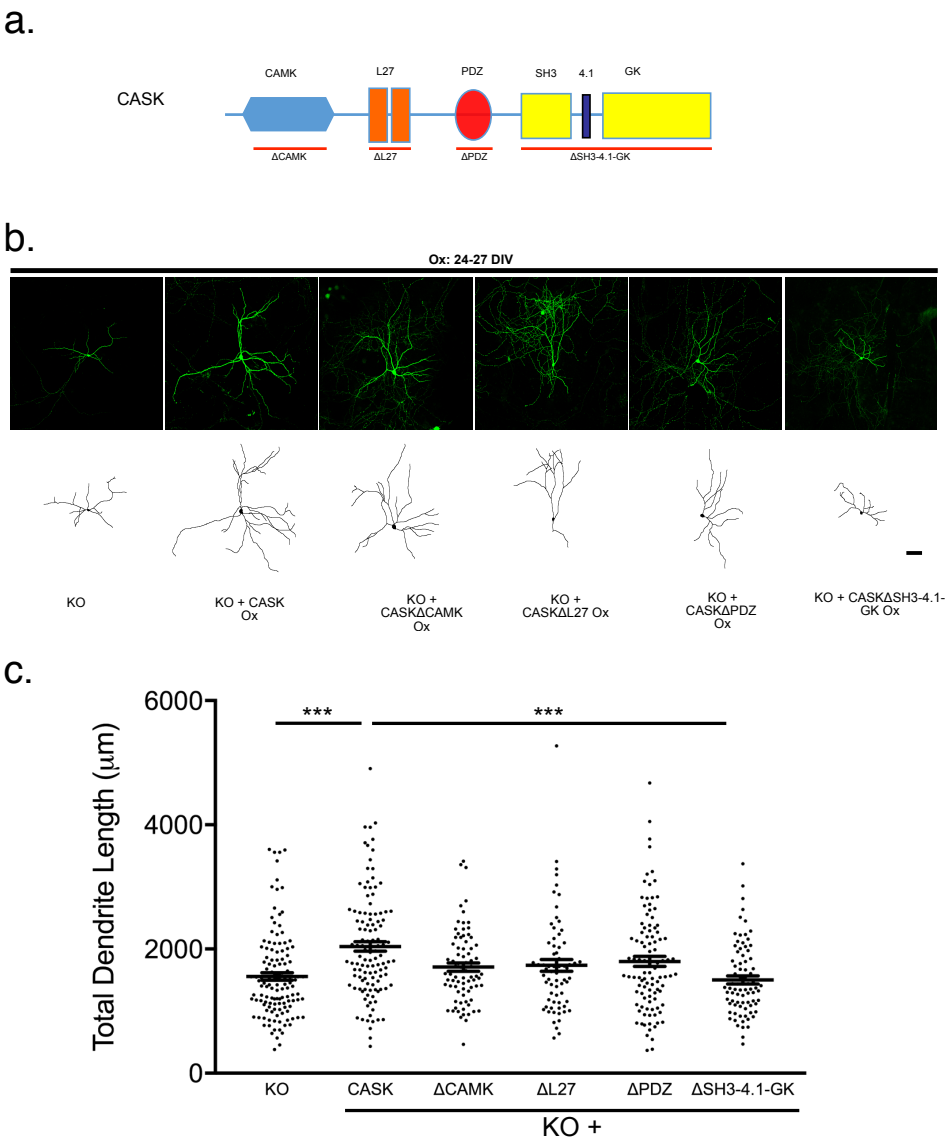


**Figure 3.16. CASK Domain Mapping in *Cntnap2* KO interneurons.** (a) Schematic of CASK domain truncations (red lines). (b) Representative images (scale bar = 50 μm) of 27 DIV KO mouse interneurons transfected (24-27 DIV) with GFP + mCherry (KO), GFP + CASK-mCherry (KO + CASK Ox), GFP + CASKΔCAMK-mCherry (KO + CASKΔCAMK Ox), GFP + CASKΔL27-mCherry (KO + CASKΔL27 Ox), GFP + CASKΔPDZ-mCherry (KO + CASKΔPDZ Ox), GFP + CASKΔSH3-4.1-GK-mCherry (KO + CASKΔSH3-4.1-GK Ox) and (c) quantification of total dendrite length (n = 69-127 cells from 4 independent experiments). Values are means ± SEM. *** P≤0.001; Kruskal-Wallis test with Dunn's correction (c).

3.16. CNTNAP2 and CASK cortical expression time course *in vivo*.

To validate the above findings in intact mouse brain, we analyzed brains of *Cntnap2* WT and KO mice. We first confirmed *in vivo* the age-dependent increase of CNTNAP2 (P0: 1 ± 0.4 vs. 4 mos: 23.1 ± 4.4) and CASK (P0: 1 ± 0.1 vs. 4 mos: 1.9 ± 0.1) (Figure 3.17a-b). We then crossed *Cntnap2* WT and KO mice with an interneuron-specific reporter *Gad1-eGFP* transgenic line (Figure 3.19a) to examine interneuron morphology *in vivo*[195].

3.17. *Cntnap2* KO mice have normal cortical PV+ interneuron electrophysiological properties and arborization in layer II/III mPFC *in vivo* at 1 month.

For initial characterization of *Gad1-eGFP* Het; *Cntnap2* WT and KO mice, we decided to examine layer II/III of the medial prefrontal cortex at 1 month. *Cntnap2* KO mice have social deficiencies – a trait controlled by the medial prefrontal cortex (mPFC) – at 1 month, with optogenetic stimulation of mPFC PV interneurons sufficient to reverse this phenotype[133]. We patched 250 μm brain slices, injected biocytin, and recorded inherent membrane properties. Because the *Gad1-eGFP* labeled all types of interneurons (data not shown), we focused on PV-specific interneurons by making sure the cells were fast-spiking (data not shown). We found no changes in total dendrite length and only a modest difference in complexity between the two genotypes (WT: 496.4 ± 51.6 μm vs. KO: 459 ± 39.7 μm; Figure 3.18a). Consistently, input/output function and membrane capacitance, two electrophysiological parameters of neuronal structure, are unaltered (Figure 3.18b-c). Taken together, our data suggests no intrinsic or arbor deficits between *Cntnap2* WT and KO layer II/III mPFC PV interneurons at 1 month.

a.

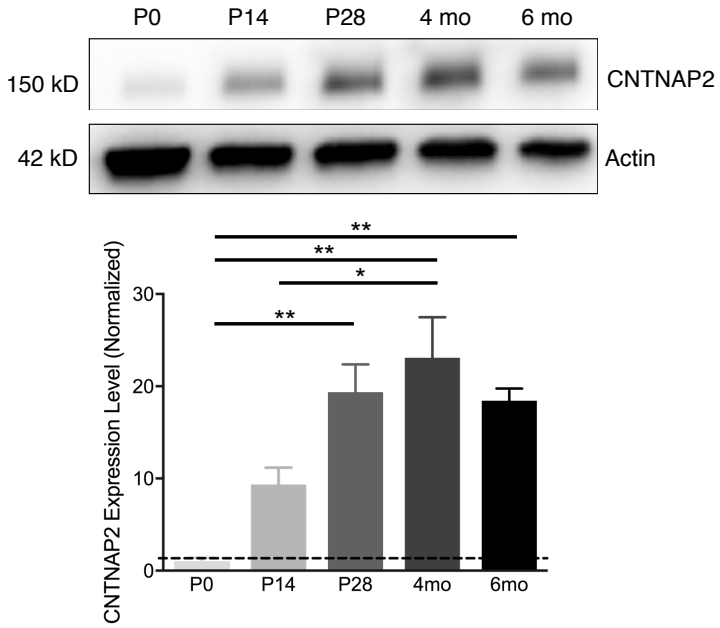
P0
P14
P28
4 mo
6 mo
150 kD
CNTNAP2
42 kD
Actin
**
**
*
**
CNTNAP2 Expression Level (Normalized)
30
20
10
0
P0
P14
P28
4mo
6mo

b.

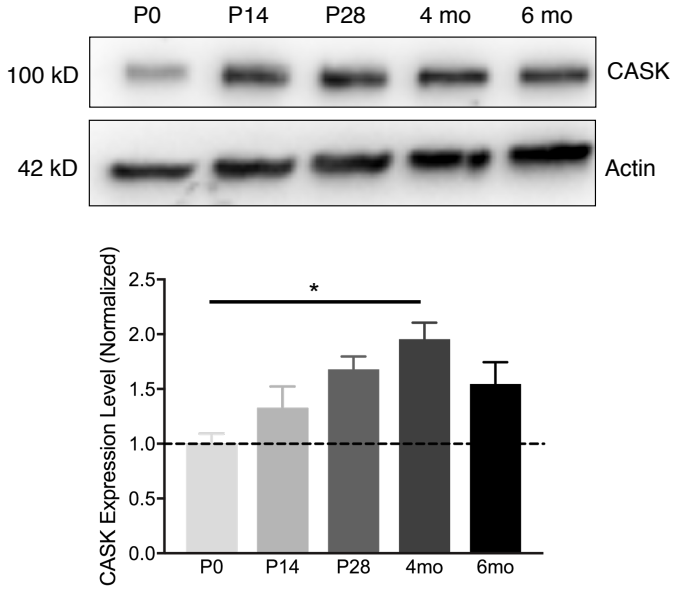
P0
P14
P28
4 mo
6 mo
100 kD
CASK
42 kD
Actin
*
CASK Expression Level (Normalized)
2.5
2.0
1.5
1.0
0.5
0.0
P0
P14
P28
4mo
6mo

**3.17. CNTNAP2 and CASK cortical expression time course *in vivo*.** (a) Cropped western blot demonstrating *in vivo* time course of CNTNAP2 expression in the cortex of P0, P14, P28, 4 months, and 6 months WT mice (n = 3 brains per time point). (b) Cropped western blot demonstrating *in vivo* time course of CASK expression in the cortex of P0, P14, P28, 4 months, and 6 months WT mice (n = 3 brains per time point). Values are means ± SEM. * P≤0.05, ** P ≤0.01, *** P ≤0.001; one-way ANOVA with Bonferroni's correction (a, b).

3.18. *Cntnap2* KO mice have normal pyramidal cell, but reduced cortical GABAergic interneuron dendrite arborization in layer IV and V, but not interneurons in layer II/III, of the cingulate cortex/M2 *in vivo* at 5 months

As our initial investigations yielded no significant results, we decided to change the conditions of our experiments. Because recent publications have shown that *Cntnap2* KO mice develop spontaneous seizures at 6 months[110], we then decided to analyze 5 month-old mice, an age immediately preceding seizure onset. Because adult male KO mice have documented local hypo-connectivity in the cingulate cortex and surrounding motor regions[196], we focused our analysis on the cingulate cortex/M2 areas (Figure 3.19b). Confocal imaging of 80 μm slices revealed a significant difference in the total dendrite length and complexity between WT and KO interneurons in layers IV and V (WT: 877.3 ± 44.2 μm vs. KO: 684.9 ± 41.5 μm; Figure 3.19c-d). Surprisingly, these changes were region-specific, as layer II/III of the same area of the same mice revealed no differences (WT: 843.9 μm ± 33.1 vs. KO: 838 ± 28.6 μm; Figure 3.19e-f). Furthermore, we found no changes in excitatory dendrite arborization in layer IV and V as well (WT: 1339 ± 71.2μm vs. KO: 1231 ± 73.9μm; Figure 3.20a-c).

3.19. CASK is mislocalized in cortices of *Cntnap2* KO mice *in vivo.*

In parallel, we detected reduced CASK protein abundance in KO cortical membrane fractions as compared to WT (KO:10% membrane decrease; Figure 3.21a-b). In summary, our data confirm *in vitro* findings (Figure 3.9), and reveal inhibitory circuit architectural deficits and CASK mislocalization in adult *Cntnap2* KO mice.

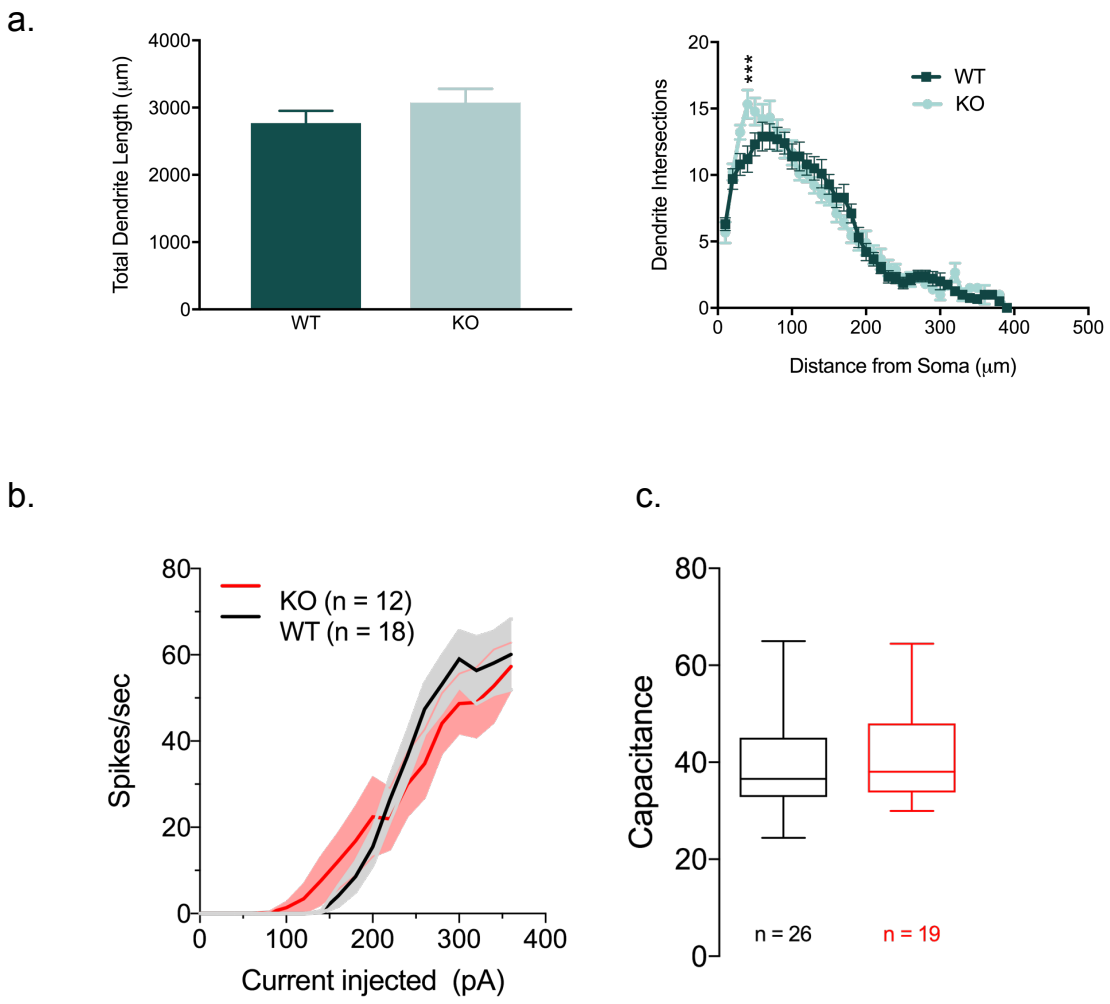


**3.18. *In vivo* morphological analysis of mPFC PV+ interneurons in 1 month *Gad1-GFP* Het; *Cntnap2* WT or KO mice.** (a) quantification of total dendrite length and (b) Sholl in *Gad1-eGFP* Het; *Cntnap2* WT or KO mice (n = 10-11 cells from 5-7 mice). Electrophysiological measurements of structural properties of layer II/III mPFC PV interneurons including (b) I/O curves (n = 12-18 cells from 5-7 mice) and (c) capacitance (n = 19-26 cells from 5-7 mice). Values are means ± SEM; *** P≤0.001; Mann-Whitney test (c, total dendrite length; a), Two-way ANOVA with Bonferroni's correction (b, Sholl; a).

3.20. Discussion.

Clinical[104, 107], electrophysiological[182, 183], and behavioral[110, 133] studies of CNTNAP2 have converged upon inhibitory neurons as key cellular, functional, and pathological substrates. However, the molecular mechanisms underlying these processes are not understood. Here, we show that CNTNAP2 participates in the stabilization of already-formed interneuron dendritic trees. This is, at least in part, mediated by the interaction of CNTNAP2's intracellular C-terminus with CASK's PDZ domain at the plasma membrane. The spatial distribution of CNTNAP2 along the dendritic tree may have a substantial contribution to dendrite stabilization. Loss of CNTNAP2 leads to simplified dendrites on GABAergic interneurons in layer IV and V of the cingulate/M2 regions of adult mouse brain. Our data provide new insight into the regulation of interneuron dendrite stabilization by two prominent neurodevelopmental disorder risk genes.

The establishment of the dendritic tree is a complex process with several distinct steps – neurite outgrowth, dendrite extension and branching, and arbor stabilization – each governed by a unique set of cell-intrinsic and extrinsic factors[186]. While much is known about the mechanisms underlying pyramidal neuron dendrite arborization[197], far less information exists on their inhibitory counterparts. Similarly, much is known about neuron dendrite outgrowth, but relatively little about stabilization.

Here we report an inhibitory-specific, age-dependent, and cell-autonomous simplification of dendritic arbors in *Cntnap2* KO neurons. We validated these findings respectively by analyzing neighboring GABA-negative pyramidal counterparts, by experimentation in younger neurons, and by reversing the deficit with recombinant CNTNAP2. In addition, acute CNTNAP2 knockdown

a.

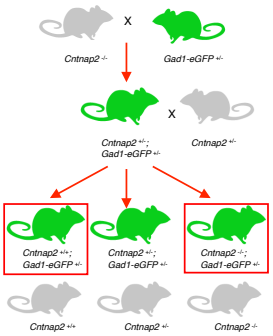
x
Cntnap2 -/-
Gad1-eGFP +/-
x
Cntnap2 +/-;
Gad1-eGFP +/-
Cntnap2 +/-
Cntnap2 +/+;
Gad1-eGFP +/-
Cntnap2 +/-;
Gad1-eGFP +/-
Cntnap2 -/-;
Gad1-eGFP +/-
Cntnap2 +/+
Cntnap2 +/-
Cntnap2 -/-

b.

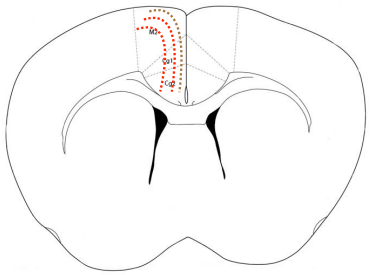

c.

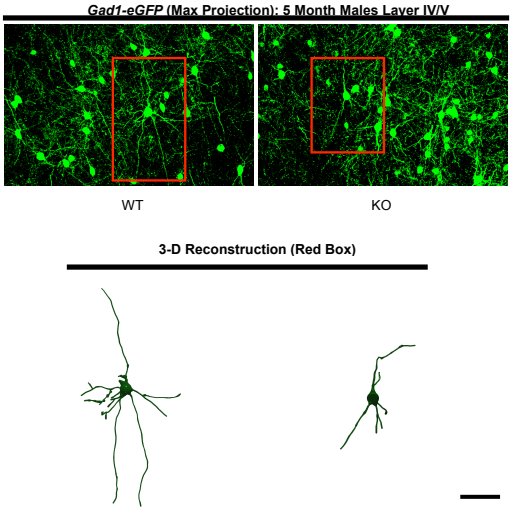
Gad1-eGFP (Max Projection): 5 Month Males Layer IV/V
WT
KO
3-D Reconstruction (Red Box)

d.

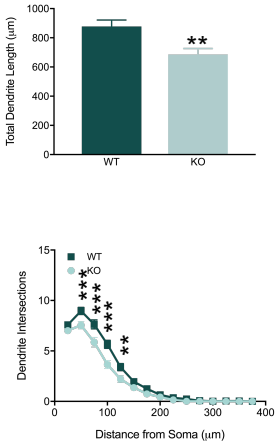
Total Dendrite Length (μm)
1000
800
600
400
200
0
**
WT
KO
Dendrite Intersections
15
10
5
0
WT
KO
***
***
**
0
100
200
300
400
Distance from Soma (μm)

e.

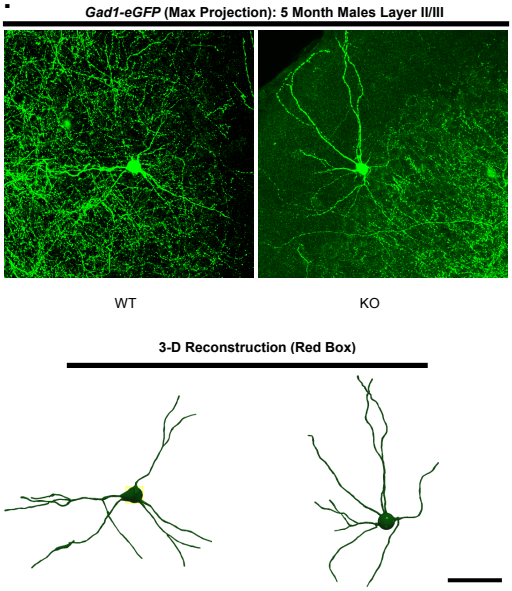
Gad1-eGFP (Max Projection): 5 Month Males Layer II/III
WT
KO
3-D Reconstruction (Red Box)

f.

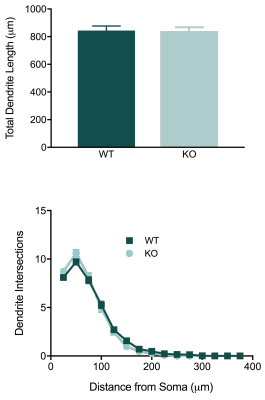
Total Dendrite Length (μm)
1000
800
600
400
200
0
WT
KO
Dendrite Intersections
15
10
5
0
WT
KO
0
100
200
300
400
Distance from Soma (μm)

**Figure 3.19. *Cntnap2* KO mice have reduced cortical interneuron dendrite arborization in layer IV and V, but not layer II/III in M2/Cingulate Cortex.** (a) Breeding scheme for *Gad1-GFP*; *Cntnap2* WT/KO mice. (b) Brain map, with double red lines and red/brown lines showing the location of layer IV and V and layer II/III and respectively in Cingulate and M2 regions. (c) Representative and 3-D reconstructed images of interneurons *in vivo* from layers IV and V of M2 and Cingulate Cortex in 5-month old male *Gad1-GFP* Het; *Cntnap2* WT/KO mice (scale bars = 50 $\mu$m) and (d) quantification of total dendrite length and Sholl (WT: n = 55 cells from 3 mice; KO: n = 51 cells from 3 mice). (e) Representative and 3-D reconstructed images of interneurons *in vivo* from layers II/III of M2 and Cingulate Cortex in 5-month old male *Gad1-GFP* Het; *Cntnap2* WT/KO mice (scale bars = 50 $\mu$m) and (f) quantification of total dendrite length and Sholl (WT = 44 cells from 3 mice; KO = 34 cells from 3 mice). Values are means $\pm$ SEM; ** P≤0.01, *** P≤0.001; Mann-Whitney test (total dendrite length; d), Student's *t*-test (total dendrite length; f), Two-way ANOVA with Bonferroni's correction (Sholl; d, f).

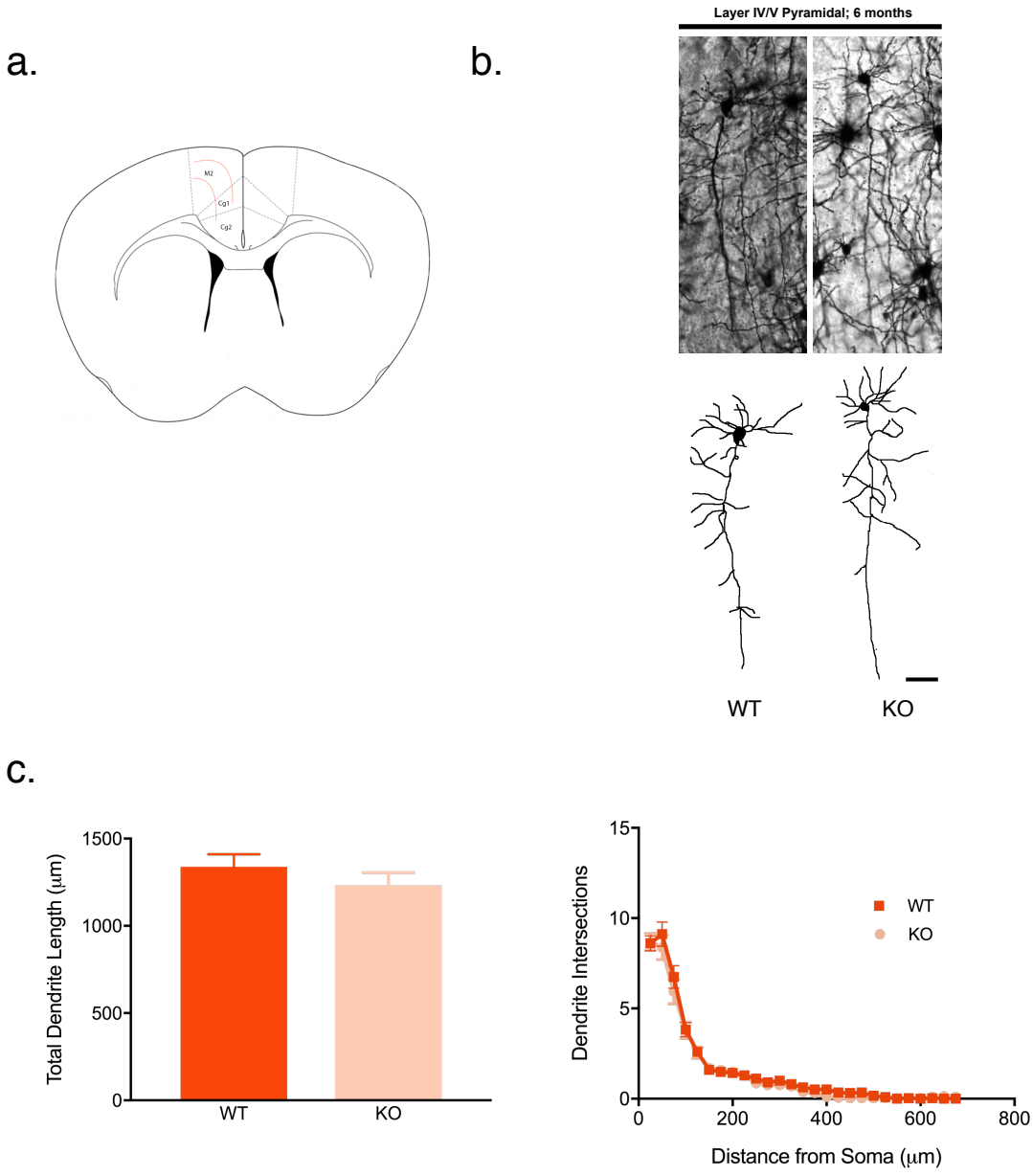


**Figure 3.20. *In vivo* analysis of cortical pyramidal neurons in *Cntnap2* WT/KO mice.** (a) Brain map, with red lines showing the location of layers IV and V in Cingulate and M2 regions. (b) Representative images of Golgi-stained pyramidal neurons *in vivo* from layers IV and V of M2 and Cingulate Cortex in 6-month old WT or KO mice (scale bar = 50 μm) and (c) quantification of total dendrite length and Sholl (WT: n = 35 cells from 4 mice; KO: n = 29 cells from 4 mice). Values are means ± SEM. Student's *t*-test (total dendrite length; c), Two-way ANOVA with Bonferroni's correction (Sholl; c).

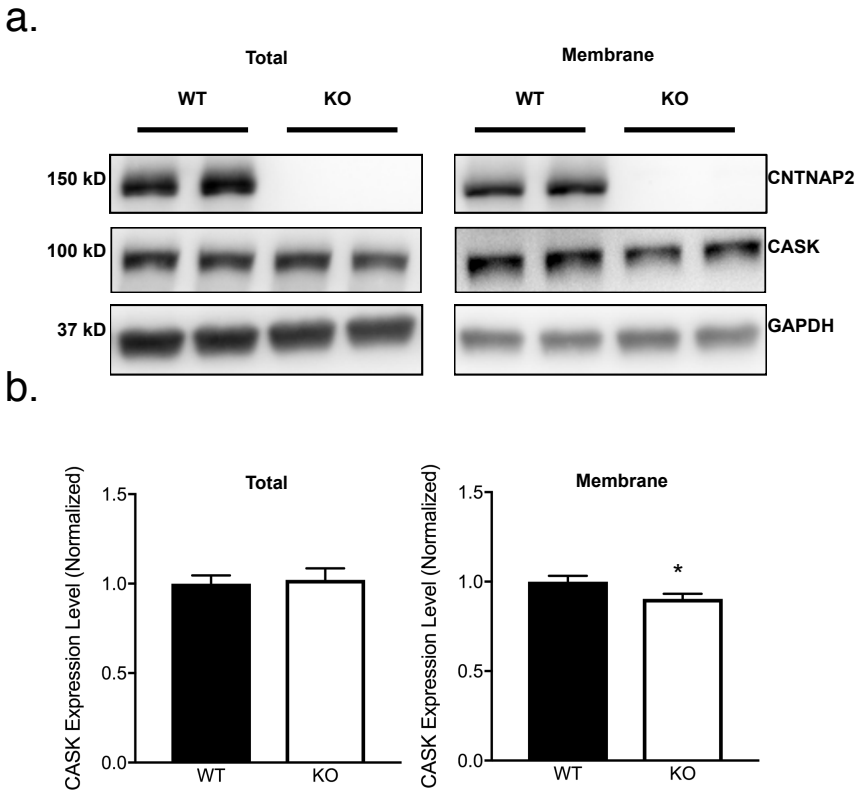


**Figure 3.21. Reduced CASK levels in membrane fractions of Cntnap2 KO cortices.** (a) Representative cropped western blots showing CASK levels in *Cntnap2* WT/KO cortical total homogenate and crude membrane fraction. GAPDH was used as a marker to determine membrane fractionation efficiency. (b) Quantification of (a) (total: n = 12 brains per genotype; membrane: n = 13 brains per genotype). Values are means ± SEM; * $P \leq 0.05$; Mann-Whitney test (total homogenate; b), Student's *t*-test (membrane fraction; b).

during a period when dendritic arbors are fully developed faithfully reproduced these observations, further supporting a role in dendrite stabilization. Finally, *in vivo* validation confirmed simplified GABAergic interneuron dendrites in adult KO mice. These data suggest CNTNAP2 plays a late-acting role in interneuronal development, which may explain why symptoms such as language regression and epilepsy have relatively delayed emergence in some clinical cases[104, 181]. Moreover, an age-dependent destabilization of interneuronal dendrites may also provide a cellular explanation for the occurrence of abnormal IPSCs only in adult KO mice[182, 183], as changes in GABAergic morphological complexity may affect inhibitory output. Our data represent, to our knowledge, the first report of an interneuron-specific mechanism for dendrite stabilization.

Intriguingly, a previous paper by Anderson et al. reported that CNTNAP2 RNAi-mediated knockdown results in reduced arborization in pyramidal neurons[131]. Here, we used mature *Cntnap2* KO mouse neurons, a model that is more pertinent to the phenotypes observed in brain slices of KO mice, where inhibitory circuits are affected but excitatory circuits are largely unaffected[182, 183]. We have shown previously that CNTNAP2 has a role in the maintenance of dendritic spines in pyramidal neurons[157], indicating that it has different functions at different stages of development, in different neuronal types. Importantly, all of these cell types and cellular structures have been implicated in the pathogenesis of disorders linked to CNTNAP2.

SIM and STED imaging provide superior spatial resolution compared to conventional microscopy, allowing for unprecedented insight into the neuronal nanoscale architecture[188, 189]. SIM imaging has been previously used to investigate how subcellular localizations of synaptic molecules affect spine morphology[198] and synapse remodeling[199] in pyramidal cells, but has not yet been utilized to

explore dendrite regulatory mechanisms in interneurons. Here, we employed SIM and STED to establish relationships between the distribution of CNTNAP2 nanostructures and detailed dendrite architectural features of interneurons. While confocal microscopy showed CNTNAP2 to be concentrated along primary dendritic branches, super-resolution imaging resolved branch-specific "bead"-like patterns of CNTNAP2 puncta. These features are found at high abundance in primary branches, but at much lower frequencies along distal dendrites. Remarkably, acute CNTNAP2 knockdown caused a loss of peripheral "bead"-like patterns along with reduced branch length, while having relatively less effect on proximal ones, suggesting a close relationship between the spatial location of CNTNAP2 nanostructures and branch stability. This and other emerging data[198, 199] reveal that investigating the detailed subcellular localization of disease-relevant molecules may provide novel insight into their function.

Clinical findings implicate the C-terminus of CNTNAP2 – a sequence entirely conserved across human/rat/mouse species – in neurodevelopmental disorders with epilepsy comorbidity. A homozygous deletion in *CNTNAP2 (I1253X)* causing premature termination, and thus absence of the C-terminus, was found in Amish children with CDFE[104]. Temporal-lobe specimens of these patients showed abnormalities of neuronal structure[104]. Deletion of the C-terminal domain was also found in several patients with epilepsy and ID[95]. Despite this, only a few intracellular protein interactors of CNTNAP2 have been characterized: the cytosolic tail is phosphorylated by protein kinase C to control protein endocytosis[129] and complexes with protein 4.1B, a cytoskeletal structural protein[123], to cluster potassium channels at the juxtaparanodes[200].

We identified a novel mechanism for intracellular signaling by CNTNAP2 through CASK. CASK is a multi-domain cytoskeletal scaffold found in multiple neuronal compartments, including pre-synaptic termini, dendritic spines, dendrites, and the nucleus, where it coordinates signal transduction pathways at the cytoskeleton, leading to regulation of neurotransmission[201], spine maintenance[194], receptor trafficking[162], and transcription of synaptic proteins[202]. While CASK has previously been shown to co-immunoprecipitate with CNTNAP2[137], here we demonstrate that the interaction is direct and is crucial for interneuron dendrite regulation. Functionally, CNTNAP2 recruits and stabilizes CASK at the plasma membrane through PDZ interactions and CNTNAP2 loss leads to overall reduction and redistribution of CASK. Our data also suggest CNTNAP2 acts upstream of CASK, as manipulation of CASK abundance does not affect CNTNAP2 distribution. CASK may regulate dendrite morphology at the membrane through several potential mechanisms, including phosphorylation (CAM-kinase domain)[146], interactions with SAP97 (L27 domain)[144, 164], cytoskeletal binding (protein 4.1 binding site)[194], and/or nuclear translocation/transcription (GK domain)[145].

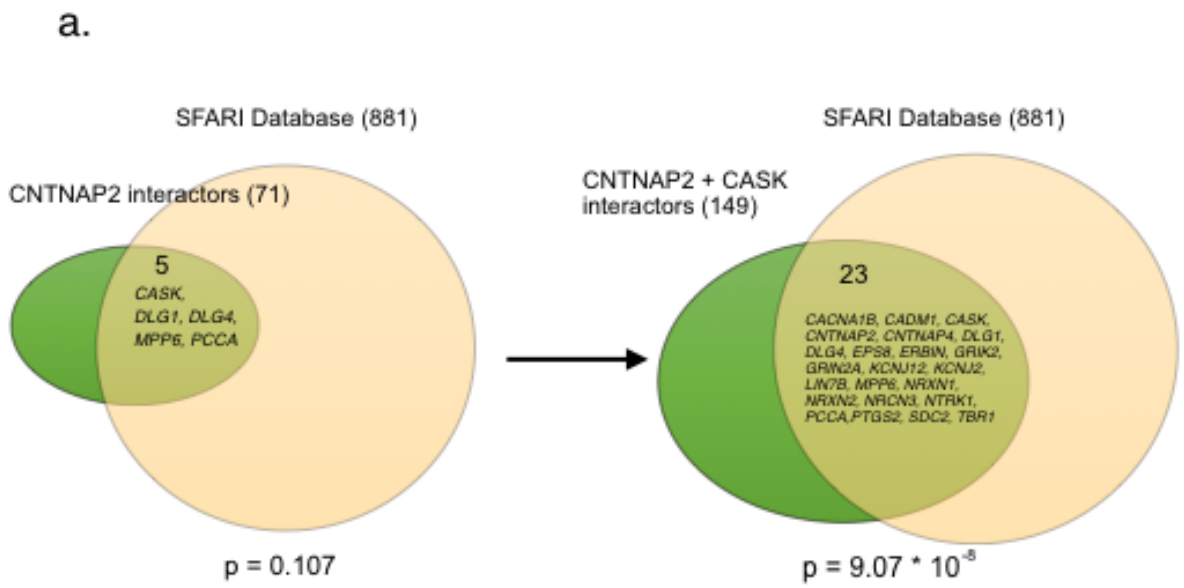


**Figure 3.22. CNTNAP2/CASK bioinformatics analysis.** (a) Venn diagram showing overlap of either CNTNAP2 interactors alone (left) or CNTNAP2 + CASK interactors (right) with the SFARI database. Numbers indicate the number of genes in each group. P values represent the significance of overlap via hypergeometric probability tests.

# DISCUSSION

## 4.1. Introduction

Interneurons, despite being numerically inferior to their excitatory counterparts, regulate pyramidal cells through highly spatiotemporal inhibitory synapses. These precise connections result in different frequencies of oscillatory excitatory rhythms, each of which is important for a particular aspect of cognition and behavior[203, 204]. Interneurons have a drastically different development than pyramidal cells: they originate in the sub-pallium and migrate into the pallium over the course of embryonic and post-natal development, where they integrate themselves into highly efficient cortical networks[27]. The importance of fully understanding the mechanisms of this process – particularly how interneurons migrate into the cortex, differentiate into distinct subtypes, and maintain their properties – has never been as relevant as today, due largely to the massive amount of genetic data that have become available in the past decade.

For example, multiple GWAS studies have consistently demonstrated complex neuropsychiatric diseases such as schizophrenia and autism share not only common genetic disruptions, but that many of these molecules are involved with interneuron development[4, 169, 205]. More specifically, multiple studies consistently implicate PV+ interneurons as a pathological cause of both conditions[88], while epilepsy – a condition that involves a chronically hyperactive state – is highly comorbid with autism[71]. Similarly, genetic analyses revealed many of the epileptic genes have roles in interneuron development and function[206]. Given the prominent role of interneuron genetics in a wide range of neuropsychiatric diseases, two critical questions – 1). figuring if/how disease genes physiologically contribute to interneuron formation and maintenance and 2). understanding how disruptions in these genes can specifically contribute to the pathophysiology

of certain mental diseases – must be answered. The solution requires years of careful molecular, electrophysiological, animal model, and human studies to seamlessly converge.

A prime example of this revelation is the discovery of *CNTNAP2* as a psychiatric risk gene. While the CAM was originally thought to be a simple spatial organizer of potassium channels in the peripheral nervous system's axonal juxtaparanodes[124], its role in neuropsychiatry was revealed by a seminal study demonstrating multiple probands of an Old Order Amish family carried a homozygous *CNTNAP2* nucleotide deletion (3709delG) predicted to produce a truncated, non-functional protein. These patients had a complex but perplexingly consistent array of symptoms, including autistic-traits, refractory seizures, ID, language/behavioral regressions, as well as cortical dysplasia – now collectively known as CDFE syndrome [104]. Soon after this study, other independent cases with the same genotypic/phenotypic characteristics were identified [104, 107, 109, 181]. Finally, other research groups quickly uncovered evidence that *CNTNAP2* heterozygous point mutations, CNVs, and several SNPs were associated with SCZ, ASD, ID, and language regression[106], with some afflicted patients sharing comorbidities resembling several CDFE symptoms.

However, complicating these seemingly straightforward findings was that deleterious heterozygous mutations have also been identified in unaffected individuals[102, 103]. Thus, the mutation type and/or genetic background may determine the extent of heterozygous disruption, thereby suggesting heterozygous mutations are far less penetrant and may contribute to disease in a polygenic manner. In line with this theory, animal studies reported spontaneous seizures as a highly penetrant endophenotype in KO *Cntnap2* models (mice, rat, and zebrafish)[110, 132, 207], but

much less so in heterozygotes. Taken together, this suggests a dose-dependent effect of CNTNAP2 on cognitive function through disruption of E/I balance. Yet, specific mechanisms for how this is achieved are highly underdeveloped.

This thesis attempts to ascertain how CNTNAP2 pathology can lead to E/I imbalance. While CNTNAP2's function at excitatory synapses in pyramidal neurons have been relatively well-documented[131, 157, 208], here we discover an interneuron-specific deficit in dendrite maintenance, but not outgrowth, in *Cntnap2* KO cultures. To ascertain a mechanism, we then validate and characterize several genuine CNTNAP2 interactors derived from an unbiased yeast two-hybrid screen. Using *Cntnap2* KO mouse cultures, we then discover that CNTNAP2 regulates interneuron dendrite maintenance through the MAGUK scaffold CASK. Our findings provide a possible mechanism to explain CNTNAP2-associated endophenotypes such as seizures: reduced expression or damaging mutations in CNTNAP2 might interfere with interneuron dendrite stabilization, which in turn may cause greater seizure susceptibility or altered information transfer from decreased inhibitory drive and overall increased circuit excitability. While these results may represent only a small functional aspect of an incredibly complex protein, it provides a theory for the cortical hyperexcitability prevalent in both animal models and patient populations.

## 4.2. CNTNAP2 regulation and interneuron specificity

While the current literature focuses on CNTNAP2 in development[98, 110, 131], there is strong evidence of its role in neuronal maturation. Our work shows via biochemical analysis that CNTNAP2 increases in cortical abundance over time (Figure 3.1a, Figure 3.17a), a finding

corroborated by an independent study examining spatiotemporal CNTNAP2 expression via a *CNTNAP2-LacZ* knock-in model[114]. Moreover, CNTNAP2 is important for spine maintenance, but not formation, in pyramidal cells[208] and cell-autonomously regulates PV+ interneuronal maturation[134]. Genetic and shRNA mediated perturbation of CNTNAP2 via KO and knockdown models respectively show no changes in dendritic arborization during the neurite outgrowth period[157] (Figure 3.2, Figure 3.5d-e). CNTNAP4, a close family member, also increases in abundance over time specifically in PV interneurons[209]. Thus, while CNTNAP2 appears to have a role in embryonic migration and development, a plethora of evidence points to responsibilities in circuit maturation, which may explain the regression of normal behavior in some clinical cases of patients with *CNTNAP2* mutations[104].

We and others also find that CNTNAP2 is more highly abundant in interneurons relative to pyramidal counterparts in mature primary cultures[187] (Figure 3.6). Since little literature currently exists as to how CNTNAP2 is regulated, it is unknown how cell-specific CNTNAP2 abundancies are achieved. Thus far, only four transcription factors – STOX1A, TCF4, FOXP2, and FOXP1 – have been shown to regulate CNTNAP2 expression[86, 92, 100, 210]. Intriguingly, some of these transcription factors (STOX1A and FOXP2) bind within the first intronic region of the gene, suggesting intron 1 is a critical regulatory region for CNTNAP2 expression[106]. Indeed, deletions within this region have also been reported[96, 111]. Hence, the relationship between human intragenic mutations and CNTNAP2-regulating transcription factors, as well as the consequential changes of CNTNAP2 expression between cell types, should be further explored.

A proteomics search revealed that FOXP1 has 3-fold higher abundance in pyramidal cells than interneurons while TCF4 has over a three-fold higher abundance in interneurons and may be involved in interneuronal migration[187, 211]. Luciferase assays reveal TCF4 upregulates CNTNAP2 expression[212] while FOXP1 downregulates it[92]. From this, we hypothesize that within each neuronal class, differing amounts of different transcription factors compete with one another for binding to promoter or intronic regions, which ultimately determines expression disparity between cell types. Since most of these published studies were performed in cell lines, more definitive spatiotemporal studies in primary culture and *in vivo*, must be performed before the nature of these relationships can be accurately determined.

4.3. CNTNAP2 and interneuronal diversity

Our work provides strong evidence that genetic disruption of *CNTNAP2* damages interneuron dendrite arbor integrity. However, the relatively low efficiency of lipofectamine transfection combined with the sparseness of GABAergic interneurons in culture makes it exceedingly difficult to study a particular subset of interneurons. We therefore do not know whether our reported interneuronal deficit is general phenomenon or specifically applicable to certain subtypes. Given the broad diversity of interneurons (for instance, the hippocampus has at least 21 different subtypes)[204], this question is critical and thus becomes a general weakness of this study. However, an elegant study by Vogt et al. showed PV+ interneuron maturation was disrupted in a cell-autonomous manner while other subtypes such as somatostatin and VIP were unaffected in *Cntnap2* KO mice. Moreover, single cell RNA sequencing from interneuron-specific Cre driver lines revealed PV+ cells to have one of the highest CNTNAP2 transcript counts relative to other subtypes postnatally[134]. Since PV+ interneurons are responsible for inducing gamma oscillations

in pyramidal cells via somatic and axon initial segment inhibition, morphological aberrancy amongst these populations would be detrimental to cognitive function and behavior. From these results, it is critical that methods of differentiating interneuronal subtypes in culture are developed so that our findings can be effectively reconciled with other discoveries from the field. One possible method is to culture primary neurons derived from *Cntnap2* WT/KO mice crossed with interneuronal-specific GFP lines.

4.4. Discrepancies between KO and knockdown techniques

Surprisingly, another paper[131] showed CNTNAP2 knockdown can also affect pyramidal arborization – a result that we were able to reproduce (data not shown) – which seemingly conflicts with our findings in the KO model, even though multiple other studies in *Cntnap2* KO mice support our findings that excitatory circuits are largely unaffected[182, 183].

However, we believe the two studies are complementary, as knockdown results in transient perturbation of CNTNAP2, while KO cultures lack the protein from embryonic genesis. The latter model, therefore, is more inclined to genetic compensatory effects while the former demonstrates the system's immediate response to acute damage. Since CNTNAP2 is more highly expressed in interneurons (Figure 3.6)[187], it is possible that *Cntnap2* KO interneurons are less prone to genetic adaptation, leading to interneuron-specific phenotypes in the KO. Our theory is backed by a recent paper demonstrating CNTNAP2 can cell-autonomously regulate electrophysiological properties in PV-interneurons and that this function is critical for interneuronal maturation[134]. On the other hand, sudden loss of CNTNAP2 via knockdown may "shock" the system, giving it little time to buffer against these insults and ultimately leading to

generalized changes in all neuronal types. Moreover, our rescue experiments only induced a partial rescue of the knockdown phenotype (Figure 3.5a-c), meaning residual off-target[213] effects are still possible[214]. Such discrepancies have been widely published and discussed in the past [215-217].

4.5. Modeling different dimensions of CNTNAP2 disruption with KO/knockdown tools

Despite the different phenotypes observed by genetic inactivation and shRNA knockdown, we believe their utilities may be useful in modeling different CNTNAP2-afflicted conditions. For instance, *Cntnap2* KO/Het mouse models have a high construct validity in replicating genetic disruptions: *Cntnap2* KO mice have been shown to recapitulate many of the major phenotypes in patients with homozygous *CNTNAP2* mutations, such as seizures, cortical dysplasia, and autistic behaviors[104, 110, 133]. Similarly, phenotypes observed in heterozygote mice are generally intermediate or nonsignificant relative to KO counterparts[110, 134, 218], which may reflect the penetrance variability of heterozygous *CNTNAP2* disruptions. For example, mutations in intron 1 – a critical regulation site for multiple transcription factors (see Chapter 4.2)[100, 219] – may affect CNTNAP2 expression more significantly than a mutation in a non-coding, non-conserved area[102]. On the other hand, a heterozygote animal is not sufficient to reflect the complexity of heterozygote human mutations, which can range from sensitive gene-dosage effects to dominant-negative loss-of-function. Thus, genetic mice harboring conditional KO/knock-ins and human-induced pluripotent stem cells (hiPSCs)/CRISPR technology need to be utilized for greater modeling precision.

Likewise, we theorize that shRNA-mediated knockdown may be useful in studying immunological conditions caused by CNTNAP2 antibodies, which are believed to temporarily disable CNTNAP2 function through disruptive binding[122]. One such instance is *in utero* exposure CNTNAP2 antibodies. Within the central nervous system, CNTNAP2 antibodies have the capability be transmitted *in utero* from mother to fetus[220] as a result of the blood-brain barrier's permeability during gestation[221]. Transmission of the antibody within this temporary window can cause elicit extensive structural and developmental damages, including simplification of pyramidal cell arborization[222]. Furthermore, a plethora of documentation exists on CNTNAP2-mediated auto-antibody neurological disorders. Here, auto-antibodies bind to VGKC-associated proteins, including CNTNAP2. The binding causes neuropathies including Issac's syndrome, Morvan's syndrome, and limbic encephalitis, with symptoms ranging from neuropathic pain and peripheral nerve hyperexcitability to cognitive decline and epilepsy[223]. The diversity of clinical cases may be spatiotemporal-selective binding events juxtaposed with high prevalence of CNTNAP2 in both the central and peripheral nervous systems. Thus, a targeted shRNA approach (i.e. injection or electroporation) can be utilized to effectively tease out the mechanistic discrepancies between the different CNTNAP2-based auto-immune syndromes.

## 4.5. Proteomics and CNTNAP2 mechanisms

Unfortunately, the literature on the molecular mechanisms of CNTNAP2 thus far has been sparse. Extracellularly, CNTNAP2 can interact with both TAG-1[115, 224] and CNTN1[118], the former of which is critical for potassium clustering. CNTNAP2 can also cluster potassium channels, bind to cytosolic adaptors, interact with multiple MAGUKs, and can be selectively endocytosed (see 1.5.4). These studies, although well-done, are not sufficient to explain the

complex phenotypes observed in both animal models and human patients with *CNTNAP2* mutations. Given the reproducibility and consistency of some endophenotypic readouts (i.e. spontaneous seizures), the field is prime for new mechanistic discoveries that can bridge the gap between cellular pathophysiology and behavioral aberrancies.

The introduction of non-biased screens such as affinity-purification mass-spectrometry (AP-MS) and yeast two-hybrid into neuroscience have uncovered a vast array of proteomics data that provide unprecedented insight into the mechanisms behind neuronal function and dysfunction. The yeast two-hybrid is a powerful tool for detecting direct protein-protein interactions by artificially tagging bait and prey proteins with transcription factors that would activate reporter genes upon binding in yeast cells. Researchers can automatically screen through millions of candidates by simply mating bait and prey-containing yeast cells. Similarly, AP-MS is a highly sensitive method that combines mass-spectrometry and pull-downs to accurate identify protein interaction partners[225]. Over the past decade, these techniques have become the foundation of high-throughput proteomics, which has revealed complex intricacies from the molecular to a system-wide level.

While these developments and trends are a boon for the field of neuroscience, one must not forget that they also have limitations. Since yeast two-hybrid assays must occur in the nucleus, the method creates an artificial environment for protein interactions, making it prone to false-positives and negatives. Protein interactions involving membrane proteins are also more difficult to detect. Furthermore, AP-MS relies on expensive equipment that not all labs can afford and results are strictly based off the quality of the reagents used (i.e. antibody, homogenate samples)

and therefore may be highly prone to background contaminants[225, 226]. Unfortunately, because of the large and sometimes ambiguous data sets that accompany these experiments, there is a need to confirm and characterize genuine interactors using multiple methods. In this work, we performed a yeast two-hybrid, thoroughly validated three candidates (CASK, PARD3, MPP6), and focused extensively on characterizing the CNTNAP2-CASK physiological relationship. Given the thorough confirmation of these candidates, our work will assist in directing CNTNAP2 proteomics in accurate directions.

4.6. CNTNAP2-CASK in disease

*CNTNAP2* has emerged as a risk gene associated with several neurodevelopmental disorders, including ID, ASD, and epilepsy. Similarly, *CASK* disruption has been established to be causative for X-linked ID, nystagmus, and microcephaly with pontine and cerebellar hypoplasia[189], and is also associated with epilepsy and ASD[147, 149]. Our findings support a model whereby disease risk molecules interact directly with each other within protein-protein-interaction networks. In addition, bioinformatics analysis shows that a combined CNTNAP2-CASK interaction module became significantly enriched with psychiatric risk genes as compared to the protein-protein interaction network built around CNTNAP2 alone, using previously known direct interactors combined with our yeast two-hybrid list (Figure 3.22a, Supplementary Table 1). The global output of these networks may regulate key cellular phenotypes, which when altered, result in disease with overlapping symptomatology. These results highlight the importance of looking beyond individual genes and into comprehensive mechanisms of molecular convergence. Elucidating the shared functions of newly identified disease-associated genes is a key step in the functional analysis of genetic findings.

Previous work has established conserved phenotypes indicative of inhibitory circuit dysfunction in KO models and human patients with *CNTNAP2* gene perturbations. Our findings provide a possible mechanism to explain these observations: reduced expression or damaging mutations in CNTNAP2 might interfere with interneuron dendrite stabilization, which in turn may cause greater seizure susceptibility or altered information transfer from decreased inhibitory drive and overall increased circuit excitability. A disparity in CNTNAP2 expression between neuronal types may be a critical factor in shaping circuit networks. Transient loss of CNTNAP2 causes a decrease in total CASK levels, while endogenous CASK is more highly expressed in interneurons – a difference that is drastically reduced in the KO model. Together, these results point to consequences of the natural discrepancy of CNTNAP2 in the expression of critical downstream factors. These differences may lead to particular aspects of circuit development that may be disrupted when CNTNAP2 is lost, ultimately serving as a possible mechanism for disease pathogenesis. Such a hypothesis may also extend to observations made *in vivo*, namely that the cortical interneurons are simplified specifically in layer IV and V but not II/III in the cingulate cortex. It is unknown how this discrepancy came about. Further studies into CASK and CNTNAP2 endogenous expression in vitro will have to be performed, but may be difficult because it appears commercial antibodies for the latter are not effective in IHC[134]. In addition, abnormal interneuron dendrite stabilization may serve as a cellular convergence point in CNTNAP2/CASK pathophysiology, thus opening up new avenues of investigation on this pathway.

# MATERIALS AND METHODS

***Antibodies and plasmids.*** A detailed antibody and primer list is presented below:

| Antibody | Species | Company | Dilution | Application | Figure |
|---|---|---|---|---|---|
| CNTNAP2 | Rabbit | Millipore (Billerica, MA, USA); AB5886-50UL | 1:2000 | WB | Figure 2.1b<br>Figure 2.3b, c<br>Figure 2.4b, d<br>Figure 3.1a<br>Figure 3.3f<br>Figure 3.4a<br>Figure 3.10d<br>Figure 3.17a<br>Figure 3.21a |
| | | | 1:400 | ICC | Figure 3.3c<br>Figure 3.6a, b<br>Figure 3.10a, c |
| CNTNAP2 | Mouse | Neuromab (Davis, CA, USA); K67/25 | 1:500 | ICC | Figure 3.3a<br>Figure 3.4b, e<br>Figure 3.7<br>Figure 3.8<br>Figure 3.11<br>Figure 3.12 |
| | | | 3 ug per sample | IP | Figure 2.3b<br>Figure 2.4b<br>Figure 2.5b |
| | | | 1:1000 | WB | Figure 2.1b<br>Figure 3.3e |
| CASK | Mouse | Neuromab; K56A/50 | 1:1000 | ICC | Figure 3.10a, c<br>Figure 3.11<br>Figure 3.12<br>Figure 3.14e<br>Figure 3.15 |
| | | | 3 ug per sample | IP | Figure 2.3c |
| CASK | Rabbit | Invitrogen; 71-5000 | 1: 1000 | WB | Figure 2.3b-d<br>Figure 3.10d, e<br>Figure 3.17b<br>Figure 3.21a |
| MAP2 | Chicken | Millipore; AB15452 | 1:1000 | ICC | Figure 3.7a |
| GABA | Rabbit | Sigma; A2052 | 1:1000 | ICC | Figure 3.1<br>Figure 3.2<br>Figure 3.4<br>Figure 3.5d, e<br>Figure 3.7<br>Figure 3.8 |

| | | | | | |
|---|---|---|---|---|---|
| | | | | | Figure 3.11<br>Figure 3.12<br>Figure 3.14 f-i<br>Figure 3.15 |
| | | | 1:500 | IHC | Figure 3.19, c, e |
| GFP | Chicken | Abcam (Cambridge, MA, USA); ab13970 | 1:10,000 | ICC | All GFP images (except Figure 3.5a, 3.14a, j) |
| | | | 1:500 | IHC | Figure 3.19, c, e |
| turboGFP | Mouse | Origene; TA150041 | 1:1000 | ICC | Figure 3.5a<br>Figure 3.14a, j |
| FLAG | Mouse | Sigma; F1804 | 1:1000 | ICC | Figure 3.1f, j<br>Figure 3.5a, c |
| | | | 3 ug per sample | IP | Figure 2.3d<br>Figure 2.4c |
| | | | 1:1000 | WB | Figure 2.3d<br>Figure 2.4c<br>Figure 3.9b<br>Figure 3.14e |
| dsRed | Rabbit | Clontech; 632496 | 1:1000 | ICC | Figure 3.13a, c, e<br>Figure 3.14a, c, j<br>Figure 3.16b |
| mCherry | Goat | Sicgen (Carcavelos, Portugal); AB0040-200 | 1:500 | WB | Figure 3.9a, c |
| FLAG-488 | Mouse | Abcam; ab117505 | 1:1000 | ICC | Figure 2.3e |
| HA-550 | Rabbit | Sysy (Goettingen, Germany); 245-003C3 | 1:1000 | ICC | Figure 2.3e |
| PLA-Mouse | Mouse | Sigma; DUO92001 | 1:5 | ICC | Figure 3.10c<br>Figure 2.3e |
| PLA-Rabbit | Rabbit | Sigma; DUO92005 | 1:5 | ICC | Figure 3.10c<br>Figure 2.3e |
| Actin | Mouse | Sigma; A2228 | 1:1000 | WB | Figure 2.3d<br>Figure 3.1a<br>Figure 3.3e-f |

| | | | | | |
|---|---|---|---|---|---|
| | | | | | Figure 3.4a<br>Figure 3.10e<br>Figure 3.14e<br>Figure 3.17a, b<br>Figure 3.21a |
| β-Tubulin | Mouse | Hybridoma (Iowa City, IA, USA); E7 | 1:1000 | WB | Figure 3.10d |
| IgG | Mouse | Santa Cruz (Dallas, TX, USA); sc-2025 | 3 ug per sample | IP | Figure 2.3b-d<br>Figure 2.4b-d<br>Figure 2.5b |
| GAPDH | Rabbit | Cell Signaling Technology (Danvers, MA, USA); D16H11 | 1:1000 | WB | Figure 3.21a |
| PARD3 | Rabbit | Millipore; 07-330 | 1:1000 | WB | Figure 2.4b |
| Myc | Mouse | Santa Cruz; sc-40 | 1:100 | WB | Figure 2.4c-d |
| | | | 3 ug per sample | IP | Figure 2.4d |
| MPP6 | Rabbit | One World Labs; 28950 | 1:1000 | WB | Figure 2.5b |

| Primer | Sequence | Vector backbone | Notes |
|---|---|---|---|
| shCNTNAP2_hairpin | 5’ TCAGACAGTGACCACTATCAATGGCTTCA 3’ | pGFP-V-RS | TG510300A |
| shCASK_hairpin | 5’ GGAAGAGATTCACGCACTTACAGACTGCA 3’ | | TG516864A |
| Scrambled_hairpin | 5’ GCACTACCAGAGCTAACTCAGATAGTACT 3’ | | TR30013 |
| pGFP-V-RS_eGFP_F | 5’ GAATCCGAGGAGATCTGCCACCATGGTGAGCAAGGGCGAGGAG 3’ | | Replace tGFP with |

| | | | |
|---|---|---|---|
| pGFP-V-RS_eGFP_R | 5’ ACCTCGAGTGCGGCCGCTTACTTGTACAGCTCGTCCATGCCGAGAG 3’ | | eGFP; BglII and NotI |
| shCNTNAP2_resistant_F | 5’ GTCTCCATCGGATAGCGATCATTACCAGTGGCTCCAGGTTGACTTTGGCA 3’ | peGFP-N2 | RNAi-resistant CNTNAP2 |
| shCNTNAP2_resistant_R | 5’ TGCCAAAGTCAACCTGGAGCCACTGGTAATGATCGCTATCCGATGGAGAC 3’ | | |
| FLAG_CNTNAP2_1_F | 5’ CGCGGGCCCGGGATCCATGCAGGCGGCTCCGCGC 3’ | | FLAG-CNTNAP2; two amplicons fused with Infusion; BamHI and Not I |
| FLAG_CNTNAP2_1_R | 5 ‘CTTGTCGTCATCGTCTTTGTAGTCCGTCCAGGCTCT 3’ | | |
| FLAG_CNTNAP2_2_F | 5’ GACGATGACGACAAGGCTCCCTCCACGTCCCAAAA | | |
| FLAG_CNTNAP2_2_R | 5’ TCTAGAGTCGCGGCCGCTCAAATGAGCCATTCCTTTTTGCTTTCATCAATGGTCTC 3’ | | |
| FLAG_CNTNAP2_d4.1B_1_F | 5’ CGCGGGCCCGGGATCCATGCAGGCGGCTCCGCGC 3’ | | FLAG-CNTNAPd4.1B; two amplicons fused with Infusion; BamHI and Not I |
| FLAG_CNTNAP2_d4.1B_1_R | 5’ GGCGGCGTCCGCGCTGAACATGTACCG GATCAGGAAGACCAGGGTGCACAGGATGGTGAAAAT 3’ | | |
| FLAG_CNTNAP2_d4.1B_2_F | 5’ AGCGCGGACGCCGCCATCATGAA 3’ | | |
| FLAG_CNTNAP2_d4.1B_2_R | 5’ TCTAGAGTCGCGGCCGCTCAAATGAGCCATTCCTTTTTGCTTTCATCAATGGTCTC 3’ | | |
| FLAG_CNTNAP2_dPDZ_F | 5’ CGCGGGCCCGGGATCCATGCAGGCGGCTCCGCGC 3’ | | FLAG-CNTNAPdPDZ; BamH |
| FLAG_CNTNAP2_dPDZ_R | 5’ TCTAGAGTCGCGGCCGCTCATTTGCTTTCATCAATGGTCTCTGTGAAGTTGGG 3’ | | |

| | | | |
|---|---|---|---|
| | | | I and Not I |
| FLAG_CNTNAP2_dCT_F | 5’ CGCGGGCCCGGGATCCATGCAGGCGGCTCCGCGC 3’ | | FLAG-CNTNAPdCT; BamH I and Not I |
| FLAG_CNTNAP2_dCT_R | 5’ TCTAGAGTCGCGGCCGCTCAGATCAGGAAGACCAGGGTGCACAGGAT 3’ | | |
| CASK_untagged_F | 5’ CGCGGGCCCGGGATCCATGGCCGACGACGACGTGCTGTTC 3’ | | CASK (no tag); BamH I and Not I |
| CASK_untagged_R | 5’ TCTAGAGTCGCGGCCGCCTAATAGACCCAGGAGACAGGGACCCAC 3’ | | |
| CASK-FLAG_F | 5’ CGCGGGCCCGGGATCCATGGCCGACGACGACGTGCTGTTC 3’ | | CASK-FLAG; BamH I and Not I |
| CASK-FLAG_R | 5’ TCTAGAGTCGCGGCCGCTTACTTGTCGTCATCGTCTTTGTAGTCTGCTGCTGCATAGACCCAGGAGACAGGGACCCACTGT 3’ | | |
| CASK-HA_F | 5’ CGCGGGCCCGGGATCCATGGCCGACGACGACGTGCTGTTCGAGGATGTG 3’ | | CASK-HA; BamH I and Not I |
| CASK-HA_R | 5’ TCTAGAGTCGCGGCCGCCTAAGCGTAATCTGGAACATCGTATGGGTA TGCTGCTGCATAGACCCAGGAGACAGGGACCCACTGTGG 3’ | | |
| CASKΔPDZ-HA_1_F | 5’ CGCGGGCCCGGGATCCATGGCCGACGACGACGTGCTGTTCGAGGATGTG 3’ | | CASKΔPDZ-HA; two amplicons fused with Infusion; BamH I and Not I |
| CASKΔPDZ-HA_1_R | 5’ TCTGGTCACATTCTCCATATCCATGTCTCCGTT 3’ | | |
| CASKΔPDZ-HA_2_F | 5’ GGAGAATGTGACCAGACCAAGTTACCGCACTCAGTCTTCGTCCT 3’ | | |
| CASKΔPDZ-HA_2_R | 5’ TCTAGAGTCGCGGCCGCCTAAGCGTAATCTGGAACATCGTATGGGTA TGCTGCTGCATAGACCCAGGAGACAGGGACCCACTGTGG 3’ | | |

| | | | |
|---|---|---|---|
| CASK-mCherry_F | 5’ CGCTAGCGCTACCGGTATGGCCGACGACGACGTGCTGTTC 3’ | pmCherry-C1 | CASK-mCherry; AgeI |
| CASK-mCherry_R | 5’ CATGGTGGCGACCGGTTTATAGACCCAGGAGACAGGGACCCACTGT 3’ | | |
| CASKΔCAMK-mCherry_F | 5’ CGCTAGCGCTACCGGTATGGCCGACGACGACGTGCTGTTCGAGGATGTGAAGGAGCGGGATCGTTACGCCTACAAGATTCATCTTC 3’ | | CASKΔCAMK-mCherry; AgeI |
| CASKΔCAMK-mCherry_R | 5’ CATGGTGGCGACCGGTTTATAGACCCAGGAGACAGGGACCCACTGT 3’ | | |
| CASKΔL27-mCherry_1_F | 5’ CGCTAGCGCTACCGGTATGGCCGACGACGACGTGCTGTTC 3’ | | CASKΔL27-mCherry; two amplicons fused with Infusion; AgeI |
| CASKΔL27-mCherry_1_R | 5’ TCCTGAGGAGGTAGGGTCTTCGGAGAAATCTGGTAA 3’ | | |
| CASKΔL27-mCherry_2_F | 5’ CCTACCTCCTCAGGAGCATTGAGGGTCACACCTCCTCCCACCTCTC 3’ | | |
| CASKΔL27-mCherry_2_R | 5’ CATGGTGGCGACCGGTTTATAGACCCAGGAGACAGGGACCCACTGT 3’ | | |
| CASKΔPDZ-mCherry_1_F | 5’ CGCTAGCGCTACCGGTATGGCCGACGACGACGTGCTGTTC 3’ | | CASKΔPDZ-mCherry; two amplicons fused with Infusion; AgeI |
| CASKΔPDZ-mCherry_1_R | 5’ TCTGGTCACATTCTCCATATCCATGTCTCCGTT 3’ | | |
| CASKΔPDZ-mCherry_2_F | 5’ GGAGAATGTGACCAGACCAAGTTACCGCACTCAGTCTTCGTCCT 3’ | | |
| CASKΔPDZ-mCherry_2_R | 5’ CATGGTGGCGACCGGTTTATAGACCCAGGAGACAGGGACCCACTGT 3’ | | |
| CASKΔSH3GK-mCherry_F | 5’ CGCTAGCGCTACCGGTATGGCCGACGACGACGTGCTGTTC 3’ | | CASKΔSH3GK- |

| | | | |
|---|---|---|---|
| CASKΔSH3GK-mCherry_R | 5’ CATGGTGGCGACCGGTTTATAGACCCAGGAGACAGGGACCCACTGTGGGGCTGTGCACACGAGCTGTCGTCCTTTTGGTTGGGTAGTTGA 3’ | | mCherry; AgeI |
| PARD3_FL_F | CGCGGGCCCGGGATCCATGGAACAGAAACTCATCTCTGAAGAGGATCTGT | pEGFP-N2 | Myc-PARD3; BamHI and Not I |
| PARD3_FL_R | TCTAGAGTCGCGGCCGCTCAGGAATAGAAGGGCCTCCCTTTCT | | |
| PARD3_dPDZ1_1_F | CGCGGGCCCGGGATCCATGGAACAGAAACTCATCTCTGAAGAGGATCTGT | | Myc-PARd3ΔPDZ1; two amplicons fused with Infusion; BamHI and Not I |
| PARD3_dPDZ1_R | ATCATCCAGAGAAAAGTTGGGTATATGCTCCA | | |
| PARD3_dPDZ2_F | TTTTCTCTGGATGATGCAGCAAATAAAGAGCAGTATGAACAACTA | | |
| PARD3_dPDZ2_R | TCTAGAGTCGCGGCCGCTCAGGAATAGAAGGGCCTCCCTTTCT | | |
| PARD3_dPDZ2_1_F | CGCGGGCCCGGGATCCATGGAACAGAAACTCATCTCTGAAGAGGATCTGT | | Myc-PARd3ΔPDZ2; two amplicons fused with Infusion; BamHI and Not I |
| PARD3_dPDZ2_1_R | AAGCCTCTTGCCTATTTTTTTGGTGTTAT | | |
| PARD3_dPDZ2_2_F | ATAGGCAAGAGGCTTCAGGAAGACGCCTTCCACCCA | | |
| PARD3_dPDZ2_2_R | TCTAGAGTCGCGGCCGCTCAGGAATAGAAGGGCCTCCCTTTCT | | |
| PARD3_dPDZ3_1_F | CGCGGGCCCGGGATCCATGGAACAGAAACTCATCTCTGAAGAGGATCTGT | | Myc-PARd3ΔPDZ3; two amplic |
| PARD3_dPDZ3_1_R | AAATGTCAGAAATTCCCTGGTGCCATCAGG | | |
| PARD3_dPDZ3_2_F | GAATTTCTGACATTT CTTATTGTTGCAAGGAGAATAAGCAAGT | | |

| | | | |
|---|---|---|---|
| PARD3_dPDZ3_2_R | TCTAGAGTCGCGGCCGCTCAGGAATAGAAGGGCCTCCCTTTCT | | ons fused with Infusion; BamH I and Not I |
| PARD3_dPDZall_1_F | CGCGGGCCCGGGATCCATGGAACAGAAACTCATCTCTGAAGAGGATCTGT | | Myc-PARd 3ΔPDZall; two amplicons fused with Infusion; BamH I and Not I |
| PARD3_dPDZall_1_R | ATCATCCAGAGAAAAGTTGGGTATATGCTCCA | | |
| PARD3_dPDZall_2_F | TTTTCTCTGGATGATCTTATTGTTGCAAGGAGAATAAGCAAGT | | |
| PARD3_dPDZall_2_R | TCTAGAGTCGCGGCCGC TCAGGAATAGAAGGGCCTCCCTTTCT | | |
| CNTNAP2_GT_WT_F | 5’ CTGCCAGCCCAGAACTGG 3’ | N/A | Genotyping; common forward |
| CNTNAP2_GT_WT_R | 5’ ACACCAGGGGCAAGAATTG 3’ | | Genotyping; WT reverse |
| CNTNAP2_GT_Neo_R | 5’ CGCTTCCTCGTGCTTTACGGTAT 3’ | | Genotyping; KO reverse |
| GAD1_GT_F | 5’ GACTCCGGGTTCCTCACACTACC 3’ | N/A | Genotyping; GAD1 GFP forward |

| | | | |
|---|---|---|---|
| GAD1_GT_R | 5’ GAGATCAGCAGCCTCTGTTCC 3’ | | Genotyping ; GAD1 GFP reverse |

pEGFP-N2 and pmCherry-C1 plasmids were purchased from Clontech (Mountain View, CA, USA). pCS2-FLAG was purchased from Addgene (Cambridge, MA, USA, #16331). FLAG-CNTNAP2 was generated by subcloning human CNTNAP2 cDNA (from a plasmid kindly provided by Dr. Elior Peles, Weizmann Institute of Science, Israel) into the peGFP-N2 vector (restriction sites BamHI and NotI, which also excises the GFP) using the Infusion cloning system from Clontech. The FLAG sequence was then inserted downstream of the signaling peptide (amino acids 1-27) using the same technique. FLAG-CNTNAP2Δ4.1B, ΔPDZ, and ΔCT mutants were generated with the same method.

Untagged CASK was generated by subcloning human CASK cDNA (Addgene #23470) into peGFP-N2 with restriction sites BamHI and NotI, while CASK-HA and CASK-FLAG were made by adding the HA and FLAG tags to the C-terminus respectively. CASK-mCherry was made by subcloning CASK cDNA into the pmCherry-C1 vector with restriction site AgeI. CASKΔPDZ was made by amplifying the cDNA upstream and downstream of the PDZ domain and ligating the pieces together (Infusion).

shRNA plasmids for *CNTNAP2* (TG510300A), *CASK* (TG516864A), and scrambled controls (TR30013) were purchased from Origene (Rockwall, MD, USA). For some knockdown experiments requiring three fluorescence channels, we replaced the turboGFP on the pGFP-V-RS

vector with eGFP (restriction sites BglII and NotI). RNAi-resistant point mutations were introduced into FLAG-CNTNAP2 using QuikChange II XL Site-Directed Mutagenesis Kit (Agilent, Santa Clara, CA, USA).

For experiments where GABA staining could not be performed, we used Dlx5/6-GFP (a gift from Dr. Daniel Vogt; Michigan State University), an expression plasmid which utilizes the Dlx5/6 enhancer to selectively express GFP in interneurons[227].

***Mice.*** All animal procedures were performed with the approval of the Institutional Animal Care and Use Committee (IACUC) at Northwestern University. *Cntnap2* KO mice (CD1) were generated by Dr. Elior Peles. *Gad1-eGFP* mice, which selectively express GFP in a PV+ subset of interneurons[195], were purchased from Jackson Laboratory (Bar Harbor, ME, USA; #007677). In our hands, we did not observe this selectivity – possibly as a result of our breeding scheme (Figure 3.19) – but found all GFP cells to be GABA-positive (data not shown); we therefore focused our analysis on GABA-positive cells. All *Gad1-eGFP* Het; *Cntnap2* WT/KO mice were male and around 5 months of age.

***Neuronal Culture and Transfections.*** High density (300 000 cells/cm$^2$) cortical neuron cultures were prepared from Sprague-Dawley rat E18 embryos (for shRNA, overexpression, and endogenous expression studies) or CD1 mouse P0 pups (for WT/KO and endogenous expression studies) as described previously[228]. Cortical neurons were transfected using Lipofectamine 2000 (Thermo Fisher Scientific, Waltham, MA, USA) following the manufacturer's recommendations (between 3-5 μg of DNA per plasmid, 4 μL of Lipofectamine 2000 per reaction) and the neurons

were maintained in the feeding media[228] for either 1 (overexpression; 6-7 days *in vitro* (DIV) for young neurons), 3 (overexpression; 24-27 DIV for mature neurons), or 5 days (knockdown; 21-26 DIV for mature neurons or 2-7 DIV for young neurons). Any signs of poor neuronal health meant the exclusion of the cell from quantification. HEK293T cells were transfected using the same protocol (2 ug of DNA per plasmid, 4 uL of Lipofectamine 2000 per reaction, 1-2 days overexpression).

***Immunocytochemistry.*** Neurons were first washed in 0.1 M phosphate buffered saline (1X PBS) and then fixed in 4% formaldehyde-sucrose-PBS for 15 min. Fixed neurons were then permeabilized and blocked simultaneously with 5% normal goat serum (NGS) and 0.3% Triton-X-100 in 1X PBS (30 minutes at 4ºC), followed by incubation of primary antibodies with 5% NGS in 1X PBS (O/N, 4ºC). The coverslips were washed three times with PBS and incubated with the corresponding fluorophore-secondary antibodies with 5% NGS in 1X PBS (Alexa Fluro 405, 488, 568, and/or 647; Thermo Fisher Scientific) for 1hr at 25ºC. The coverslips were then washed (3x) and mounted onto slides using ProLong Antifade reagent (Invitrogen, Carlsbad, CA, USA), and stored at 4ºC until the acquisition of the images.

***Immunohistochemistry.*** *Gad1-eGFP* Het; *Cntnap2* WT/KO male mice at five months of age were anesthetized with Euthasol (Virbac, Fort Worth, Texas, USA) and fixed by transcardial perfusion using 4% paraformaldehyde (PFA) in 1X PBS. Brains were dissected and further incubated in 4% PFA at 25ºC for 4 hours before being placed in 30% sucrose at 4ºC for 3 days and frozen in OCT embedding medium (Fisher Scientific, Hampton, NH, USA). Brains were sectioned into 80 μm coronal slices (floating sections) with a cryostat, permeabilized/blocked

with 3% bovine serum albumin (BSA) + 0.3% Triton X-100 in 1X PBS at 25ºC for 1 hour, immunostained with GFP chicken and GABA rabbit antibodies (2 days at 4ºC), followed by Alexa Fluro 488 and 568 incubation (2 days at 4ºC), before being mounted onto glass slides with Dako mounting medium (Agilent) and covered with glass coverslips. Cells exhibiting intact dendritic structures were imaged (see **Confocal Microscopy Imaging**). Representative 3-D images were reconstructed with the neuTube program (neutracing.com).

***Golgi Staining.*** The Rapid GolgiStain Kit (FD Technologies, Columbia, MD, USA) was used. Briefly, brains were dissected and immersed in impregnation solution (Solutions A+B) for 2 weeks in the dark at room temperature. The brains were then transferred into Solution C and kept for 3 days in the dark at room temperature before being flash frozen, sliced into 180 μm sections, and mounted onto gelatin-coated slides (FD Technologies). The slides were rinsed with a mixture of Solution D, E, and milli-Q water before being dehydrated with increasing concentrations (50%, 75%, 95%, and 100%) of ethanol, cleared with Xylene (Sigma, St. Louis, MO, USA), mounted using Permount (Thermo Fischer Scientific), and covered with glass coverslips. Mice (male and female) were on CD1 background and were around 6 months of age.

***PLA.*** FLAG-CNTNAP2 and CASK-HA were overexpressed for 2-3 days in either HEK293T cells (ATCC, Manassas, VA, USA; line authenticated by company before shipment) or neurons. Coverslips were processed, fixed, and permabilized using aforementioned immunocytochemistry methods, with mouse FLAG-488 and rabbit HA-550 as primary probes (O/N, 4ºC). From here, the DUOLINK kit (Sigma) was used. Briefly, mouse and rabbit PLA antibodies were used as secondary probes (37°C, 1 hr). Coverslips were then washed with Buffer A, incubated with ligase

diluted in ligation solution (37°C, 30 minutes), washed again with Buffer A, and incubated with polymerase diluted in amplification solution (37ºC, 100 min). The coverslips were then carefully washed with Buffer B and mounted. For PLA experiments examining endogenous CNTNAP2-CASK interactions in neurons, the same procedure was followed, except GFP was expressed for 3 days and CNTNAP2 (Millipore) and CASK (Neuromab) antibodies were used as primary probes.

***Immunoprecipitation.*** Mouse cortex or HEK293T cells were homogenized in immunoprecipitation buffer (50 mM Tris pH 7.4, 150 mM NaCl, 0.5% Triton X-100, with protease inhibitor cocktail from Roche, Basel, Switzerland) and solubilized for 1 hour at 4°C. Solubilized material was centrifuged at 20 000 g for 10 minutes at 4°C and the supernatant was precleared with protein A/G sepharose beads (Thermo Fisher Scientific) for 30 minutes. Proteins in the precleared supernatant were then immunoprecipitated with 3 μg of antibody overnight at 4°C, followed by a 1 hour incubation with protein A/G sepharose beads the following day. Beads were then washed 3 times with IP buffer before adding 2x Laemmli buffer (Biorad, Hercules, CA, USA). Samples were analyzed by SDS-PAGE and western blotting.

***Expression Time Course.*** Cortices from CD1 WT mice aged P0, P14, P28, 4 months, and 6 months (sex not determined at P0, P14; males for P28, 4 months, 6 months) were homogenized in immunoprecipitation buffer (50 mM Tris pH 7.4, 150 mM NaCl, 0.5% Triton X-100 with Roche protease inhibitor cocktail) and solubilized for 1 hour at 4°C. Solubilized material was centrifuged at 16 000 g for 10 minutes at 4°C and 10 ug supernatant per sample was loaded for western blotting. For *in vitro* studies, the same procedure was performed on cultured WT rat neurons aged 7, 14, 21, and 28 DIV.

***Fractionation.*** Subcellular fractionation was performed essentially as previously described[229]. Briefly, cortices from 6-week old mice were homogenized in cold sucrose buffer (20 mM HEPES pH 7.4, 320 mM sucrose, 5 mM EDTA) supplemented with protease inhibitor cocktail (Roche). Homogenates were centrifuged at low speed to pellet nuclei and cell debris (3 000 g for 20 min at 4°C) and the supernatant (S1) was then centrifuged at high speed (38 000 g for 30 min at 4°C) to obtain a membrane pellet (P2). P2 was re-suspended in potassium iodide buffer (20 mM HEPES pH 7.4, 1 M KI, 5 mM EDTA) to remove membrane-associated proteins (S3), and membranes were again collected by centrifugation (38 000 g for 20 min at 4°C). Membranes were washed (20 mM HEPES pH 7.4, 5 mM EDTA) and pelleted once more (S4) before solubilizing in CHAPS buffer (20 mM HEPES pH 7.4, 100 mM NaCl, 5 mM EDTA, 1% CHAPS) supplemented with protease inhibitors for 2 hr at 4°C. Solubilized membranes were clarified by centrifugation for 30 min at 100 000 g, 4°C (S5). The final CHAPS-insoluble pellet was re-suspended in SDS buffer (50mM TRIS pH 7.4, 150 mM NaCl, 1% SDS) supplemented with protease inhibitors, solubilized at 37°C for 20 mins and clarified by centrifugation (S6). For *Cntnap2* WT/KO mice (cortices from 4-6 month males) and HEK293T membrane fractionation experiments, the above fractionation procedure was performed until the P2 step. The P2 pellet (crude membrane fraction) was then resuspended with Tris buffer (50 mM Tris pH 7.4, 150 mM NaCl, 5 mM EDTA with inhibitors) before a 2X RIPA solution (50 mM Tris pH 7.4, 150 mM NaCl, 5 mM EDTA, 2% TritonX-100, 1% deoxycholate, 0.2% SDS + inhibitors) was added 1:1; similarly, the same ratio of 2X RIPA was also added to S1 (cytosolic fraction) and total homogenate. All RIPA-treated fractions were agitated for 1 hour and spun down at 16 000 g to isolate the supernatant. For western blotting, 10 μg of each sample was loaded.

***Yeast Two-Hybrid Screening.*** Briefly, from the Matchmaker Gold Yeast Two-Hybrid manual (Clontech), CNTNAP2's C-terminal region (amino acids 1284-1331) was cloned into the bait vector (pGBKT7) and transformed into yeast. Bait-positive yeast were then mated with yeast containing cDNA (pGADT7) from a mouse brain library. Mated yeast were then plated onto double amino acid (-Leu/-Trp) dropout, Aureobasidin-A positive (A), and X-α-Gal positive (X) plates (DDO/X/A), a low stringency medium that selects for mated yeast containing both bait and prey vectors. DDO/X/A colonies that were blue, indicative of a possible interaction between bait-prey, were streaked onto quadruple amino acid (-Leu/-Trp/-His/-Ade) dropout, Aureobasidin-A positive (A), and X-α-Gal positive (X) plates (QDO/X/A), which require a genuine bait-prey interaction for growth. The blue colonies from QDO/X/A plates were isolated and plasmids sequenced.

***Electrophysiology and Biocytin Injections.*** One-month *Gad1-eGFP* Het; *Cntnap2* WT/KO mice (both male and female) were anesthetized with ketamine/xylazine and perfused with ice-cold artificial CSF (aCSF). Brains were extracted and sliced (coronal) at a thickness of 250 μm via Vibratome. Electrophysiological recordings and biotin injections of GFP-positive neurons in layer II/III of the mPFC were performed as described previously[230]. Each patched cell was confirmed to be fast-spiking (PV+) before any data was collected. After biocytin injection, cells were fixed (4% PFA) and stained with streptavidin-AlexaFluor 594 (Invitrogen) with methods documented previously[231]. Afterward, samples were imaged using a LSM510 Zeiss confocal microscope on a 40X/1NA oil-immersion objective at 1 μm intervals and reconstructed/analyzed with Neurolucida software (Williston, VT, USA).

***Confocal Microscopy/Camera Imaging and Analysis.*** Confocal images of neurons were obtained as described previously[157]. Briefly, for protein localization and expression studies, images were acquired by a Nikon (Amsterdam, Netherlands) C2 confocal microscope using a 63X oil immersion objective with numerical aperture (NA) = 1.4 with 0.4 μm z-stacks. All images were acquired in the linear range of fluorescence intensity and the best single plane image from the stack was selected for analysis (for antibody validation analysis, z-projections were used instead). The acquisition parameters were kept the same for all conditions and images were analyzed using Fiji software. For puncta analysis, the "Analyze Particle" function was employed on a background-subtracted GFP-defined region-of-interest (ROI); puncta with areas less than 0.025 $\mu m^2$ were excluded from the analysis. For immunofluorescence intensity, the mean pixel intensity of an ROI was measured; images were not background subtracted in this case (except for antibody validation studies). For *in vivo* dendritic arborization studies, images were taken with the C2 confocal using a 10X objective (NA = 0.3) with 1.0 μm z-stacks. For cultured dendrite morphological studies and *in vivo* Golgi-treated brain slices, images were acquired using a Zeiss (Oberkochen, Germany) Axioplan2 upright microscope. Images were taken with a 10X objective (NA = 0.3) and micrographs acquired using a Zeiss AxioCam MRM CCD camera. Dendrite arbors (*in vivo* and *in vitro*) were manually traced in Fiji. Sholl analysis was done using the Sholl plugin (Ghosh Lab), while total dendrite length and branch information were derived with Neuronstudio (Mt. Sinai School of Medicine) and analyzed with Lmeasure[232].

***Structured Illuminated Microscopy (SIM) imaging and analysis.*** Neurons were fixed, and immunocytochemistry was performed as described above. Three-channel images were taken

using a Nikon SIM microscope with a 100X 1.49 NA objective (Cell Imaging Facility & Nikon Imaging Center, Northwestern University, Chicago, IL, USA) that allows a resolution range of 110-130 nm. Images were reconstructed and analyzed with Fiji as described previously[198]. For determining co-localization, Fiji's Colocalization plugin was used (Ratio: 50%, Threshold 1: 15, Threshold 2: 15, Display: 255). For analyzing puncta location, the distance from the center of the visible puncta to the closest peripheral edge of an overlay dendrite ROI was measured. To control for dendritic width variability, which can confound measurements, this value was normalized by the total dendritic width at that point and multiplied by 100 to achieve a percentage value. For determining puncta density, the number of puncta within a ROI was counted and divided by the ROI's area. Interneuron dendrites were considered positive for "bead-like" CNTNAP2 nanostructures if a group of puncta were proximal to and highly aligned with one another. All SIM images were processed for background subtraction before analysis. Analysis of CNTNAP2 and CASK immunofluorescence was restricted to signal strictly within ROI defined by GFP expression in individual neurons. All peripheral co-localized puncta outside of the ROI were not analyzed to exclude the possibility of presynaptic complexes confounding our calculations.

***Stimulated Emission Depletion (STED) Microscopy.*** Super resolution images were acquired on a STED-capable Leica (Wetzlar, Germany) SP8 confocal microscope, and images were acquired with a 100X objective. Mature cortical interneurons were transfected with GFP, fixed, and stained with a CNTNAP2 antibody (Neuromab) as described previously. Alexa 488 and Alexa 594 secondary antibodies were used for GFP and CNTNAP2, respectively. An adjustable white laser was used for excitation at the optimum wavelength, and a standard confocal image was taken with the cell-fill GFP. Pulsed stimulation at 594nm and depletion laser of 775nm were simultaneously

used for gated acquisition of CNTNAP2 at 594nm between 0.5 and 6 ns. In post processing, Huygens deconvolution software was used to enhance image clarity and resolution.

***Bioinformatics Analysis.*** The list of candidate CNTNAP2-interacting proteins combined data from the BIOGRID database (via NCBI), proteomic data from published literature[125], and the yeast two-hybrid hits from this paper. The list of CASK-interacting proteins consisted of candidates from BIND/BIOGRID/HRPD databases (via NCBI; Supplementary Table 1). A list of candidate ASD susceptibility genes was retrieved from the SFARI website (sfari.org, May 2017). A hypergeometric probability calculator was used (Geneprof.org) to determine the significance of overlap between data sets, with total gene set assumed to be 20 310 genes (Ensembl, July 2017) for all calculations.

***Blinding and Statistical Analysis.*** Data from morphological (both *in vivo* and *in vitro*) and protein expression/localization studies were obtained and analyzed under blinded conditions (coverslip identity hidden, cells selected randomly, and raw data pooled during quantification).

Time course, fractionation (both *in vivo* and *in vitro*), immunoprecipitation, and antibody/shRNA validation experiments were not blinded. Cells of visibly poor health (i.e. blebs, broken dendrites, poor expression, etc.) were excluded from quantification. No animals were excluded from the analysis and no method of animal randomization was employed. Sample sizes, particularly for morphological studies, were on average between 30 – 60 cells to account for inherent cellular diversity. At least three animals per genotype were used for each *in vivo* experiment, which was sufficient for statistical significance.

All statistical tests were performed with GraphPad Prism (Version 7). Before analysis, data were first tested for normality with D'Agostino and Pearson in order to determine whether parametric or nonparametric tests were to be used. Tests involving symmetrical distributions (i.e. *t-test* or Mann-Whitney) were always two-sided. Post-hoc tests were always used in multiple comparison analysis. P values $\leq 0.05$ were considered significant.

# REFERENCES

1. de Lacy N, King BH. Revisiting the relationship between autism and schizophrenia: toward an integrated neurobiology. *Annu Rev Clin Psychol* 2013; **9:** 555-587.

2. Penzes P, Cahill ME, Jones KA, VanLeeuwen JE, Woolfrey KM. Dendritic spine pathology in neuropsychiatric disorders. *Nat Neurosci* 2011; **14**(3)**:** 285-293.

3. Harrison PJ, Weinberger DR. Schizophrenia genes, gene expression, and neuropathology: on the matter of their convergence. *Mol Psychiatry* 2005; **10**(1)**:** 40-68; image 45.

4. Toro R, Konyukh M, Delorme R, Leblond C, Chaste P, Fauchereau F *et al.* Key role for gene dosage and synaptic homeostasis in autism spectrum disorders. *Trends Genet* 2010; **26**(8)**:** 363-372.

5. Owen MJ, Williams NM, O'Donovan MC. The molecular genetics of schizophrenia: new findings promise new insights. *Mol Psychiatry* 2004; **9**(1)**:** 14-27.

6. Rapin I, Tuchman RF. Autism: definition, neurobiology, screening, diagnosis. *Pediatr Clin North Am* 2008; **55**(5)**:** 1129-1146, viii.

7. Cheung C, Yu K, Fung G, Leung M, Wong C, Li Q *et al.* Autistic disorders and schizophrenia: related or remote? An anatomical likelihood estimation. *PLoS One* 2010; **5**(8)**:** e12233.

8. Toal F, Bloemen OJ, Deeley Q, Tunstall N, Daly EM, Page L *et al.* Psychosis and autism: magnetic resonance imaging study of brain anatomy. *Br J Psychiatry* 2009; **194**(5)**:** 418-425.

9. Kolvin I. Studies in the childhood psychoses. I. Diagnostic criteria and classification. *Br J Psychiatry* 1971; **118**(545)**:** 381-384.

10. Kolvin I, Ounsted C, Humphrey M, McNay A. Studies in the childhood psychoses. II. The phenomenology of childhood psychoses. *Br J Psychiatry* 1971; **118**(545)**:** 385-395.

11. Penzes P, Buonanno A, Passafaro M, Sala C, Sweet RA. Developmental vulnerability of synapses and circuits associated with neuropsychiatric disorders. *J Neurochem* 2013; **126**(2)**:** 165-182.

12. Chattopadhyaya B, Cristo GD. GABAergic circuit dysfunctions in neurodevelopmental disorders. *Front Psychiatry* 2012; **3:** 51.

13. Glausier JR, Lewis DA. Dendritic spine pathology in schizophrenia. *Neuroscience* 2013; **251:** 90-107.

14. Hutsler JJ, Zhang H. Increased dendritic spine densities on cortical projection neurons in autism spectrum disorders. *Brain Res* 2010; **1309:** 83-94.

15. Fritschy JM, Brunig I. Formation and plasticity of GABAergic synapses: physiological mechanisms and pathophysiological implications. *Pharmacol Ther* 2003; **98**(3)**:** 299-323.

16. Lynch JW. Molecular structure and function of the glycine receptor chloride channel. *Physiol Rev* 2004; **84**(4)**:** 1051-1095.

17. Gatto CL, Broadie K. Genetic controls balancing excitatory and inhibitory synaptogenesis in neurodevelopmental disorder models. *Front Synaptic Neurosci* 2010; **2:** 4.

18. Wu GY, Zou DJ, Rajan I, Cline H. Dendritic dynamics in vivo change during neuronal maturation. *J Neurosci* 1999; **19**(11)**:** 4472-4483.

19. Koleske AJ. Molecular mechanisms of dendrite stability. *Nat Rev Neurosci* 2013; **14**(8)**:** 536-550.

20. Spruston N. Pyramidal neurons: dendritic structure and synaptic integration. *Nat Rev Neurosci* 2008; **9**(3)**:** 206-221.

21. Holtmaat A, Svoboda K. Experience-dependent structural synaptic plasticity in the mammalian brain. *Nat Rev Neurosci* 2009; **10**(9)**:** 647-658.

22. Zuo Y, Lin A, Chang P, Gan WB. Development of long-term dendritic spine stability in diverse regions of cerebral cortex. *Neuron* 2005; **46**(2)**:** 181-189.

23. Alvarez VA, Sabatini BL. Anatomical and physiological plasticity of dendritic spines. *Annu Rev Neurosci* 2007; **30:** 79-97.

24. Tada T, Sheng M. Molecular mechanisms of dendritic spine morphogenesis. *Curr Opin Neurobiol* 2006; **16**(1)**:** 95-101.

25. Penzes P, Jones KA. Dendritic spine dynamics--a key role for kalirin-7. *Trends Neurosci* 2008; **31**(8)**:** 419-427.

26. Penzes P, Cahill ME, Jones KA, Srivastava DP. Convergent CaMK and RacGEF signals control dendritic structure and function. *Trends Cell Biol* 2008; **18**(9)**:** 405-413.

27. Markram H, Toledo-Rodriguez M, Wang Y, Gupta A, Silberberg G, Wu C. Interneurons of the neocortical inhibitory system. *Nat Rev Neurosci* 2004; **5**(10)**:** 793-807.

28. McBain CJ, Fisahn A. Interneurons unbound. *Nat Rev Neurosci* 2001; **2**(1)**:** 11-23.

29. Gonzalez-Burgos G, Krimer LS, Povysheva NV, Barrionuevo G, Lewis DA. Functional properties of fast spiking interneurons and their synaptic connections with pyramidal cells in primate dorsolateral prefrontal cortex. *J Neurophysiol* 2005; **93**(2)**:** 942-953.

30. Kawaguchi Y. Physiological subgroups of nonpyramidal cells with specific morphological characteristics in layer II/III of rat frontal cortex. *J Neurosci* 1995; **15**(4)**:** 2638-2655.

31. Lewis DA, Lund JS. Heterogeneity of chandelier neurons in monkey neocortex: corticotropin-releasing factor- and parvalbumin-immunoreactive populations. *J Comp Neurol* 1990; **293**(4)**:** 599-615.

32. Freund TF, Katona I. Perisomatic inhibition. *Neuron* 2007; **56**(1)**:** 33-42.

33. Williams S, Boksa P. Gamma oscillations and schizophrenia. *J Psychiatry Neurosci* 2010; **35**(2)**:** 75-77.

34. DeFelipe J, Lopez-Cruz PL, Benavides-Piccione R, Bielza C, Larranaga P, Anderson S *et al.* New insights into the classification and nomenclature of cortical GABAergic interneurons. *Nat Rev Neurosci* 2013; **14**(3)**:** 202-216.

35. Megias M, Emri Z, Freund TF, Gulyas AI. Total number and distribution of inhibitory and excitatory synapses on hippocampal CA1 pyramidal cells. *Neuroscience* 2001; **102**(3)**:** 527-540.

36. Eichler SA, Meier JC. E-I balance and human diseases - from molecules to networking. *Front Mol Neurosci* 2008; **1:** 2.

37. Liu G. Local structural balance and functional interaction of excitatory and inhibitory synapses in hippocampal dendrites. *Nat Neurosci* 2004; **7**(4)**:** 373-379.

38. Gulyas AI, Megias M, Emri Z, Freund TF. Total number and ratio of excitatory and inhibitory synapses converging onto single interneurons of different types in the CA1 area of the rat hippocampus. *J Neurosci* 1999; **19**(22)**:** 10082-10097.

39. Turrigiano GG, Leslie KR, Desai NS, Rutherford LC, Nelson SB. Activity-dependent scaling of quantal amplitude in neocortical neurons. *Nature* 1998; **391**(6670)**:** 892-896.

40. Turrigiano G. Too many cooks? Intrinsic and synaptic homeostatic mechanisms in cortical circuit refinement. *Annu Rev Neurosci* 2011; **34:** 89-103.

41. Beierlein M, Gibson JR, Connors BW. A network of electrically coupled interneurons drives synchronized inhibition in neocortex. *Nat Neurosci* 2000; **3**(9)**:** 904-910.

42. Moran LV, Hong LE. High vs low frequency neural oscillations in schizophrenia. *Schizophr Bull* 2011; **37**(4)**:** 659-663.

43. Szabadics J, Lorincz A, Tamas G. Beta and gamma frequency synchronization by dendritic gabaergic synapses and gap junctions in a network of cortical interneurons. *J Neurosci* 2001; **21**(15)**:** 5824-5831.

44. Tamas G, Buhl EH, Lorincz A, Somogyi P. Proximally targeted GABAergic synapses and gap junctions synchronize cortical interneurons. *Nat Neurosci* 2000; **3**(4)**:** 366-371.

45. Uhlhaas PJ, Singer W. Abnormal neural oscillations and synchrony in schizophrenia. *Nat Rev Neurosci* 2010; **11**(2)**:** 100-113.

46. Bartos M, Vida I, Jonas P. Synaptic mechanisms of synchronized gamma oscillations in inhibitory interneuron networks. *Nat Rev Neurosci* 2007; **8**(1)**:** 45-56.

47. Bateup HS, Johnson CA, Denefrio CL, Saulnier JL, Kornacker K, Sabatini BL. Excitatory/inhibitory synaptic imbalance leads to hippocampal hyperexcitability in mouse models of tuberous sclerosis. *Neuron* 2013; **78**(3)**:** 510-522.

48. Yizhar O, Fenno LE, Prigge M, Schneider F, Davidson TJ, O'Shea DJ *et al.* Neocortical excitation/inhibition balance in information processing and social dysfunction. *Nature* 2011; **477**(7363)**:** 171-178.

49. Zoghbi HY. Postnatal neurodevelopmental disorders: meeting at the synapse? *Science* 2003; **302**(5646)**:** 826-830.

50. Fatemi SH, Folsom TD. The neurodevelopmental hypothesis of schizophrenia, revisited. *Schizophr Bull* 2009; **35**(3)**:** 528-548.

51. Selemon LD, Goldman-Rakic PS. The reduced neuropil hypothesis: a circuit based model of schizophrenia. *Biol Psychiatry* 1999; **45**(1)**:** 17-25.

52. Thompson PM, Vidal C, Giedd JN, Gochman P, Blumenthal J, Nicolson R *et al.* Mapping adolescent brain change reveals dynamic wave of accelerated gray matter loss in very early-onset schizophrenia. *Proc Natl Acad Sci U S A* 2001; **98**(20)**:** 11650-11655.

53. Vita A, De Peri L, Deste G, Sacchetti E. Progressive loss of cortical gray matter in schizophrenia: a meta-analysis and meta-regression of longitudinal MRI studies. *Transl Psychiatry* 2012; **2:** e190.

54. Glantz LA, Lewis DA. Decreased dendritic spine density on prefrontal cortical pyramidal neurons in schizophrenia. *Arch Gen Psychiatry* 2000; **57**(1)**:** 65-73.

55. Sweet RA, Henteleff RA, Zhang W, Sampson AR, Lewis DA. Reduced dendritic spine density in auditory cortex of subjects with schizophrenia. *Neuropsychopharmacology* 2009; **34**(2)**:** 374-389.

56. Steen RG, Mull C, McClure R, Hamer RM, Lieberman JA. Brain volume in first-episode schizophrenia: systematic review and meta-analysis of magnetic resonance imaging studies. *Br J Psychiatry* 2006; **188:** 510-518.

57. Kolomeets NS, Orlovskaya DD, Rachmanova VI, Uranova NA. Ultrastructural alterations in hippocampal mossy fiber synapses in schizophrenia: a postmortem morphometric study. *Synapse* 2005; **57**(1)**:** 47-55.

58. Gonzalez-Burgos G, Lewis DA. GABA neurons and the mechanisms of network oscillations: implications for understanding cortical dysfunction in schizophrenia. *Schizophr Bull* 2008; **34**(5)**:** 944-961.

59. Wilson FA, O'Scalaidhe SP, Goldman-Rakic PS. Functional synergism between putative gamma-aminobutyrate-containing neurons and pyramidal neurons in prefrontal cortex. *Proc Natl Acad Sci U S A* 1994; **91**(9)**:** 4009-4013.

60. Rao SG, Williams GV, Goldman-Rakic PS. Destruction and creation of spatial tuning by disinhibition: GABA(A) blockade of prefrontal cortical neurons engaged by working memory. *J Neurosci* 2000; **20**(1)**:** 485-494.

61. Sawaguchi T, Matsumura M, Kubota K. Delayed response deficits produced by local injection of bicuculline into the dorsolateral prefrontal cortex in Japanese macaque monkeys. *Exp Brain Res* 1989; **75**(3)**:** 457-469.

62. Haenschel C, Bittner RA, Waltz J, Haertling F, Wibral M, Singer W *et al.* Cortical oscillatory activity is critical for working memory as revealed by deficits in early-onset schizophrenia. *J Neurosci* 2009; **29**(30)**:** 9481-9489.

63. Barr MS, Farzan F, Tran LC, Chen R, Fitzgerald PB, Daskalakis ZJ. Evidence for excessive frontal evoked gamma oscillatory activity in schizophrenia during working memory. *Schizophr Res* 2010; **121**(1-3)**:** 146-152.

64. Lewis DA, Hashimoto T, Volk DW. Cortical inhibitory neurons and schizophrenia. *Nat Rev Neurosci* 2005; **6**(4)**:** 312-324.

65. Hashimoto T, Volk DW, Eggan SM, Mirnics K, Pierri JN, Sun Z *et al.* Gene expression deficits in a subclass of GABA neurons in the prefrontal cortex of subjects with schizophrenia. *J Neurosci* 2003; **23**(15)**:** 6315-6326.

66. Woo TU, Whitehead RE, Melchitzky DS, Lewis DA. A subclass of prefrontal gamma-aminobutyric acid axon terminals are selectively altered in schizophrenia. *Proc Natl Acad Sci U S A* 1998; **95**(9)**:** 5341-5346.

67. Volk DW, Pierri JN, Fritschy JM, Auh S, Sampson AR, Lewis DA. Reciprocal alterations in pre- and postsynaptic inhibitory markers at chandelier cell inputs to pyramidal neurons in schizophrenia. *Cereb Cortex* 2002; **12**(10)**:** 1063-1070.

68. Parellada M, Penzol MJ, Pina L, Moreno C, Gonzalez-Vioque E, Zalsman G *et al.* The neurobiology of autism spectrum disorders. *Eur Psychiatry* 2014; **29**(1)**:** 11-19.

69. Rubenstein JL, Merzenich MM. Model of autism: increased ratio of excitation/inhibition in key neural systems. *Genes Brain Behav* 2003; **2**(5)**:** 255-267.

70. Courchesne E, Redcay E, Kennedy DP. The autistic brain: birth through adulthood. *Curr Opin Neurol* 2004; **17**(4)**:** 489-496.

71. Tuchman R, Rapin I. Epilepsy in autism. *Lancet Neurol* 2002; **1**(6)**:** 352-358.

72. Irwin SA, Patel B, Idupulapati M, Harris JB, Crisostomo RA, Larsen BP *et al.* Abnormal dendritic spine characteristics in the temporal and visual cortices of patients with fragile-X syndrome: a quantitative examination. *Am J Med Genet* 2001; **98**(2)**:** 161-167.

73. Guerin P, Lyon G, Barthelemy C, Sostak E, Chevrollier V, Garreau B *et al.* Neuropathological study of a case of autistic syndrome with severe mental retardation. *Dev Med Child Neurol* 1996; **38**(3)**:** 203-211.

74. Raymond GV, Bauman ML, Kemper TL. Hippocampus in autism: a Golgi analysis. *Acta Neuropathol* 1996; **91**(1)**:** 117-119.

75. Gadad BS, Hewitson L, Young KA, German DC. Neuropathology and animal models of autism: genetic and environmental factors. *Autism Res Treat* 2013; **2013:** 731935.

76. Geschwind DH. Autism: many genes, common pathways? *Cell* 2008; **135**(3)**:** 391-395.

77. Wass S. Distortions and disconnections: disrupted brain connectivity in autism. *Brain Cogn* 2011; **75**(1)**:** 18-28.

78. Fatemi SH, Halt AR, Stary JM, Kanodia R, Schulz SC, Realmuto GR. Glutamic acid decarboxylase 65 and 67 kDa proteins are reduced in autistic parietal and cerebellar cortices. *Biol Psychiatry* 2002; **52**(8)**:** 805-810.

79. Yau HJ, Wang HF, Lai C, Liu FC. Neural development of the neuregulin receptor ErbB4 in the cerebral cortex and the hippocampus: preferential expression by interneurons tangentially migrating from the ganglionic eminences. *Cereb Cortex* 2003; **13**(3)**:** 252-264.

80. Collins AL, Ma D, Whitehead PL, Martin ER, Wright HH, Abramson RK *et al.* Investigation of autism and GABA receptor subunit genes in multiple ethnic groups. *Neurogenetics* 2006; **7**(3)**:** 167-174.

81. Fatemi SH, Reutiman TJ, Folsom TD, Thuras PD. GABA(A) receptor downregulation in brains of subjects with autism. *J Autism Dev Disord* 2009; **39**(2)**:** 223-230.

82. Abrahams BS, Geschwind DH. Advances in autism genetics: on the threshold of a new neurobiology. *Nat Rev Genet* 2008; **9**(5)**:** 341-355.

83. Brooks-Kayal A. Epilepsy and autism spectrum disorders: are there common developmental mechanisms? *Brain Dev* 2010; **32**(9)**:** 731-738.

84. Zikopoulos B, Barbas H. Altered neural connectivity in excitatory and inhibitory cortical circuits in autism. *Front Hum Neurosci* 2013; **7:** 609.

85. DeFelipe J. Chandelier cells and epilepsy. *Brain* 1999; **122 ( Pt 10):** 1807-1822.

86. Forrest MP, Parnell E, Penzes P. Dendritic structural plasticity and neuropsychiatric disease. *Nat Rev Neurosci* 2018; **19**(4)**:** 215-234.

87. Schaafsma SM, Gagnidze K, Reyes A, Norstedt N, Mansson K, Francis K *et al.* Sex-specific gene-environment interactions underlying ASD-like behaviors. *Proc Natl Acad Sci U S A* 2017; **114**(6)**:** 1383-1388.

88. Gao R, Penzes P. Common mechanisms of excitatory and inhibitory imbalance in schizophrenia and autism spectrum disorders. *Curr Mol Med* 2015; **15**(2)**:** 146-167.

89. Bakkaloglu B, O'Roak BJ, Louvi A, Gupta AR, Abelson JF, Morgan TM *et al.* Molecular cytogenetic analysis and resequencing of contactin associated protein-like 2 in autism spectrum disorders. *Am J Hum Genet* 2008; **82**(1)**:** 165-173.

90. Rossi E, Verri AP, Patricelli MG, Destefani V, Ricca I, Vetro A *et al.* A 12Mb deletion at 7q33-q35 associated with autism spectrum disorders and primary amenorrhea. *Eur J Med Genet* 2008; **51**(6)**:** 631-638.

91. Poot M, Beyer V, Schwaab I, Damatova N, Van't Slot R, Prothero J *et al.* Disruption of CNTNAP2 and additional structural genome changes in a boy with speech delay and autism spectrum disorder. *Neurogenetics* 2010; **11**(1)**:** 81-89.

92. O'Roak BJ, Deriziotis P, Lee C, Vives L, Schwartz JJ, Girirajan S *et al.* Exome sequencing in sporadic autism spectrum disorders identifies severe de novo mutations. *Nat Genet* 2011; **43**(6)**:** 585-589.

93. Ji W, Li T, Pan Y, Tao H, Ju K, Wen Z *et al.* CNTNAP2 is significantly associated with schizophrenia and major depression in the Han Chinese population. *Psychiatry Res* 2013; **207**(3)**:** 225-228.

94. Friedman JI, Vrijenhoek T, Markx S, Janssen IM, van der Vliet WA, Faas BH *et al.* CNTNAP2 gene dosage variation is associated with schizophrenia and epilepsy. *Mol Psychiatry* 2008; **13**(3)**:** 261-266.

95. Gregor A, Albrecht B, Bader I, Bijlsma EK, Ekici AB, Engels H *et al.* Expanding the clinical spectrum associated with defects in CNTNAP2 and NRXN1. *BMC Med Genet* 2011; **12:** 106.

96. Elia J, Gai X, Xie HM, Perin JC, Geiger E, Glessner JT *et al.* Rare structural variants found in attention-deficit hyperactivity disorder are preferentially associated with neurodevelopmental genes. *Mol Psychiatry* 2010; **15**(6)**:** 637-646.

97. Verkerk AJ, Mathews CA, Joosse M, Eussen BH, Heutink P, Oostra BA *et al.* CNTNAP2 is disrupted in a family with Gilles de la Tourette syndrome and obsessive compulsive disorder. *Genomics* 2003; **82**(1)**:** 1-9.

98. Zweier C, de Jong EK, Zweier M, Orrico A, Ousager LB, Collins AL *et al.* CNTNAP2 and NRXN1 are mutated in autosomal-recessive Pitt-Hopkins-like mental retardation and determine the level of a common synaptic protein in Drosophila. *Am J Hum Genet* 2009; **85**(5)**:** 655-666.

99. Al-Murrani A, Ashton F, Aftimos S, George AM, Love DR. Amino-Terminal Microdeletion within the CNTNAP2 Gene Associated with Variable Expressivity of Speech Delay. *Case Rep Genet* 2012; **2012:** 172408.

100. Vernes SC, Newbury DF, Abrahams BS, Winchester L, Nicod J, Groszer M *et al.* A functional genetic link between distinct developmental language disorders. *N Engl J Med* 2008; **359**(22)**:** 2337-2345.

101. Sehested LT, Moller RS, Bache I, Andersen NB, Ullmann R, Tommerup N *et al.* Deletion of 7q34-q36.2 in two siblings with mental retardation, language delay, primary amenorrhea, and dysmorphic features. *Am J Med Genet A* 2010; **152A**(12)**:** 3115-3119.

102. Murdoch JD, Gupta AR, Sanders SJ, Walker MF, Keaney J, Fernandez TV *et al.* No evidence for association of autism with rare heterozygous point mutations in Contactin-Associated Protein-Like 2 (CNTNAP2), or in Other Contactin-Associated Proteins or Contactins. *PLoS Genet* 2015; **11**(1)**:** e1004852.

103. Sampath S, Bhat S, Gupta S, O'Connor A, West AB, Arking DE *et al.* Defining the contribution of CNTNAP2 to autism susceptibility. *PLoS One* 2013; **8**(10)**:** e77906.

104. Strauss KA, Puffenberger EG, Huentelman MJ, Gottlieb S, Dobrin SE, Parod JM *et al.* Recessive symptomatic focal epilepsy and mutant contactin-associated protein-like 2. *N Engl J Med* 2006; **354**(13)**:** 1370-1377.

105. Falivelli G, De Jaco A, Favaloro FL, Kim H, Wilson J, Dubi N *et al.* Inherited genetic variants in autism-related CNTNAP2 show perturbed trafficking and ATF6 activation. *Hum Mol Genet* 2012; **21**(21)**:** 4761-4773.

106. Rodenas-Cuadrado P, Ho J, Vernes SC. Shining a light on CNTNAP2: complex functions to complex disorders. *Eur J Hum Genet* 2014; **22**(2)**:** 171-178.

107. Smogavec M, Cleall A, Hoyer J, Lederer D, Nassogne MC, Palmer EE *et al.* Eight further individuals with intellectual disability and epilepsy carrying bi-allelic CNTNAP2 aberrations allow delineation of the mutational and phenotypic spectrum. *J Med Genet* 2016; **53**(12)**:** 820-827.

108. Jackman C, Horn ND, Molleston JP, Sokol DK. Gene associated with seizures, autism, and hepatomegaly in an Amish girl. *Pediatr Neurol* 2009; **40**(4)**:** 310-313.

109. Watson CM, Crinnion LA, Tzika A, Mills A, Coates A, Pendlebury M *et al.* Diagnostic whole genome sequencing and split-read mapping for nucleotide resolution breakpoint identification in CNTNAP2 deficiency syndrome. *Am J Med Genet A* 2014; **164A**(10)**:** 2649-2655.

110. Penagarikano O, Abrahams BS, Herman EI, Winden KD, Gdalyahu A, Dong H *et al.* Absence of CNTNAP2 leads to epilepsy, neuronal migration abnormalities, and core autism-related deficits. *Cell* 2011; **147**(1)**:** 235-246.

111. Alarcon M, Abrahams BS, Stone JL, Duvall JA, Perederiy JV, Bomar JM *et al.* Linkage, association, and gene-expression analyses identify CNTNAP2 as an autism-susceptibility gene. *Am J Hum Genet* 2008; **82**(1)**:** 150-159.

112. Abrahams BS, Tentler D, Perederiy JV, Oldham MC, Coppola G, Geschwind DH. Genome-wide analyses of human perisylvian cerebral cortical patterning. *Proc Natl Acad Sci U S A* 2007; **104**(45)**:** 17849-17854.

113. Panaitof SC, Abrahams BS, Dong H, Geschwind DH, White SA. Language-related Cntnap2 gene is differentially expressed in sexually dimorphic song nuclei essential for vocal learning in songbirds. *J Comp Neurol* 2010; **518**(11)**:** 1995-2018.

114. Gordon A, Salomon D, Barak N, Pen Y, Tsoory M, Kimchi T *et al.* Expression of Cntnap2 (Caspr2) in multiple levels of sensory systems. *Mol Cell Neurosci* 2016; **70:** 42-53.

115. Traka M, Goutebroze L, Denisenko N, Bessa M, Nifli A, Havaki S *et al.* Association of TAG-1 with Caspr2 is essential for the molecular organization of juxtaparanodal regions of myelinated fibers. *J Cell Biol* 2003; **162**(6)**:** 1161-1172.

116. Denaxa M, Chan CH, Schachner M, Parnavelas JG, Karagogeos D. The adhesion molecule TAG-1 mediates the migration of cortical interneurons from the ganglionic eminence along the corticofugal fiber system. *Development* 2001; **128**(22)**:** 4635-4644.

117. Scott R, Sanchez-Aguilera A, van Elst K, Lim L, Dehorter N, Bae SE *et al.* Loss of Cntnap2 Causes Axonal Excitability Deficits, Developmental Delay in Cortical Myelination, and Abnormal Stereotyped Motor Behavior. *Cereb Cortex* 2017.

118. Rubio-Marrero EN, Vincelli G, Jeffries CM, Shaikh TR, Pakos IS, Ranaivoson FM *et al.* Structural Characterization of the Extracellular Domain of CASPR2 and Insights into Its Association with the Novel Ligand Contactin1. *J Biol Chem* 2016; **291**(11)**:** 5788-5802.

119. Fukata Y, Adesnik H, Iwanaga T, Bredt DS, Nicoll RA, Fukata M. Epilepsy-related ligand/receptor complex LGI1 and ADAM22 regulate synaptic transmission. *Science* 2006; **313**(5794)**:** 1792-1795.

120. Ogawa Y, Oses-Prieto J, Kim MY, Horresh I, Peles E, Burlingame AL *et al.* ADAM22, a Kv1 channel-interacting protein, recruits membrane-associated guanylate kinases to juxtaparanodes of myelinated axons. *J Neurosci* 2010; **30**(3)**:** 1038-1048.

121. Seagar M, Russier M, Caillard O, Maulet Y, Fronzaroli-Molinieres L, De San Feliciano M *et al.* LGI1 tunes intrinsic excitability by regulating the density of axonal Kv1 channels. *Proc Natl Acad Sci U S A* 2017; **114**(29)**:** 7719-7724.

122. van Sonderen A, Petit-Pedrol M, Dalmau J, Titulaer MJ. The value of LGI1, Caspr2 and voltage-gated potassium channel antibodies in encephalitis. *Nat Rev Neurol* 2017; **13**(5)**:** 290-301.

123. Denisenko-Nehrbass N, Oguievetskaia K, Goutebroze L, Galvez T, Yamakawa H, Ohara O *et al.* Protein 4.1B associates with both Caspr/paranodin and Caspr2 at paranodes and juxtaparanodes of myelinated fibres. *Eur J Neurosci* 2003; **17**(2)**:** 411-416.

124. Poliak S, Salomon D, Elhanany H, Sabanay H, Kiernan B, Pevny L *et al.* Juxtaparanodal clustering of Shaker-like K+ channels in myelinated axons depends on Caspr2 and TAG-1. *J Cell Biol* 2003; **162**(6)**:** 1149-1160.

125. Chen N, Koopmans F, Gordon A, Paliukhovich I, Klaassen RV, van der Schors RC *et al.* Interaction proteomics of canonical Caspr2 (CNTNAP2) reveals the presence of two Caspr2 isoforms with overlapping interactomes. *Biochim Biophys Acta* 2015; **1854**(7)**:** 827-833.

126. Gao R, Piguel NH, Melendez-Zaidi AE, Martin-de-Saavedra MD, Yoon S, Forrest MP *et al.* CNTNAP2 stabilizes interneuron dendritic arbors through CASK. *Mol Psychiatry* 2018.

127. Tanabe Y, Fujita-Jimbo E, Momoi MY, Momoi T. CASPR2 forms a complex with GPR37 via MUPP1 but not with GPR37(R558Q), an autism spectrum disorder-related mutation. *J Neurochem* 2015; **134**(4)**:** 783-793.

128. Pinatel D, Hivert B, Saint-Martin M, Noraz N, Savvaki M, Karagogeos D *et al.* The Kv1-associated molecules TAG-1 and Caspr2 are selectively targeted to the axon initial segment in hippocampal neurons. *J Cell Sci* 2017; **130**(13)**:** 2209-2220.

129. Bel C, Oguievetskaia K, Pitaval C, Goutebroze L, Faivre-Sarrailh C. Axonal targeting of Caspr2 in hippocampal neurons via selective somatodendritic endocytosis. *J Cell Sci* 2009; **122**(Pt 18)**:** 3403-3413.

130. Huttlin EL, Jedrychowski MP, Elias JE, Goswami T, Rad R, Beausoleil SA *et al.* A tissue-specific atlas of mouse protein phosphorylation and expression. *Cell* 2010; **143**(7)**:** 1174-1189.

131. Anderson GR, Galfin T, Xu W, Aoto J, Malenka RC, Sudhof TC. Candidate autism gene screen identifies critical role for cell-adhesion molecule CASPR2 in dendritic arborization and spine development. *Proc Natl Acad Sci U S A* 2012; **109**(44)**:** 18120-18125.

132. Hoffman EJ, Turner KJ, Fernandez JM, Cifuentes D, Ghosh M, Ijaz S *et al.* Estrogens Suppress a Behavioral Phenotype in Zebrafish Mutants of the Autism Risk Gene, CNTNAP2. *Neuron* 2016; **89**(4)**:** 725-733.

133. Selimbeyoglu A, Kim CK, Inoue M, Lee SY, Hong ASO, Kauvar I *et al.* Modulation of prefrontal cortex excitation/inhibition balance rescues social behavior in CNTNAP2-deficient mice. *Sci Transl Med* 2017; **9**(401).

134. Vogt D, Cho KKA, Shelton SM, Paul A, Huang ZJ, Sohal VS *et al.* Mouse Cntnap2 and Human CNTNAP2 ASD Alleles Cell Autonomously Regulate PV+ Cortical Interneurons. *Cereb Cortex* 2017**:** 1-12.

135. Biederer T, Sudhof TC. CASK and protein 4.1 support F-actin nucleation on neurexins. *J Biol Chem* 2001; **276**(51)**:** 47869-47876.

136. Pinatel D, Hivert B, Boucraut J, Saint-Martin M, Rogemond V, Zoupi L *et al.* Inhibitory axons are targeted in hippocampal cell culture by anti-Caspr2 autoantibodies associated with limbic encephalitis. *Front Cell Neurosci* 2015; **9:** 265.

137. Horresh I, Poliak S, Grant S, Bredt D, Rasband MN, Peles E. Multiple molecular interactions determine the clustering of Caspr2 and Kv1 channels in myelinated axons. *J Neurosci* 2008; **28**(52)**:** 14213-14222.

138. Mellacheruvu D, Wright Z, Couzens AL, Lambert JP, St-Denis NA, Li T *et al.* The CRAPome: a contaminant repository for affinity purification-mass spectrometry data. *Nat Methods* 2013; **10**(8)**:** 730-736.

139. Spiegel I, Salomon D, Erne B, Schaeren-Wiemers N, Peles E. Caspr3 and caspr4, two novel members of the caspr family are expressed in the nervous system and interact with PDZ domains. *Mol Cell Neurosci* 2002; **20**(2)**:** 283-297.

140. Poepsel S, Sprengel A, Sacca B, Kaschani F, Kaiser M, Gatsogiannis C *et al.* Determinants of amyloid fibril degradation by the PDZ protease HTRA1. *Nat Chem Biol* 2015; **11**(11)**:** 862-869.

141. Zumbrunn J, Trueb B. Primary structure of a putative serine protease specific for IGF-binding proteins. *FEBS Lett* 1996; **398**(2-3)**:** 187-192.

142. Hsueh YP. Calcium/calmodulin-dependent serine protein kinase and mental retardation. *Ann Neurol* 2009; **66**(4)**:** 438-443.

143. Leonoudakis D, Conti LR, Radeke CM, McGuire LM, Vandenberg CA. A multiprotein trafficking complex composed of SAP97, CASK, Veli, and Mint1 is associated with inward rectifier Kir2 potassium channels. *J Biol Chem* 2004; **279**(18)**:** 19051-19063.

144. Lee S, Fan S, Makarova O, Straight S, Margolis B. A novel and conserved protein-protein interaction domain of mammalian Lin-2/CASK binds and recruits SAP97 to the lateral surface of epithelia. *Mol Cell Biol* 2002; **22**(6)**:** 1778-1791.

145. Hsueh YP, Wang TF, Yang FC, Sheng M. Nuclear translocation and transcription regulation by the membrane-associated guanylate kinase CASK/LIN-2. *Nature* 2000; **404**(6775)**:** 298-302.

146. Mukherjee K, Sharma M, Urlaub H, Bourenkov GP, Jahn R, Sudhof TC *et al.* CASK Functions as a Mg2+-independent neurexin kinase. *Cell* 2008; **133**(2)**:** 328-339.

147. Atasoy D, Schoch S, Ho A, Nadasy KA, Liu X, Zhang W *et al.* Deletion of CASK in mice is lethal and impairs synaptic function. *Proc Natl Acad Sci U S A* 2007; **104**(7)**:** 2525-2530.

148. Mertens AE, Pegtel DM, Collard JG. Tiam1 takes PARt in cell polarity. *Trends Cell Biol* 2006; **16**(6)**:** 308-316.

149. Renschler FA, Bruekner SR, Salomon PL, Mukherjee A, Kullmann L, Schutz-Stoffregen MC *et al.* Structural basis for the interaction between the cell polarity proteins Par3 and Par6. *Sci Signal* 2018; **11**(517).

150. Terada N, Saitoh Y, Ohno N, Komada M, Saitoh S, Peles E *et al.* Essential function of protein 4.1G in targeting of membrane protein palmitoylated 6 into Schmidt-Lanterman incisures in myelinated nerves. *Mol Cell Biol* 2012; **32**(1)**:** 199-205.

151. Terada N, Saitoh Y, Ohno N, Komada M, Yamauchi J, Ohno S. Involvement of Src in the membrane skeletal complex, MPP6-4.1G, in Schmidt-Lanterman incisures of mouse myelinated nerve fibers in PNS. *Histochem Cell Biol* 2013; **140**(2)**:** 213-222.

152. Tseng TC, Marfatia SM, Bryant PJ, Pack S, Zhuang Z, O'Brien JE *et al.* VAM-1: a new member of the MAGUK family binds to human Veli-1 through a conserved domain. *Biochim Biophys Acta* 2001; **1518**(3)**:** 249-259.

153. Kaech SM, Whitfield CW, Kim SK. The LIN-2/LIN-7/LIN-10 complex mediates basolateral membrane localization of the C. elegans EGF receptor LET-23 in vulval epithelial cells. *Cell* 1998; **94**(6)**:** 761-771.

154. Dalva MB, McClelland AC, Kayser MS. Cell adhesion molecules: signalling functions at the synapse. *Nat Rev Neurosci* 2007; **8**(3)**:** 206-220.

155. Zhang H, Macara IG. The polarity protein PAR-3 and TIAM1 cooperate in dendritic spine morphogenesis. *Nat Cell Biol* 2006; **8**(3)**:** 227-237.

156. Joberty G, Petersen C, Gao L, Macara IG. The cell-polarity protein Par6 links Par3 and atypical protein kinase C to Cdc42. *Nat Cell Biol* 2000; **2**(8)**:** 531-539.

157. Varea O, Martin-de-Saavedra MD, Kopeikina KJ, Schurmann B, Fleming HJ, Fawcett-Patel JM *et al.* Synaptic abnormalities and cytoplasmic glutamate receptor aggregates in contactin associated protein-like 2/Caspr2 knockout neurons. *Proc Natl Acad Sci U S A* 2015; **112**(19)**:** 6176-6181.

158. Chen X, Macara IG. Par-3 controls tight junction assembly through the Rac exchange factor Tiam1. *Nat Cell Biol* 2005; **7**(3)**:** 262-269.

159. Duman JG, Tzeng CP, Tu YK, Munjal T, Schwechter B, Ho TS *et al.* The adhesion-GPCR BAI1 regulates synaptogenesis by controlling the recruitment of the Par3/Tiam1 polarity complex to synaptic sites. *J Neurosci* 2013; **33**(16)**:** 6964-6978.

160. Lin D, Gish GD, Songyang Z, Pawson T. The carboxyl terminus of B class ephrins constitutes a PDZ domain binding motif. *J Biol Chem* 1999; **274**(6)**:** 3726-3733.

161. Ahmed SM, Macara IG. The Par3 polarity protein is an exocyst receptor essential for mammary cell survival. *Nat Commun* 2017; **8:** 14867.

162. Jeyifous O, Waites CL, Specht CG, Fujisawa S, Schubert M, Lin EI *et al.* SAP97 and CASK mediate sorting of NMDA receptors through a previously unknown secretory pathway. *Nat Neurosci* 2009; **12**(8)**:** 1011-1019.

163. Lin EI, Jeyifous O, Green WN. CASK regulates SAP97 conformation and its interactions with AMPA and NMDA receptors. *J Neurosci* 2013; **33**(29)**:** 12067-12076.

164. Zhou W, Zhang L, Guoxiang X, Mojsilovic-Petrovic J, Takamaya K, Sattler R *et al.* GluR1 controls dendrite growth through its binding partner, SAP97. *J Neurosci* 2008; **28**(41)**:** 10220-10233.

165. Cooper GM, Coe BP, Girirajan S, Rosenfeld JA, Vu TH, Baker C *et al.* A copy number variation morbidity map of developmental delay. *Nat Genet* 2011; **43**(9)**:** 838-846.

166. Chen CH, Chen HI, Chien WH, Li LH, Wu YY, Chiu YN *et al.* High resolution analysis of rare copy number variants in patients with autism spectrum disorder from Taiwan. *Sci Rep* 2017; **7**(1)**:** 11919.

167. Lee BH, Smith T, Paciorkowski AR. Autism spectrum disorder and epilepsy: Disorders with a shared biology. *Epilepsy Behav* 2015; **47:** 191-201.

168. Hackett A, Tarpey PS, Licata A, Cox J, Whibley A, Boyle J *et al.* CASK mutations are frequent in males and cause X-linked nystagmus and variable XLMR phenotypes. *Eur J Hum Genet* 2010; **18**(5)**:** 544-552.

169. Marin O. Interneuron dysfunction in psychiatric disorders. *Nat Rev Neurosci* 2012; **13**(2)**:** 107-120.

170. Srivastava DP, Copits BA, Xie Z, Huda R, Jones KA, Mukherji S *et al.* Afadin is required for maintenance of dendritic structure and excitatory tone. *J Biol Chem* 2012; **287**(43)**:** 35964-35974.

171. Kulkarni VA, Firestein BL. The dendritic tree and brain disorders. *Mol Cell Neurosci* 2012; **50**(1)**:** 10-20.

172. Kalus P, Bondzio J, Federspiel A, Muller TJ, Zuschratter W. Cell-type specific alterations of cortical interneurons in schizophrenic patients. *Neuroreport* 2002; **13**(5)**:** 713-717.

173. Magloczky Z, Wittner L, Borhegyi Z, Halasz P, Vajda J, Czirjak S *et al.* Changes in the distribution and connectivity of interneurons in the epileptic human dentate gyrus. *Neuroscience* 2000; **96**(1)**:** 7-25.

174. Redolfi N, Galla L, Maset A, Murru L, Savoia E, Zamparo I *et al.* Oligophrenin-1 regulates number, morphology and synaptic properties of adult-born inhibitory interneurons in the olfactory bulb. *Hum Mol Genet* 2016; **25**(23)**:** 5198-5211.

175. Cahill ME, Jones KA, Rafalovich I, Xie Z, Barros CS, Muller U *et al.* Control of interneuron dendritic growth through NRG1/erbB4-mediated kalirin-7 disinhibition. *Mol Psychiatry* 2012; **17**(1)**:** 1, 99-107.

176. Cobos I, Calcagnotto ME, Vilaythong AJ, Thwin MT, Noebels JL, Baraban SC *et al.* Mice lacking Dlx1 show subtype-specific loss of interneurons, reduced inhibition and epilepsy. *Nat Neurosci* 2005; **8**(8)**:** 1059-1068.

177. Gomez-Climent MA, Guirado R, Castillo-Gomez E, Varea E, Gutierrez-Mecinas M, Gilabert-Juan J *et al.* The polysialylated form of the neural cell adhesion molecule (PSA-NCAM) is expressed in a subpopulation of mature cortical interneurons characterized by reduced structural features and connectivity. *Cereb Cortex* 2011; **21**(5)**:** 1028-1041.

178. Wirth MJ, Brun A, Grabert J, Patz S, Wahle P. Accelerated dendritic development of rat cortical pyramidal cells and interneurons after biolistic transfection with BDNF and NT4/5. *Development* 2003; **130**(23)**:** 5827-5838.

179. Anney R, Klei L, Pinto D, Almeida J, Bacchelli E, Baird G *et al.* Individual common variants exert weak effects on the risk for autism spectrum disorders. *Hum Mol Genet* 2012; **21**(21)**:** 4781-4792.

180. Lee IS, Carvalho CM, Douvaras P, Ho SM, Hartley BJ, Zuccherato LW *et al.* Characterization of molecular and cellular phenotypes associated with a heterozygous CNTNAP2 deletion using patient-derived hiPSC neural cells. *NPJ schizophrenia* 2015; **1**.

181. Rodenas-Cuadrado P, Pietrafusa N, Francavilla T, La Neve A, Striano P, Vernes SC. Characterisation of CASPR2 deficiency disorder--a syndrome involving autism, epilepsy and language impairment. *BMC Med Genet* 2016; **17:** 8.

182. Jurgensen S, Castillo PE. Selective Dysregulation of Hippocampal Inhibition in the Mouse Lacking Autism Candidate Gene CNTNAP2. *J Neurosci* 2015; **35**(43)**:** 14681-14687.

183. Bridi MS, Park SM, Huang S. Developmental Disruption of GABAAR-Meditated Inhibition in Cntnap2 KO Mice. *eNeuro* 2017; **4**(5).

184. Ramanathan S, Wong CH, Rahman Z, Dale RC, Fulcher D, Bleasel AF. Myoclonic status epilepticus as a presentation of caspr2 antibody-associated autoimmune encephalitis. *Epileptic Disord* 2014; **16**(4)**:** 477-481.

185. van Sonderen A, Arino H, Petit-Pedrol M, Leypoldt F, Kortvelyessy P, Wandinger KP *et al.* The clinical spectrum of Caspr2 antibody-associated disease. *Neurology* 2016; **87**(5)**:** 521-528.

186. Scott EK, Luo L. How do dendrites take their shape? *Nat Neurosci* 2001; **4**(4)**:** 359-365.

187. Mo A, Mukamel EA, Davis FP, Luo C, Henry GL, Picard S *et al.* Epigenomic Signatures of Neuronal Diversity in the Mammalian Brain. *Neuron* 2015; **86**(6)**:** 1369-1384.

188. Gustafsson MG. Nonlinear structured-illumination microscopy: wide-field fluorescence imaging with theoretically unlimited resolution. *Proc Natl Acad Sci U S A* 2005; **102**(37)**:** 13081-13086.

189. Hell SW, Wichmann J. Breaking the diffraction resolution limit by stimulated emission: stimulated-emission-depletion fluorescence microscopy. *Opt Lett* 1994; **19**(11)**:** 780-782.

190. Cavallaro U, Dejana E. Adhesion molecule signalling: not always a sticky business. *Nat Rev Mol Cell Biol* 2011; **12**(3)**:** 189-197.

191. Hata Y, Butz S, Sudhof TC. CASK: a novel dlg/PSD95 homolog with an N-terminal calmodulin-dependent protein kinase domain identified by interaction with neurexins. *J Neurosci* 1996; **16**(8)**:** 2488-2494.

192. Hsueh YP, Yang FC, Kharazia V, Naisbitt S, Cohen AR, Weinberg RJ *et al.* Direct interaction of CASK/LIN-2 and syndecan heparan sulfate proteoglycan and their overlapping distribution in neuronal synapses. *J Cell Biol* 1998; **142**(1)**:** 139-151.

193. Frese CK, Mikhaylova M, Stucchi R, Gautier V, Liu Q, Mohammed S *et al.* Quantitative Map of Proteome Dynamics during Neuronal Differentiation. *Cell Rep* 2017; **18**(6)**:** 1527-1542.

194. Chao HW, Hong CJ, Huang TN, Lin YL, Hsueh YP. SUMOylation of the MAGUK protein CASK regulates dendritic spinogenesis. *J Cell Biol* 2008; **182**(1)**:** 141-155.

195. Chattopadhyaya B, Di Cristo G, Higashiyama H, Knott GW, Kuhlman SJ, Welker E *et al.* Experience and activity-dependent maturation of perisomatic GABAergic innervation in primary visual cortex during a postnatal critical period. *J Neurosci* 2004; **24**(43)**:** 9598-9611.

196. Liska A, Bertero A, Gomolka R, Sabbioni M, Galbusera A, Barsotti N *et al.* Homozygous Loss of Autism-Risk Gene CNTNAP2 Results in Reduced Local and Long-Range Prefrontal Functional Connectivity. *Cereb Cortex* 2017**:** 1-13.

197. Jan YN, Jan LY. Branching out: mechanisms of dendritic arborization. *Nat Rev Neurosci* 2010; **11**(5)**:** 316-328.

198. Smith KR, Kopeikina KJ, Fawcett-Patel JM, Leaderbrand K, Gao R, Schurmann B *et al.* Psychiatric risk factor ANK3/ankyrin-G nanodomains regulate the structure and function of glutamatergic synapses. *Neuron* 2014; **84**(2)**:** 399-415.

199. Yam PT, Pincus Z, Gupta GD, Bashkurov M, Charron F, Pelletier L *et al.* N-cadherin relocalizes from the periphery to the center of the synapse after transient synaptic stimulation in hippocampal neurons. *PLoS One* 2013; **8**(11)**:** e79679.

200. Horresh I, Bar V, Kissil JL, Peles E. Organization of myelinated axons by Caspr and Caspr2 requires the cytoskeletal adapter protein 4.1B. *J Neurosci* 2010; **30**(7)**:** 2480-2489.

201. Samuels BA, Hsueh YP, Shu T, Liang H, Tseng HC, Hong CJ *et al.* Cdk5 promotes synaptogenesis by regulating the subcellular distribution of the MAGUK family member CASK. *Neuron* 2007; **56**(5)**:** 823-837.

202. Wang GS, Hong CJ, Yen TY, Huang HY, Ou Y, Huang TN *et al.* Transcriptional modification by a CASK-interacting nucleosome assembly protein. *Neuron* 2004; **42**(1)**:** 113-128.

203. Kahana MJ. The cognitive correlates of human brain oscillations. *J Neurosci* 2006; **26**(6)**:** 1669-1672.

204. Klausberger T, Somogyi P. Neuronal diversity and temporal dynamics: the unity of hippocampal circuit operations. *Science* 2008; **321**(5885)**:** 53-57.

205. Fromer M, Pocklington AJ, Kavanagh DH, Williams HJ, Dwyer S, Gormley P *et al.* De novo mutations in schizophrenia implicate synaptic networks. *Nature* 2014; **506**(7487)**:** 179-184.

206. Epi KC. De Novo Mutations in SLC1A2 and CACNA1A Are Important Causes of Epileptic Encephalopathies. *Am J Hum Genet* 2016; **99**(2)**:** 287-298.

207. Thomas AM, Schwartz MD, Saxe MD, Kilduff TS. Cntnap2 Knockout Rats and Mice Exhibit Epileptiform Activity and Abnormal Sleep-Wake Physiology. *Sleep* 2017; **40**(1).

208. Gdalyahu A, Lazaro M, Penagarikano O, Golshani P, Trachtenberg JT, Geschwind DH. The Autism Related Protein Contactin-Associated Protein-Like 2 (CNTNAP2) Stabilizes New Spines: An In Vivo Mouse Study. *PLoS One* 2015; **10**(5)**:** e0125633.

209. Karayannis T, Au E, Patel JC, Kruglikov I, Markx S, Delorme R *et al.* Cntnap4 differentially contributes to GABAergic and dopaminergic synaptic transmission. *Nature* 2014; **511**(7508)**:** 236-240.

210. van Abel D, Michel O, Veerhuis R, Jacobs M, van Dijk M, Oudejans CB. Direct downregulation of CNTNAP2 by STOX1A is associated with Alzheimer's disease. *J Alzheimers Dis* 2012; **31**(4)**:** 793-800.

211. Birey F, Andersen J, Makinson CD, Islam S, Wei W, Huber N *et al.* Assembly of functionally integrated human forebrain spheroids. *Nature* 2017; **545**(7652)**:** 54-59.

212. Forrest M, Chapman RM, Doyle AM, Tinsley CL, Waite A, Blake DJ. Functional analysis of TCF4 missense mutations that cause Pitt-Hopkins syndrome. *Hum Mutat* 2012; **33**(12)**:** 1676-1686.

213. Jones CA, Watson DJ, Fone KC. Animal models of schizophrenia. *Br J Pharmacol* 2011; **164**(4)**:** 1162-1194.

214. Alvarez VA, Ridenour DA, Sabatini BL. Retraction of synapses and dendritic spines induced by off-target effects of RNA interference. *J Neurosci* 2006; **26**(30)**:** 7820-7825.

215. Golzio C, Willer J, Talkowski ME, Oh EC, Taniguchi Y, Jacquemont S *et al.* KCTD13 is a major driver of mirrored neuroanatomical phenotypes of the 16p11.2 copy number variant. *Nature* 2012; **485**(7398)**:** 363-367.

216. Escamilla CO, Filonova I, Walker AK, Xuan ZX, Holehonnur R, Espinosa F *et al.* Kctd13 deletion reduces synaptic transmission via increased RhoA. *Nature* 2017; **551**(7679)**:** 227-231.

217. Rossi A, Kontarakis Z, Gerri C, Nolte H, Holper S, Kruger M *et al.* Genetic compensation induced by deleterious mutations but not gene knockdowns. *Nature* 2015; **524**(7564)**:** 230-233.

218. Canali G, Garcia M., Hivert B., Pinatel D, Goullancourt A., Oguievetskaia K *et al.* Genetic variants in autism-related CNTNAP2 impair axonal growth of cortical neurons. *Hum Mol Genet* 2018.

219. Polimanti R, Squitti R, Pantaleo M, Giglio S, Zito G. Duplication of FOXP2 binding sites within CNTNAP2 gene in a girl with neurodevelopmental delay. *Minerva Pediatr* 2017; **69**(2)**:** 162-164.

220. Coutinho E, Jacobson L, Pedersen MG, Benros ME, Norgaard-Pedersen B, Mortensen PB *et al.* CASPR2 autoantibodies are raised during pregnancy in mothers of children with mental retardation and disorders of psychological development but not autism. *J Neurol Neurosurg Psychiatry* 2017; **88**(9)**:** 718-721.

221. Braniste V, Al-Asmakh M, Kowal C, Anuar F, Abbaspour A, Toth M *et al.* The gut microbiota influences blood-brain barrier permeability in mice. *Sci Transl Med* 2014; **6**(263)**:** 263ra158.

222. Brimberg L, Mader S, Jeganathan V, Berlin R, Coleman TR, Gregersen PK *et al.* Caspr2-reactive antibody cloned from a mother of an ASD child mediates an ASD-like phenotype in mice. *Mol Psychiatry* 2016; **21**(12)**:** 1663-1671.

223. Dawes JM, Weir GA, Middleton SJ, Patel R, Chisholm KI, Pettingill P *et al.* Immune or Genetic-Mediated Disruption of CASPR2 Causes Pain Hypersensitivity Due to Enhanced Primary Afferent Excitability. *Neuron* 2018; **97**(4)**:** 806-822 e810.

224. Lu Z, Reddy MV, Liu J, Kalichava A, Liu J, Zhang L *et al.* Molecular Architecture of Contactin-associated Protein-like 2 (CNTNAP2) and Its Interaction with Contactin 2 (CNTN2). *J Biol Chem* 2016; **291**(46)**:** 24133-24147.

225. Bruckner A, Polge C, Lentze N, Auerbach D, Schlattner U. Yeast two-hybrid, a powerful tool for systems biology. *Int J Mol Sci* 2009; **10**(6)**:** 2763-2788.

226. Lavallee-Adam M, Cloutier P, Coulombe B, Blanchette M. Modeling contaminants in AP-MS/MS experiments. *J Proteome Res* 2011; **10**(2)**:** 886-895.

227. Fazzari P, Paternain AV, Valiente M, Pla R, Lujan R, Lloyd K *et al.* Control of cortical GABA circuitry development by Nrg1 and ErbB4 signalling. *Nature* 2010; **464**(7293)**:** 1376-1380.

228. Srivastava DP, Woolfrey KM, Penzes P. Analysis of dendritic spine morphology in cultured CNS neurons. *Journal of visualized experiments : JoVE* 2011; (53)**:** e2794.

229. Nakagawa T, Cheng Y, Ramm E, Sheng M, Walz T. Structure and different conformational states of native AMPA receptor complexes. *Nature* 2005; **433**(7025)**:** 545-549.

230. Gertler TS, Chan CS, Surmeier DJ. Dichotomous anatomical properties of adult striatal medium spiny neurons. *J Neurosci* 2008; **28**(43)**:** 10814-10824.

231. Sebel LE, Graves SM, Chan CS, Surmeier DJ. Haloperidol Selectively Remodels Striatal Indirect Pathway Circuits. *Neuropsychopharmacology* 2017; **42**(4)**:** 963-973.

232. Scorcioni R, Polavaram S, Ascoli GA. L-Measure: a web-accessible tool for the analysis, comparison and search of digital reconstructions of neuronal morphologies. *Nat Protoc* 2008; **3**(5)**:** 866-876.